CLOSED LOOP PERFORMANCE OF NEW SLIP POWER RECOVERY SCHEME WITH IMPROVED POWER FACTOR

A Thesis Submitted
In Partial Fulfilment of the Requirements
for the Degree of

MASTER OF TECHNOLOGY

by

SUDARSHAN CHAKRAVORTY

to the

DEPARTMENT OF ELECTRICAL ENGINEERING
INDIAN INSTITUTE OF TECHNOLOGY, KANPUR
OCTOBER, 1984

EE-1984-M-CHA--CLO

DEDICATED

TO

MY PARENTS

CERTIFICATE

Certified that this work on ''Closed Loop Control of a New Slip-Power Recovery Scheme with improved power-factor'' has been carried out by Sudarshan Chakravorty under our supervisions and that it has not been submitted elsewhere for a degree.

K.E. Holé
Asst. Professor
Department of Electrical Engg.
Indian Institute of Technology
Kanpur- 208016

S.R. Doradla
Asst. Professor
Department of Electrical Engg.
Indian Institute of Technology
Kanpur- 208016

ACKNOWLEDGEMENT

I am grateful to Dr.S.R. Doradla and Dr.K.E. Hole for their guidance throughout the course of this work. I express my sincere gratitude to Dr.G.K. Dubey for the useful discussions with him at the begining stages of the work.

I sincerely thank Mr.O.P. Arora and Mr.D.N. Joshi for their unflinching help in carrying out the experimental work of the project. Also my thanks to M/s. J. Usmani, S.P. Tyagi, M.L. Gupta, Ramavatar Chaurasia and S.V. Gharpade for their kind help in different stages of the experimental work.

I am extremely grateful to Royda for his moral support during a very crucial part of the experimental work.

I am thankful to my friends, specially Mukund and Deshpande, for the useful discussions with them in different stages of the work. Also my special thanks to Durga Prasad for giving moral support in this work.

Thanks are due to Mr.B.D. Bisras for excellent typing, Mr.A.K. Ganguli for the drawing of the figures, Mr.D.K. Sarkar for taking the excellent photographs and Mr.Sri Ram for careful cyclostyling.

I.I.T. Kanpur

SUDARSHAN CHAKRAVORTY

September, 1984

CONTENTS

CHAPTER			Page
1	INTRODUCTION		1
	1.1	Introduction	1
	1.2	Thesis outline	7
2	A NEW SLIP POWER RECOVERY SCHEME		11
	2.1	Block diagram of the scheme	11
	2.2	Forced commutated inverter	16
	2.2.1	Starting process	18
	2.2.2	Speed and power factor control	20
	2.3	Operation of the PWM inverter	20
	2.4	Control circuit	28
	2.4.1	Firing circuit for the starting thyristor	28
	2.4.2	Control circuit for thyristors T_1, T_3 and T_5	30
	2.4.3	Control circuit for thyristors T_4, T_6 and T_2	33
3	STEADY STATE PERFORMANCE CHARACTERISTICS OF SLIP POWER RECOVERY SCHEME EMPLOYING PWM CONVERTER IN THE ROTOR CIRCUIT		37
	3.1	Introduction	37
	3.2	DC equivalent circuit	38
	3.3	AC equivalent circuit	49
	3.3.1	Calculation of the fundamental component of the inverter current	50
	3.3.2	Determination of the overall power factor of the drive	54

4	CLOSED LOOP CONTROL OF THE NEW SLIP POWER RECOVERY SCHEME		60
	4.1	Overall description of the closed loop scheme	60
	4.2	Mathemetical model for the closed loop	62
	4.3	Transducers	66
	4.3.1	Speed transducer	66
	4.3.2	Current transducer	66
	4.4	Filters	69
	4.4.1	Speed feedback filter	69
	4.5	Derivation of the transfer function of various elements	70
	4.5.1	PWM inverter	70
	4.5.2	Current controller	71
	4.5.3	Speed controller	71
	4.6	Limiters	72
	4.7	Design of controllers	72
	4.7.1	Current controller	72
	4.7.2	Realisation of current controller	77
	4.7.3	Speed controller	77
	4.7.4	Realisation of speed controller	83
	4.8	Power factor correction loop	83
5	CONCLUSIONS		90
	APPENDIX 'A'		92
	APPENDIX 'B'		97
	APPENDIX 'C'		101
	APPENDIX 'D'		103
	REFERENCES		104

LIST OF SYMBOLS

V_D	Rectified rotor emf, V
s	Slip
V_{DO}	Average inverter counter emf, V
V, V_a	Phase to neutral voltage, V
m	Modulation index
a	Stator to rotor turns ratio
n	3-phase transformer turns ratio
I_D	DC link current, A
I_2	Rotor current, A
I_{21}	Fundamental component of rotor current, A
X_1'	Stator leakage reactance when reflected to the rotor side, Ω
X_2	Rotor reactance, Ω
R_1'	Stator resistance when reflected in the rotor, Ω
R_2	Rotor resistance, Ω
R_F	Filter resistance, Ω
w_s	Synchronous speed of the machine, radians
θ_{21}	Angle between E_2 and I_{21}
P_{mech}	Mechanical power output from the machine
I_s	Stator current, A
I_{if}	Fundamental component of the inverter current, A
T	Torque, N-m
I_n	Harmonic components of inverter phase current, A

R_s	Shunt resistance in the rotor circuit, Ω
L_F	Filter inductance, H
ΔV	Drops across thyristors of the inverter, V
$\Delta V'$	Drops across diodes, V
P_r	Rotor power, W
E	Average rectified rotor voltage at unity slip, V
S	Laplace transform variable
K_1	Gain of the current controller
K_2	Gain of the speed controller
T_2	Time constant of the speed controller
T_i	Time constant of the current filter
T_w	Time constant of the speed filter
H_w	Steady state feedback factor of the speed filter

LIST OF FIGURES

		Page
1.1	Schematic diagram of slip power recovery scheme	3
1.2	Schematic diagram of slip power recovery schemes reported so far	9,10
2.1	Experimental set-up	12
2.2	Phasor diagram of the new scheme	14
2.3	Circuit configuration of the EPWM inverter	17
2.4	Pulse layout of the PWM inverter	19
2.5	Equivalent circuit of the duty interval	23
2.6	Equivalent of the interval for commutation of starting interval	25
2.7	Equivalent circuit for the freewheeling interval	26
2.8	Equivalent circuit for the interval for the change of bottom group thyristors	27
2.9	Control circuit for the starting thyristor and its pulse layout	29
2.10	General block diagram of the control circuit for the thyristors T_1,T_3 and T_5	31
2.11	Wave forms at different stages for the firing CKT in Fig.2.9	32
2.12	General block diagram of the control circuit for the thyristors T_2,T_4 and T_6	34
2.13	Wave forms at different stages for the firing circuit in Fig.2.12	35
3.1(a)	Representation of the drive system	39
3.1(b)	Representation of drive system by transferring the stator impedances to the rotor side	39

3.2(a)	Rotor voltage and current	40
3.2(b)	Derivation of DC equivalent circuit	40
3.3	Pulse layout and the inverter counter EMF for the phase shift angle 0-30 degrees	42
3.4	Pulse layout and the inverter counter EMF for the phase angle 30-60 degrees	43
3.5	Pulse layout and the inverter counter EMF for the phase angles of 60-90 degrees	44
3.6	Inverter counter EMF vs. modulation index for a transformer turns ratio of 10:1	45
3.7	DC link current vs. speed for different values of modulation index	47
3.8	Torque vs. speed characteristics for different values of modulation index	48
3.9	AC equivalent circuit referred to the stator	51
3.10	Phasor diagram of the AC equivalent circuit	52
3.11	Phase to neutral voltages and inverter phase a current	53
3.12	Inverter current harmonic spectrum	55
3.13	Power factor vs. speed for different values of modulation index	57
4.1	Closed loop speed control scheme for 3-phase slip-ring induction motor	61
4.2	Simplified block diagram of the plant	67
4.3	Sensing of link current using opto-isolator	68
4.4	Block diagram of current control loop	73
4.5	Equivalent approximate block diagram of current control loop	75
4.6	Circuit diagram of the current controller	78
4.7	Block diagram of speed controller loop	80

4.8	Realization of the speed-controller	84
4.9	Block diagram of the power factor correction loop	85
4.10	System block diagram	88
4.11	Closed loop speed-torque characteristics	89

ABSTRACT

Slip power recovery scheme employing a new control strategy for improving the supply power factor is investigated. A diode bridge and a PWM converter are used in the rotor circuit giving subsynchronous speed control range. The induction motor drive is started initially with a starting thyristor in series with a current limiting resistor. The inverter gating circuit is designed such that the starting thyristor is line commutated. Simple DC and AC equivalent circuits are used to compute the steady state performance. Because of pulse width modulation, the input current harmonic spectrum has shifted from lower order to higher order. This has a beneficial effect on the size of input filters for the inverter. Closed loop scheme for speed control of the system, for a limited sub-synchronous range is given. Controller design is also presented. A new scheme for controlling the displacement factor of the inverter in closed loop is suggested. Experimental results confirming the theoretical results are given for open-loop study.

CHAPTER 1

1.1 INTRODUCTION

The speed control of induction motors has been of much interest in recent times because of several advantages associated with induction motors over dc motors. Where high performance is a must over a wide range of speed, inverter fed squirrel cage induction motors are preferred since the high cost of the inverter is compensated by the relatively low cost of squirrel cage induction motor. Generally wound rotor induction motors are also employed in many industrial applications. All the methods of speed control of squirrel cage induction motors are also equally applicable to wound rotor induction motors. In addition, continuous speed control can be obtained by inserting a resistance or injecting a counter EMF in the rotor circuit. The former method of speed control is quite attractive if high starting torque is required but is highly inefficient while the latter method provides efficient means of speed control. Auxiliary machines were used for generating slip-frequency EMF, since this is required for controlling the speed of an induction motor [1]. Such schemes were not economical and did not find much acceptance in the variable speed drives employing induction motors. With the availability of high power semiconductor switches, there has been a revival of interest in the speed control of wound rotor induction motors by the injection of

counter EMF at slip-frequency in the rotor circuit. The speed control is achieved by efficiently utilizing the power crossing the air gap and entering the rotor circuit. This method of speed control is often referred to as 'slip power recovery scheme' in the literature. It is also commonly known as 'Static Scherbius system' since it is an analog of the well known Scherbius scheme of speed control [2]. Fig.1.1 shows the basic block diagram of slip power recovery scheme. The slip frequency rotor EMFs,are rectified by a diode bridge and the dc power is returned to the ac supply system through a line commutated converter operated as an inverter. Since the power can flow from the rotor circuit to the supply line with the arrangement shown in Fig.1.1, only sub-synchronous speeds are possible. If the diode bridge is replaced by a line commutated converter, it is possible to achieve power flow in either direction between the rotor circuit and the supply source. Speed control in the super-synchronous speed range is thus obtained by supplying power to the rotor from the three phase ac supply system.

The main limitations of slip power recovery scheme are :

1. This scheme requires a large number of thyristors for speed control above and below the synchronous speed. At near synchronous speed, no rotor EMFs are available and hence the commutation of thyristors may not be possible. An

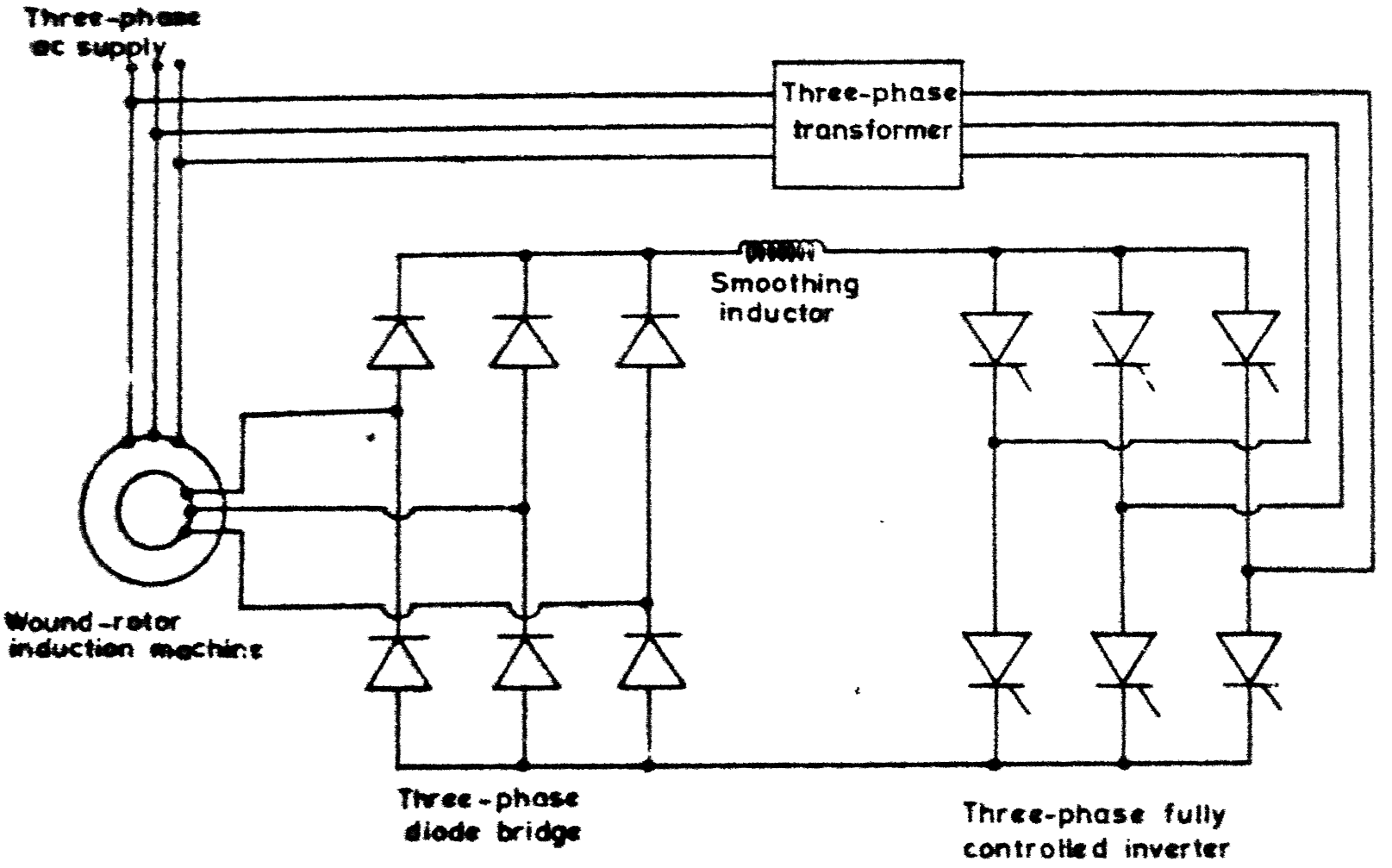

1.1 Schematic diagram of slip power recovery scheme

auxiliary dc bus or some other means must be provided to ensure proper commutation of the devices at synchronous speed.

2. The resultant supply power factor is poor particularly at low speeds when the power output of the motor is low. Both fundamental and harmonic currents drawn by the converter contribute to reactive power. Because of the presence of leakage inductances of the stator and the rotor windings, commutation overlap takes place in the diode bridge and some reactive power is drawn from the source.

3. The device ratings are considerably reduced if the speed control range is limited. If the power crossing the air gap is P_{ag}, and the slip is to be controlled from say zero to s, then the converters are designed to handle s P_{ag}. Thus, as the speed control range decreases, the converter rating also decreases. This drive is quite attractive for large fans and pumps where the speed control range is small.

Many papers appeared in the literature on different aspects of slip power recovery scheme. The gists of these papers are briefly reported. And finally the scope of the present work is mentioned.

Erlicki [3] investigated static Scherbius method of speed control on a laboratory sized induction motor and suggested, the suitability of such a drive for industrial applications requiring variable speed of operation. In order to obtain super-synchronous speeds, three single phase parallel inverters were used in the rotor circuit.

Lavi and Polge [4] reported a method of analysis for determining the steady state performance of a wound rotor induction motor with a diode bridge and a line commutated converter in the rotor circuit. The theoretical performance characteristics are corroborated experimentally. It was pointed out that this drive system had the characteristics of a seperately excited dc motor. The transient performance was also discussed qualitatively.

Shepherd and Stanway [5] investigated the slip power recovery scheme employing auxiliary stator windings for the improvement of power factor and current waveform, but the efficiency was found to be much less two stator windings are required for implementing this drive system.

Shepherd and Khalil [6] studied the improvement of power factor by using external capacitances. It was reported that the drive system provided high torque and torque/supply current ratio, better speed regulation, greater efficiency, good power factor at low speeds in comparison with the uncompensated slip energy recovery scheme. However, the performance deteriorated specially at low slips or high speeds.

Miljanic [7] studied the rotor slip power recovery scheme using a through pass inverter instead of a line commutated inverter specially for improving the power factor of the drive system. The forced commutated converter employed a single pulse per phase in each half-cycle.

Drury et al. [8] and Rao et al. [9] studied sub-synchronous slip power recovery schemes employing fully controlled converters with half controlled characteristics. Some improvement in supply power factor was reported. The former investigated the scheme with a three-phase converter while the latter used a single phase converter. DC and AC equivalent circuits were used for the determination of the performance [9].

Guy Oliver et al. [10] investigated the drive performance characteristics of a slip power recovery scheme with three types of line commutated converters and presented a comparative study. The improvement of the performance characteristics by employing a converter having eight thyristors instead of a conventional 6-thyristor bridge was pointed out.

Smith [11] presented a complete drive system capable of providing driving and braking characteristics below and above synchronous speed. A current source inverter was used in the place of a diode bridge. Conceptually, the treatment was indeed exhaustive.

In this thesis, slip energy recovery scheme using a diode bridge and a forced commutated converter in the rotor circuit is studied. Speed control in the sub-synchronous speed range is considered. A starting thyristor is employed to start the drive. No special control and commutation circuitry are required to turn on and commutate the starting thyristor. The logic has been built into the main control circuit for the inverter.

A PWM converter is used to improve the supply power factor. The inverter is operated in such a way that the active power and the reactive power corresponding to the fundamental component is returned to the supply source. Since multipulse width modulation is employed within the inverter, a number of lower order harmonics are eliminated from the input current of the inverter. Thus the harmonic reactive power is reduced. The overall power factor of the complete drive system is greatly improved. DC and AC equivalent circuits are used to determince the performance characteristics [4]. The performance characteristics such as speed torque, power factor-speed, dc link current-speed, inverter EMF vs. speed etc. are determined theoretically and verified experimentaly. There is a good agreement between experimental and theoretical results. Oscillograms of typical waveforms from the experimental set-up are also given.

1.2 THESIS OUTLINE

In this thesis, the slip power recovery scheme with a diode bridge and a PWM converter in the rotor circuit is studied. The supply power factor variation as a function of speed is determined theoretically and verified experimentally also. Apart from the study of open loop performance, the closed poop operation of speed is investigated. The chapter wise contents of the thesis are :

In chapter 2, the speed and power factor control and the starting of the induction motor drive employing the forced commutated inverter are discussed. The generator of trigger pulses for the PWM strategy in the inverter is explained. The operation of the inverter, commutation of the starting thyristor are clearly explained.

In chapter 3, the open loop analysis of the drive system using both the dc as well as the ac equivalent circuit approch is presented. Performance characteristics such as torque-speed, power factor versus speed, inverter current harmonic spectrum etc. are determined theoretically and verified experimentally. Oscillograms of typical waveforms obtained from the experimental set-up are illustrated to verify the basic principles of operation.

In chapter 4, the closed loop operation of the drive system is discussed in detail. Design of controllers for the current as well as the speed control loop are presented. A new method for controlling the power factor in closed loop conditions is also presented. Lastly some closed loop performance characteristics are also given.

Chapter 5 gives the conclusions along with suggestions for further research in this area of investigation.

The schematic diagrams of the papers discussed in Sec.1.1 are shown in Fig. 1.2.

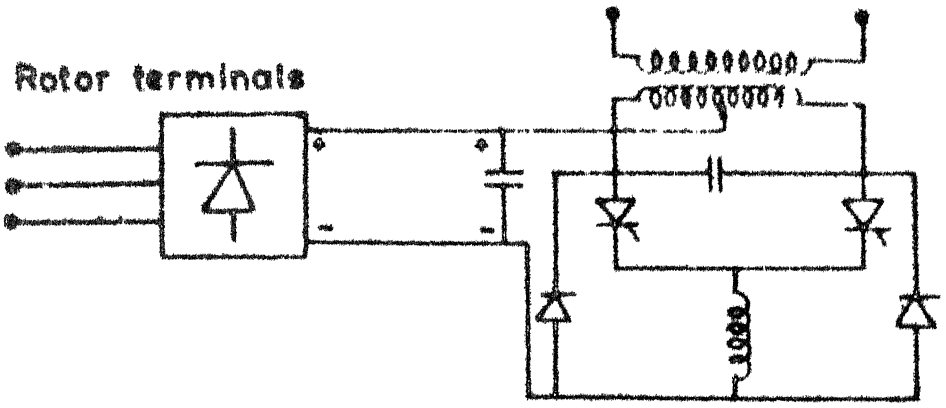

(a) Diode bridge and parallel inverter

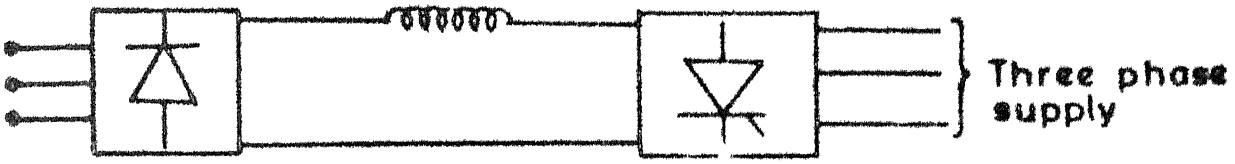

(b) Diode bridge and three-phase FCC

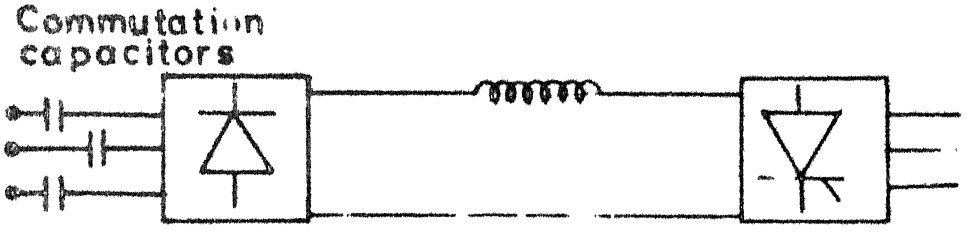

(c) Diode bridge with capacitors on the rotorside and three-phase FCC

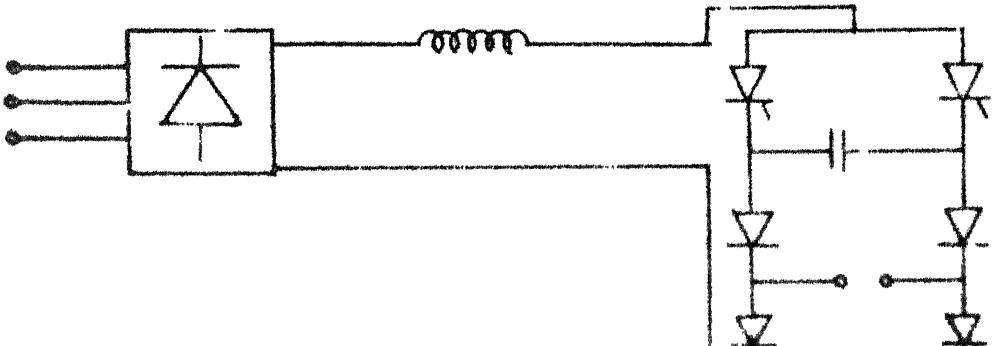

(d) Diode bridge and single phase through pass inverter

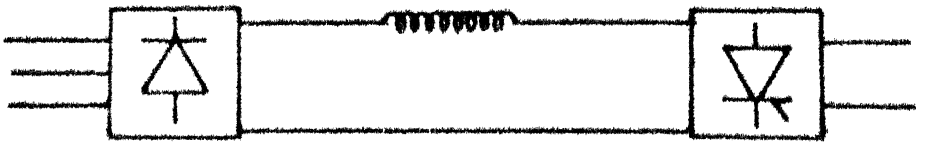

(e) Diode bridge and single phase FCC with half controlled characteristics

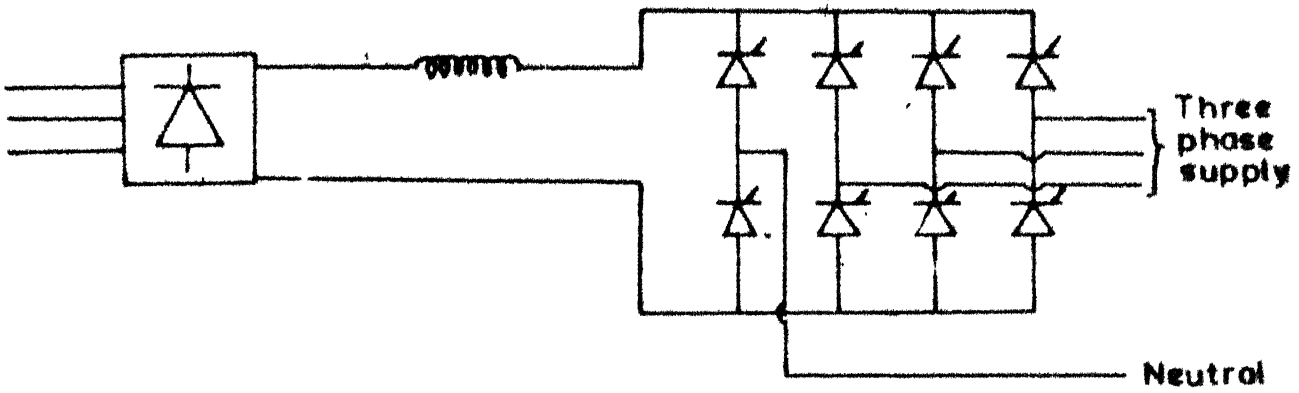

(f) Diode bridge and eight thyristor bridge

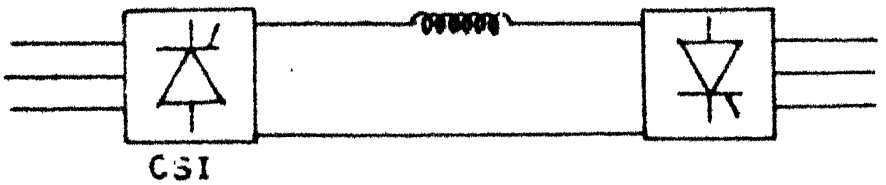

(g) CSI and three-phase FCC

CHAPTER 2

A NEW SLIP POWER RECOVERY SCHEME

2.1 BLOCK DIAGRAM OF THE SCHEME

The block diagram of the slip power recovery scheme in which the speed of a three phase slip ring induction motor is to be controlled is shown in Fig.2.1. Mechanically coupled to the induction motor is a dc motor acting as a generator for loading purposes. The three phase diode bridge is connected to the rotor terminals of the induction motor to convert the slip power at the slip frequency to dc power. The diodes are line commutated by the rotor voltages. A smoothing reactor is connected to reduce the ripple in the dc link current. A three phase converter employing equal pulse width modulation (EPWM) is used to convert dc power to ac power at the line frequency. The speed of the drive is varied from standstill to near synchronous speed by varying the modulation index of the inverter from unity to zero if the stator to rotor turns ratio is unity. The average rectified rotor voltage, V_D, at some slip s is given by,

$$V_D = s.\ \frac{3\sqrt{6}}{\pi}\ .\ E_2 = 2.34sE_2 \qquad \ldots\ldots\ (2.1)$$

where E_2 is the rotor rms voltage/phase at standstill.

The average inverter counter emf across the PWM inverter can be written as ,

$$V_{DO} = \frac{V}{n} \sum_{K=1}^{P} f\ (m,K) \qquad \ldots\ldots\ (2.2)$$

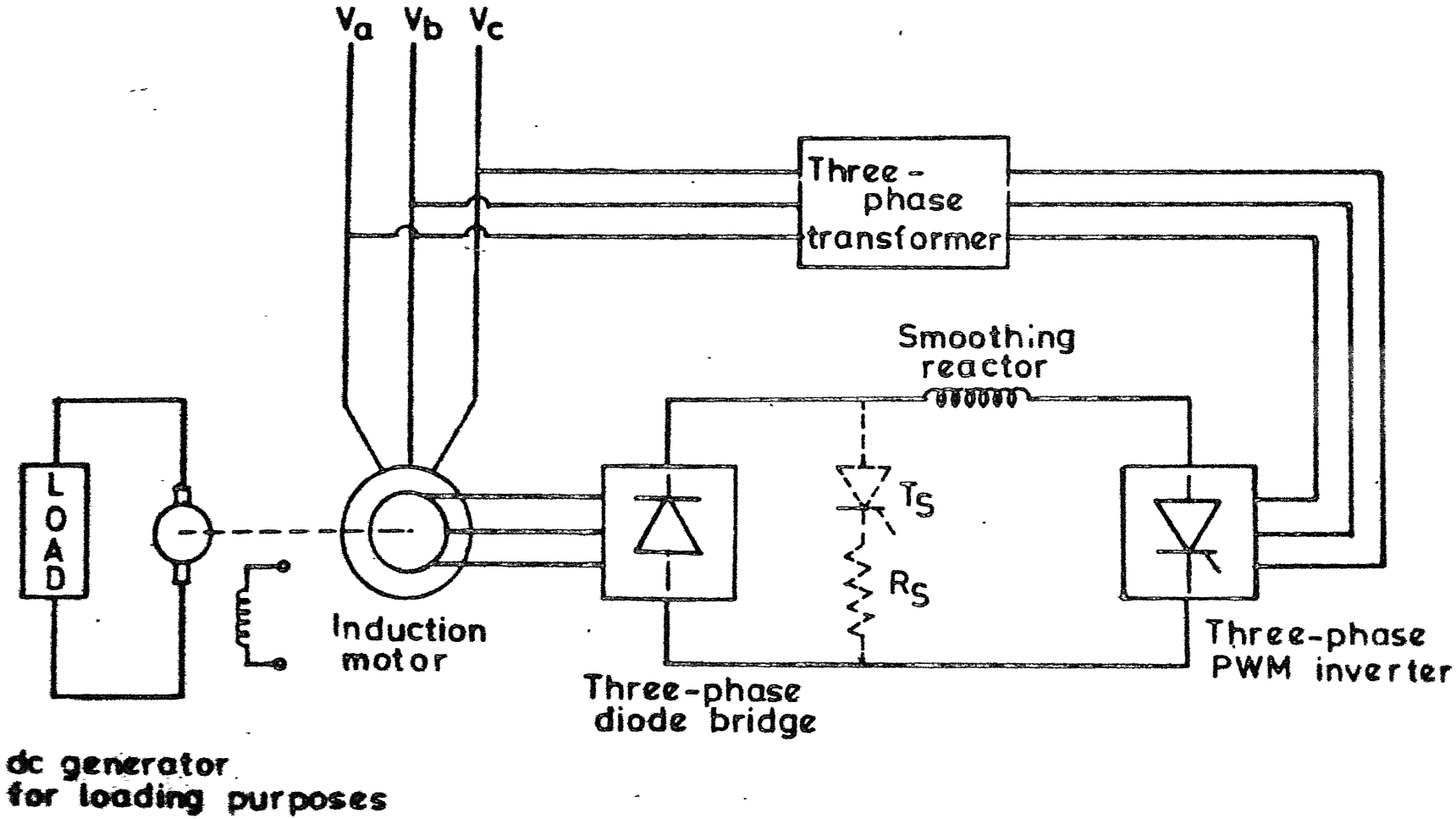

2.1 Experimental set-up

where f(m,K) is a function of the modulation index m and the number K, P is the number of pulses/phase/half-cycle and n is the turns ratio of the transformer interposed between the inverter and the ac supply.

On no load, the rectified rotor current is almost zero, then these two voltages must balance i.e.

$$2.34 s E_2 = \frac{V}{n} \sum_{K=1}^{P} f(m,K)$$

$$\text{or} \quad s = 0.38 \frac{V}{E_2 . n} \sum_{K=1}^{P} f(m,K) \qquad \ldots\ldots (2.3)$$

But $\frac{V}{E_2}$ = a = stator to rotor turns ratio

Therefore, $s = 0.38 \frac{a}{n} \sum_{K=1}^{P} f(m,K)$ $\qquad \ldots\ldots (2.4)$

Most of the commercially available induction motors have stator/rotor turns ratios more than 1. The second factor in eqn.(2.4) can vary from zero to unity. In order to vary the slip in proportion to this factor, 0.38a/n must be kept at unity. In otherwards, a transformer is interposed between the supply and the inverter and the turns ratio n, is selected as 0.38a. Thus the slip is controlled from unity to near zero values. Moreover, the devices having lower breakover voltage ratings can be used by using a step down transformer.

The basic principle of this new scheme is described by the phasor diagram in Fig.2.2. The slip power recovery

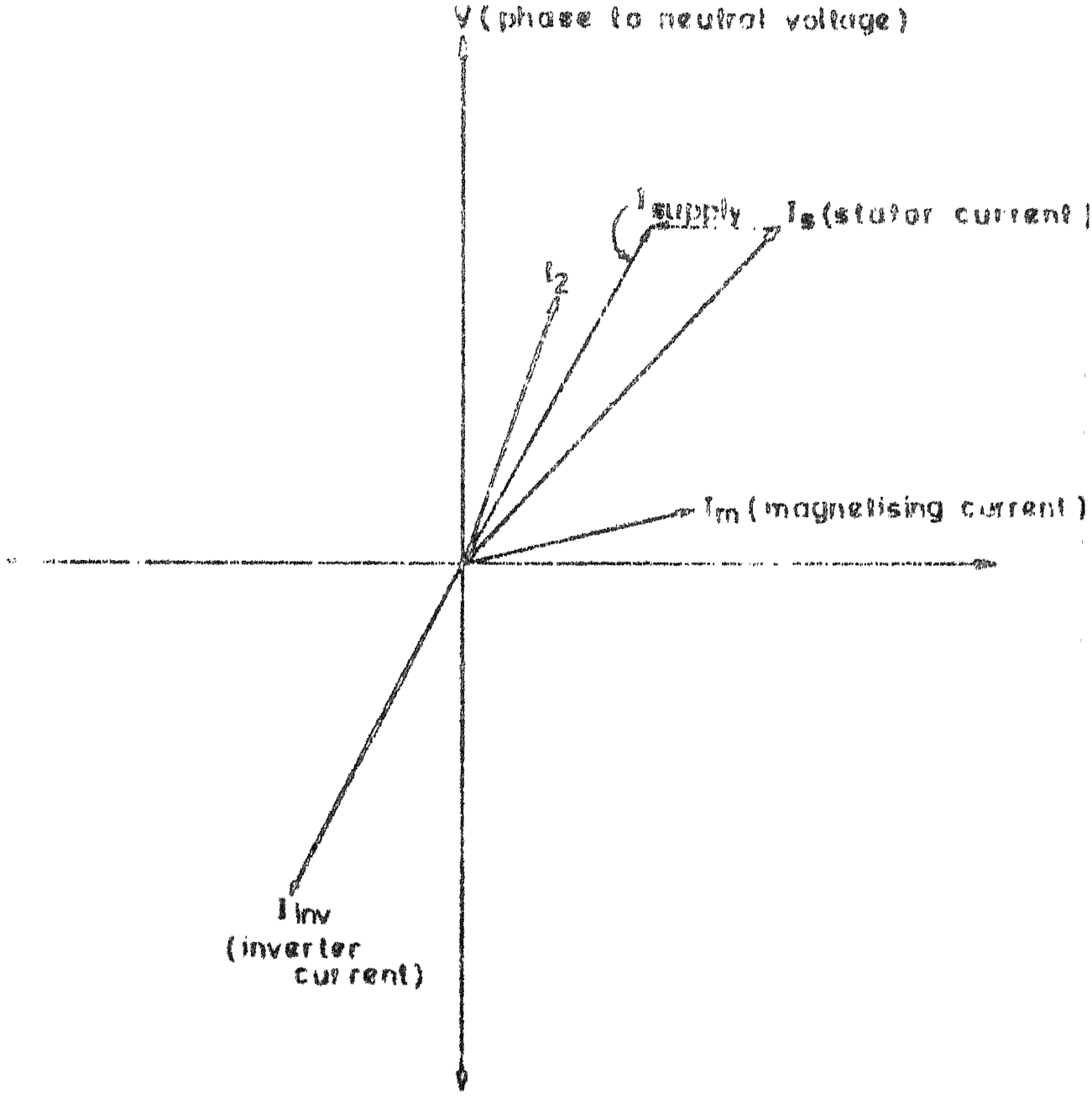

2.2 Phasor diagram of the new scheme

scheme employing phase controlled thyristor inverter provide poor overall supply power factor [4,5,6,9]. Because of the phase delay control technique within the inverter, reactive power is drawn from the supply source by the fundamental and harmonic currents although the active power is returned to the supply source. By replacing the line commutated inverter by forced commutated type of inverter, the power factor is improved to some extent by maintaining the displacement angle (phase difference between the inverter input voltage and current) at 180°[7]. The supply power factor can be significantly improved by incorporating the following features in the forced commutated inverter.

1. If we place the fundamental component of the inverter current in the third quadrant with reference to the supply voltage, the active and reactive powers corresponding to the fundamental are returned to the source. Some of the reactive power drawn by the induction motor is supplied by the inverter. The overall reactive power requirement of the drive system is thus reduced. The phasor diagram illustrating stator current, inverter current and resultant supply current is given in Fig.2.2.

2. By operating the forced commutated inverter with multipulse control, the predominant lower order harmonics can be either eliminated or reduced. The harmonic reactive power requirement of the inverter is considerably reduced. The actual control technique adopted for the inverter is described in section 2.4.

The inverter circuit configuration which makes the above features possible is described in the latter portion of this chapter. The static Scherbius scheme of speed control is cost competitive in comparison with a converter-fed dc drive specially when the sub-synchronous speed control is required over a limited range. However a starting mechanism is required before the speed is controlled in the desired range. This is achieved by a starting thyristor in series with a starting resistance as shown by the dotted lines in Fig.2.1. It provides fast start-up of the drive and the device ratings are considerably reduced. No forced commutation circuitry is required for the starting thyristor since line commutation is employed. After the drive has acquired enough speed, the starting thyristor is first commutated and the forced commutated converter is operated in the inverting mode.

2.2 FORCED COMMUTATED INVERTER

The circuit configuration of the forced commutated inverter is shown in Fig.2.3. Since pulse width modulation is used, hereafter the inverter is referred as PWM inverter in the text. T_1-T_6 are turned off by forced commutation. Thyristors T_1,T_3 and T_5 are turned on and off each four times in each half cycle of the respective phase voltage while thyristors T_2,T_4 and T_6 are turned on and off once in each cycle of the respective phase voltage. The trigger pulse layout showing the on intervals of the thyristors T_1 to T_6 is given in Fig.2.4.

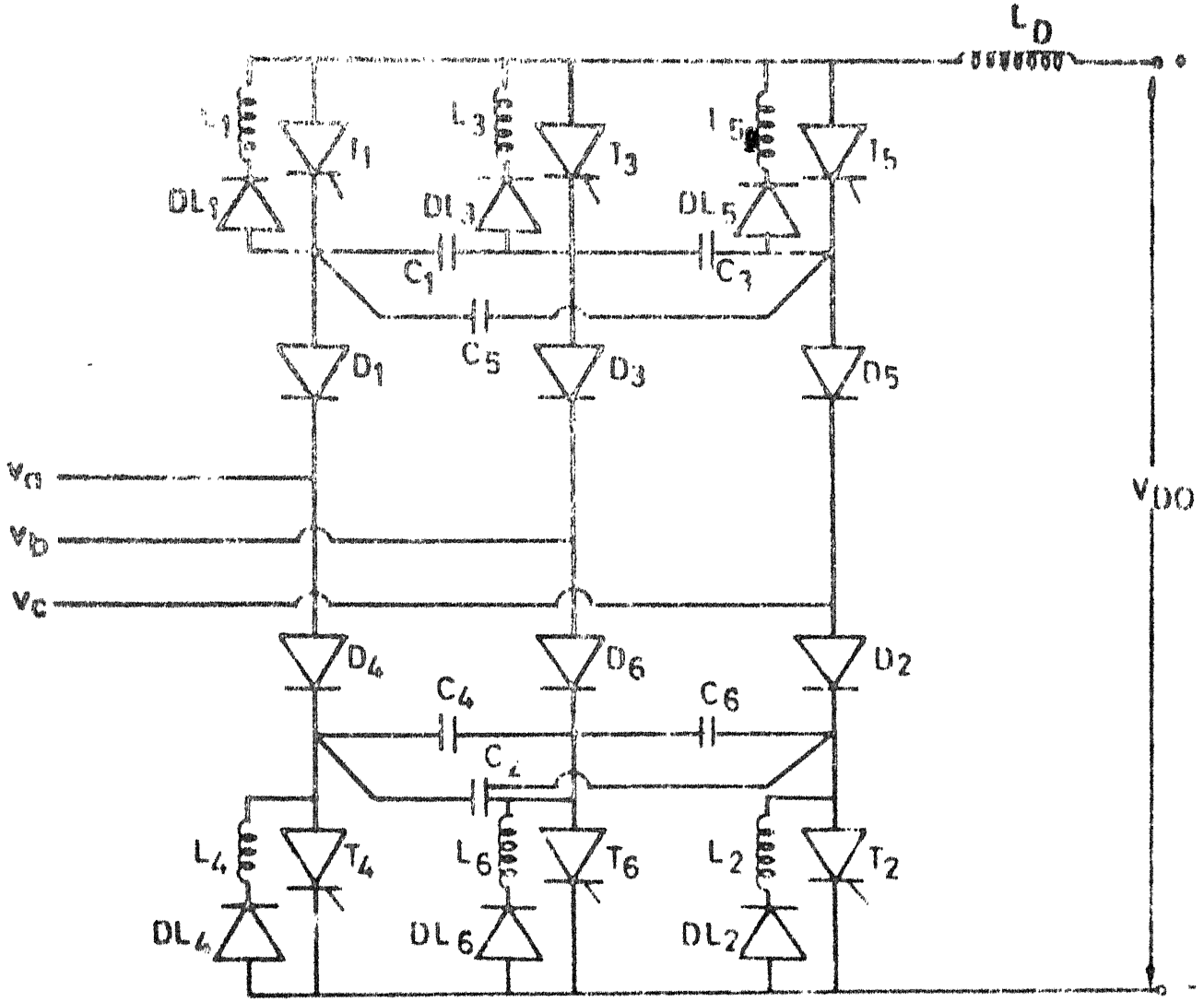

2.3 Circuit configuration of the EPWM inverter

Capacitors C_1-C_6 are used to commutate the thyristors T_1-T_6 respectively. Diodes D_1-D_6 are used to prevent the capacitors from discharging into the load. DL_1,L_1, ... DL_6,L_6 form the local discharging loops which provide quick reversal of capacitor voltages.

In a current source inverter, the commutation capacitors discharge only through the load. Due to almost constant current fed to the inverter, the capacitors also discharge at a constant rate. The capacitor takes more time to recharge in the opposite direction as the capacitance is increased. Thus there is a possibility of commutation overlap which also affects the performance of the inverter due to undesirable modes of operation. Hence to overcome this defect, a local discharging loop consisting of a diode in series with an inductance is connected across each thyristor to quicken the commutation process thereby improving the inverter performance [12].

2.2.1 STARTING PROCESS

The gate pulses for a particular output voltage of the inverter are shown in Fig.2.4, while the pulse for the starting thyristor T_s is shown in Fig.2.9. From Fig.2.4, it can be seen that at the 180° crossing point of each of the phase voltage, the pulse layout of the inverter is such that the counter EMF is negative. But at the instant when next pulse appears, the counter EMF becomes positive which is of right polarity to commutate the starting thyristor. This does not affect the performance of the system because the average back emf across the inverter still remains negative.

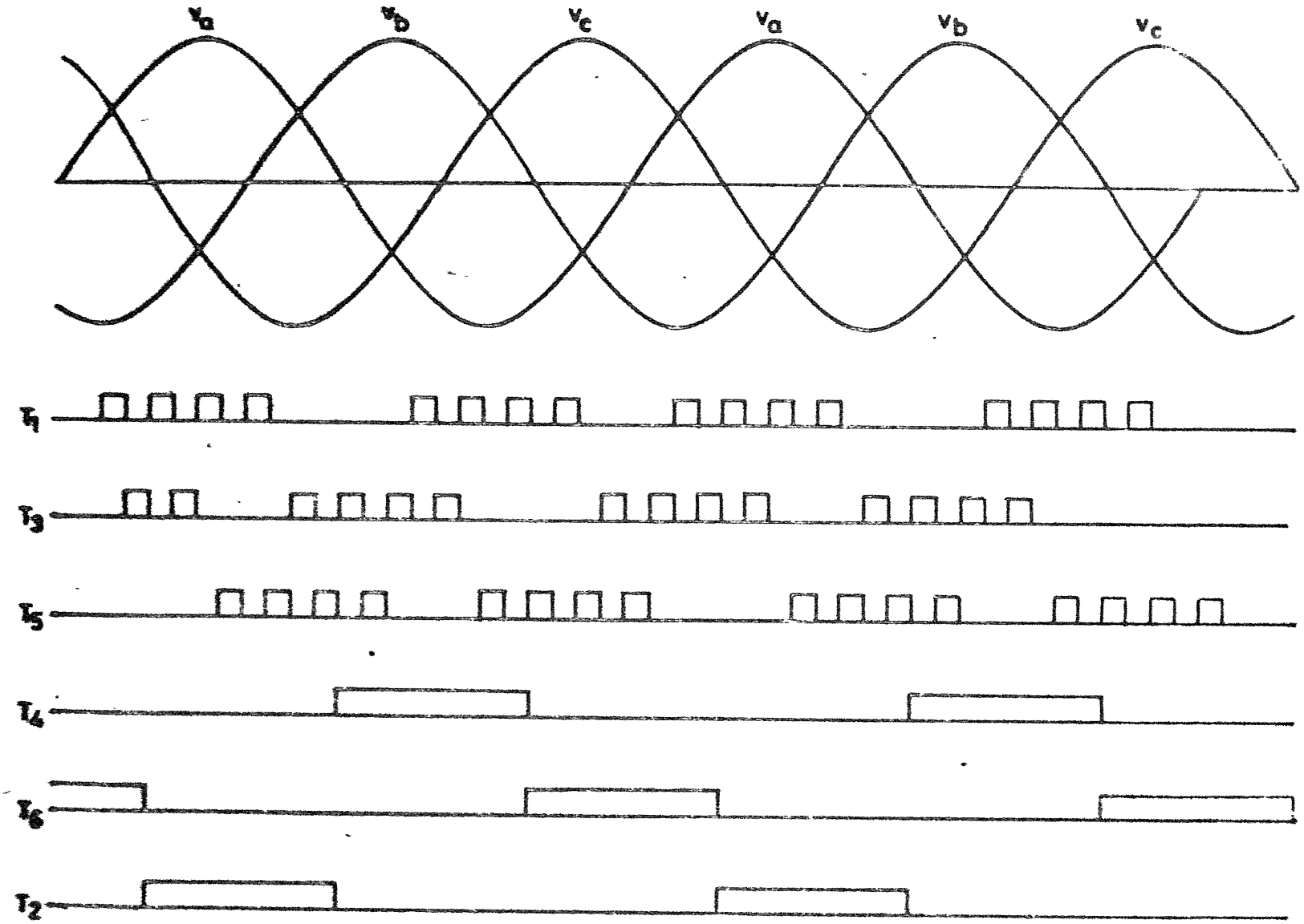

2.4 Pulse layout of the PWM inverter

2.2.2 SPEED AND POWER FACTOR CONTROL

The modulation index in this scheme is defined as the ratio of the on time to one period (1.83 msec). The average counter EMF across the inverter can be varied by changing the modulation index i.e. by varying the on time of the trigger pulses. The speed is thus varied by varying the modulation index. The gate pulses for the thyristors T_2,T_4 and T_6 can be placed anywhere lagging between 180° to 270° points in their respective phase to neutral voltages. The desplacement angle of the inverter can be controlled from $0^{\circ}$to 90° lagging.

2.3 OPERATION OF THE PWM INVERTER

The operation of the inverter is explained with the help of the pulse layout shown in Fig.2.4. The sequence of events start with the triggering of the starting thyristor. The drive starts and after an interval of about 0.1 sec., the trigger pulses to the inverter are activated. The whole operation before the inverter completely takes over after commutating the starting thyristor can be broadly classified into four intervals in the order in which they occur are explained below :

Power interval : In this interval, one thyristor in the top group of thyristors (T_1,T_3 and T_5) and one thyristor in the bottom group of thyristors (T_4,T_6 and T_2) conduct such that the counter EMF of the inverter is negative. Obviously, two

thyristors in the same leg will not conduct. During this interval, apart of the rotor power is being returned to the three phase ac supply system.

Interval for commutation of the starting thyristor : During this interval, the pulses to different thyristors in the inverter are such that its counter emf becomes positive. The starting thyristor is reverse biased and is thus commutated.

Freewheeling interval : During this interval, two thyristors in the same leg of the inverter conduct during which period the counter EMF of the inverter becomes zero.

Commutation interval of bottom group thyristors : In this interval, the thyristor conducting in the bottom group is commutated by turning on another thyristor in the same group. During this period, apart of the rotor power is returned to the three phase ac supply system. This is therefore a power interval.

In what follows, all these intervals are explained with reference to one particular set of thyristors. Depending upon the switching instant of the inverter in the ac supply cycle, the starting thyristor and the inverter may conduct simultaneously before the above intervals take place while commutating the starting thyristor.

From Fig.2.4, it can be seen that the thyristors T_3 and T_4 are triggered at the 180° point of the phase voltage V_A. This makes the inverter back emf negative. Current flows through the path T_3-D_3-V_{ba}-D4-T_4 and feeds ac power to the

supply. The equivalent circuit of the inverter in power interval along with the capacitor voltage polarities is shown in Fig.2.5. The flow of current is shown by the arrows in the figure. At the next instant of trigger pulse layout, thyristor T_5 is triggered, the power interval ends.

As the thyristor T_5 is turned on, the interval for commutation of starting thyristor starts. The full voltage across C_3 will be applied across the thyristor T_3, thus reverse biasing it and turning it off. The capacitor C_3 will start discharging along two paths [12]. One path is T_5-C_3-D3-V_{ba}-D4-T_4-dc supply-T_5. This is the discharging path through the supply. The other path will be the local discharging loop comprising of T_5-C_3-DL_3-L_3-T_5. Diode D3 still conducts and when the voltage across the capacitor C_3 becomes equal to the line voltage V_{bc}, D5 will start conducting. Because of the presence of sufficient inductance at the line, D3 will continue to conduct but current through it will gradually decrease and ultimately D3 will stop conducting. It can be seen from Fig.2.4, that due to the conduction of T_5 and T_4, the back emf across the inverter becomes positive. This helps in the commutation of the starting thyristor T_s and thus the inverter takes over from T_s. Due to the local discharging loop, the charging of the capacitor C_3 in the opposite direction becomes independent of the load current. The equivalent circuit of the interval for commutation of the

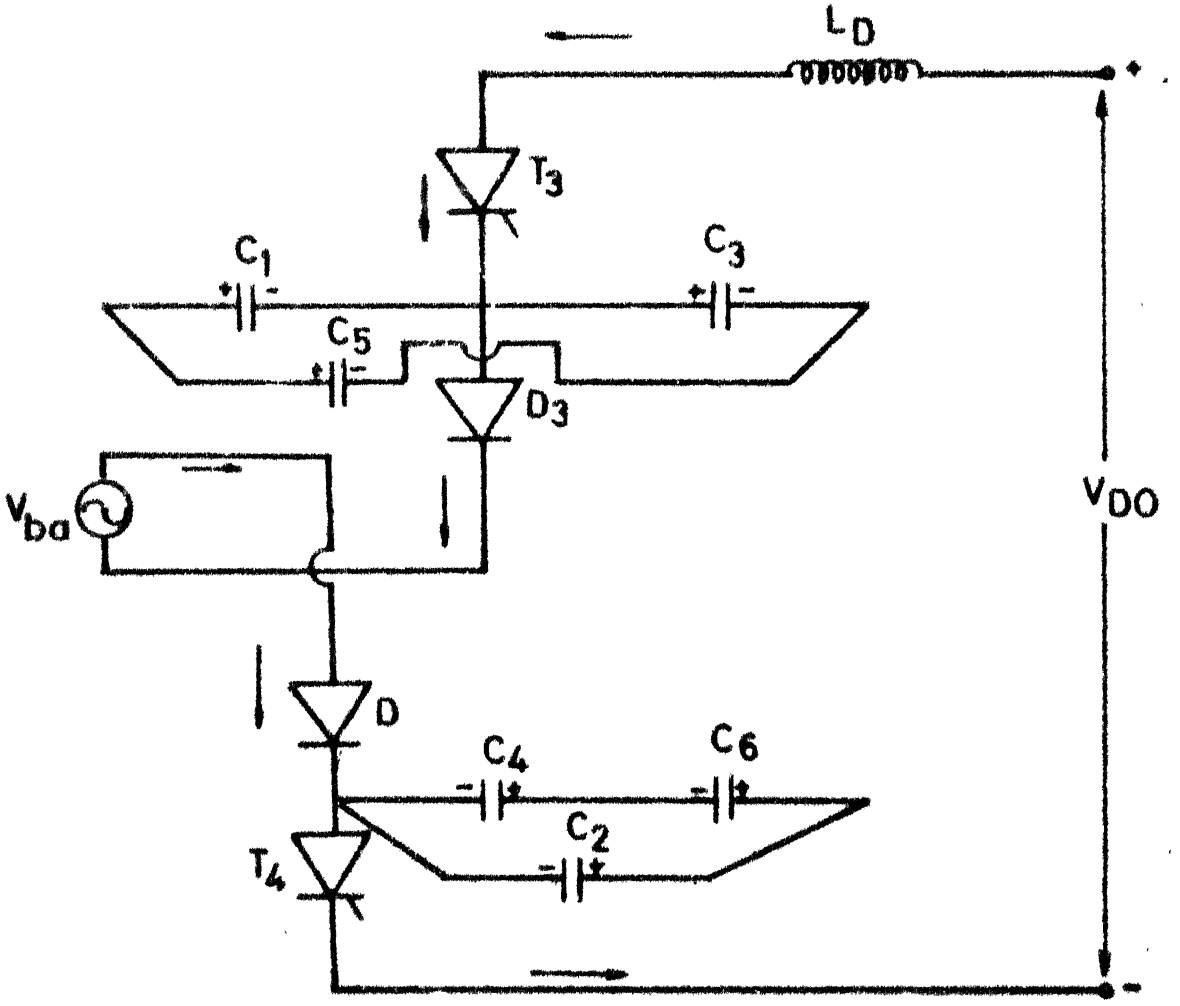

2.5 Equivalent circuit of the duty interval

starting thyristor alongwith the capacitor voltage polarities are shown in Fig. 2.6. At the next instant of the pulse layout, again T_3 is turned on and power interval repeats. At the next instant, T_1 is again turned on and thus free wheeling interval starts.

When T_1 is turned on, the inverter back emf goes to zero. The free wheeling current path is given by T_1-D1-D4-T_4-T_1. Change over of current from D3 to D1 is not instantaneous due to sufficient line inductance. The equivalent circuit of the inverter in the free wheeling mode is shown in Fig.2.7. After this instant, power interval and free wheeling interval repeats alternatively. At the 180° instant of the phase voltage V_b, thyristor T_6 is triggered. This marks the beginning of the interval for change over of thyristors in the bottom half of the inverter.

When T_6 triggers, the full voltage across the capacitor C_4 comes across the thyristor T_4 and turns it off. The capacitor C_4 starts discharging in two directions [12]. One is through the supply consisting of the path T_5-D5-V_{ca}-D4-C_4-T_6-dc supply- T_5. Other path is through the local discharging loop of T_6-DL_4-L_4-C_4-T_6. The transfer of current from D4 to D6 is not instantaneous and when voltage across $C_4 = V_{ab}$, then D6 starts conducting and D4 turns off. The equivalent citcuit at this interval is shown in Fig.2.8.

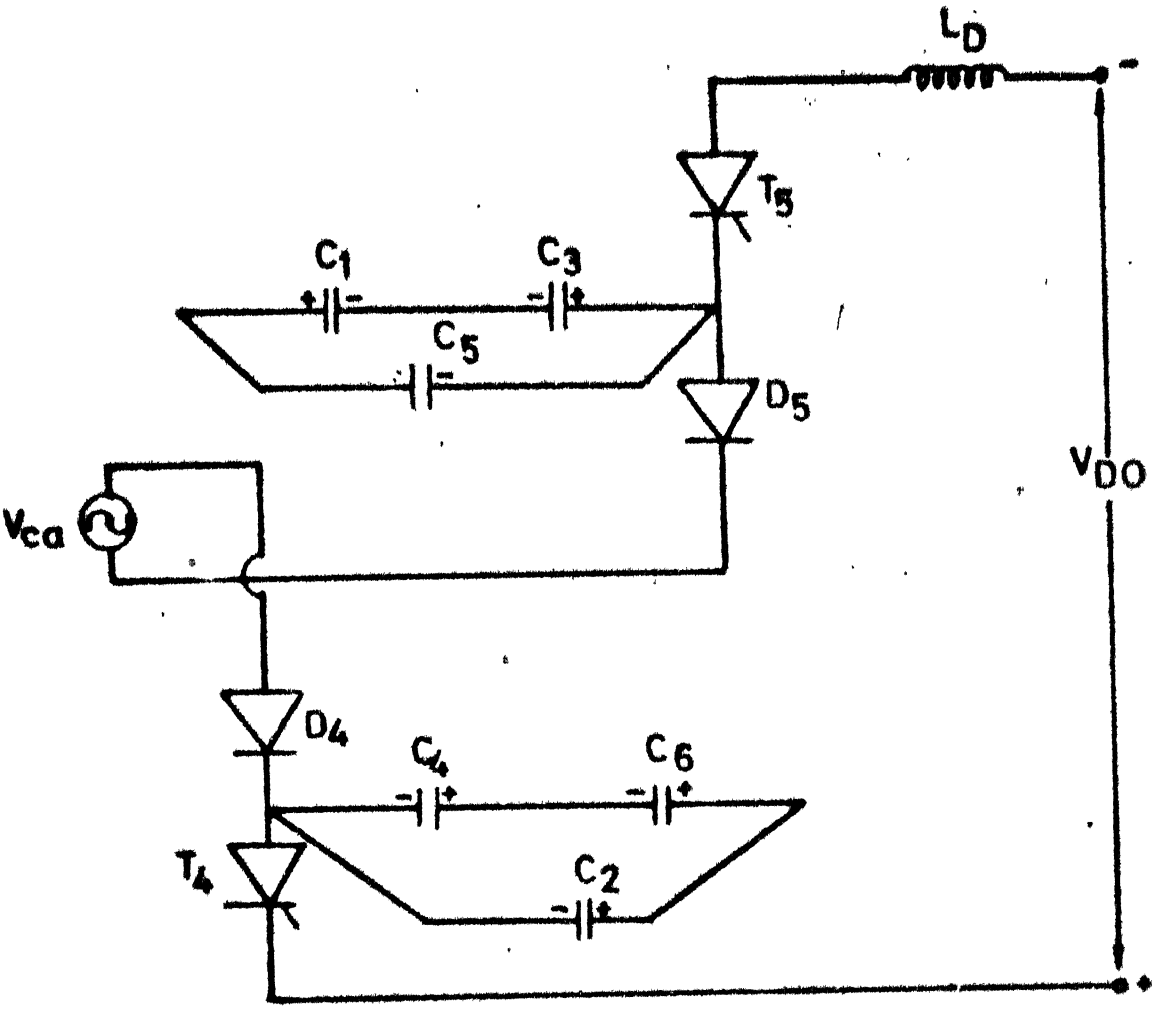

2.6 Equivalent of the interval for commutation of starting interval

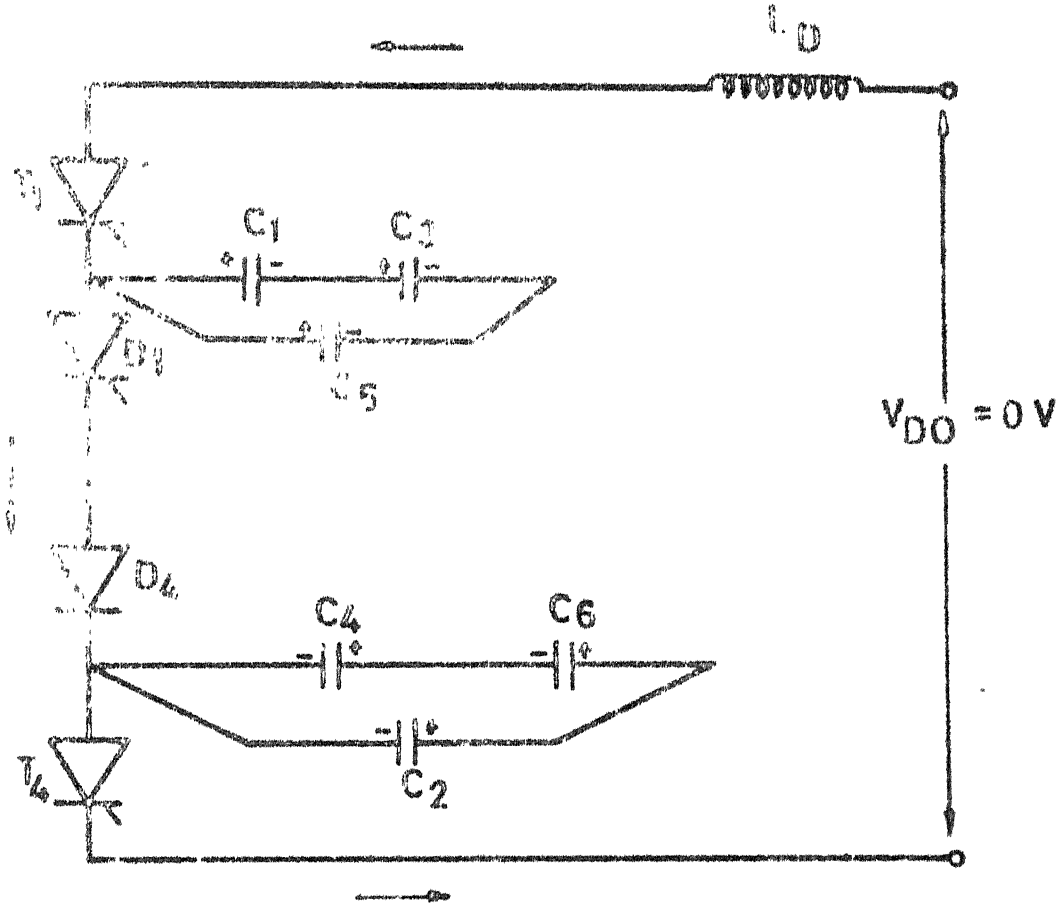

2.7 Equivalent circuit for the freewheeling interval

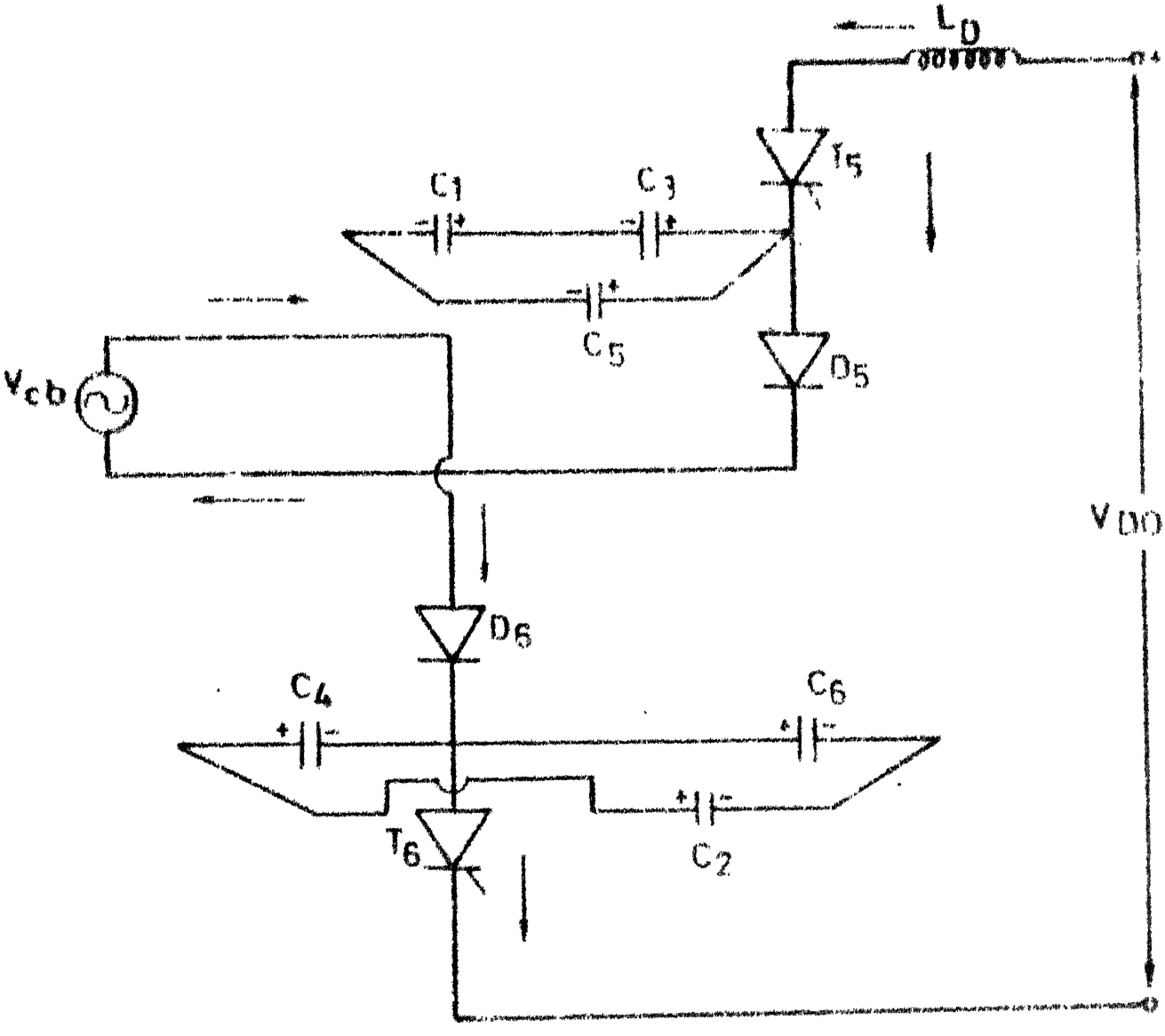

2.8 Equivalent circuit for the interval for the change of bottom group thyristors

2.4 CONTROL CIRCUIT

2.4.1 FIRING CIRCUIT FOR THE STARTING THYRISTOR

The firing circuit for thyristor T_s is shown in Fig. 2.9. The requirement of starting the induction motor to a speed in the control range of the drive system is explained in section 2.2.1. This is important particularly when the speed control is in the subsynchronous speed range. The device ratings are reduced and the whole system may be cost competitive. No additional circuitry is needed to turn off the starting thyristor. The supply voltages are utilized for commutating the starting thyristor.

An RC charging circuit is connected between the supply (+5V) and the ground. The waveforms of voltages at different points are also illustrated. The waveform at point A is fed to a schmitt trigger NOT gate to get a very sharp falling edge as shown at point B. The output at B is given to the monostable 1 the timing of which is adjusted to 5ms. The output of the monostable 1 is used as a trigger pulse for the starting thyristor and its width is adjusted to 5ms. to ensure reliable turn-on. The trigger pulse waveform is shown at C. The output of the schmitt trigger NOT gate B is given to the monostable 2 to provide a delay between the turn on instants of the starting thyristor and the inverter. The total delay of the two monostable stages is kept equal to 0.1 sec. and this is found quite satisfactory. This output is shown in D. The outputs

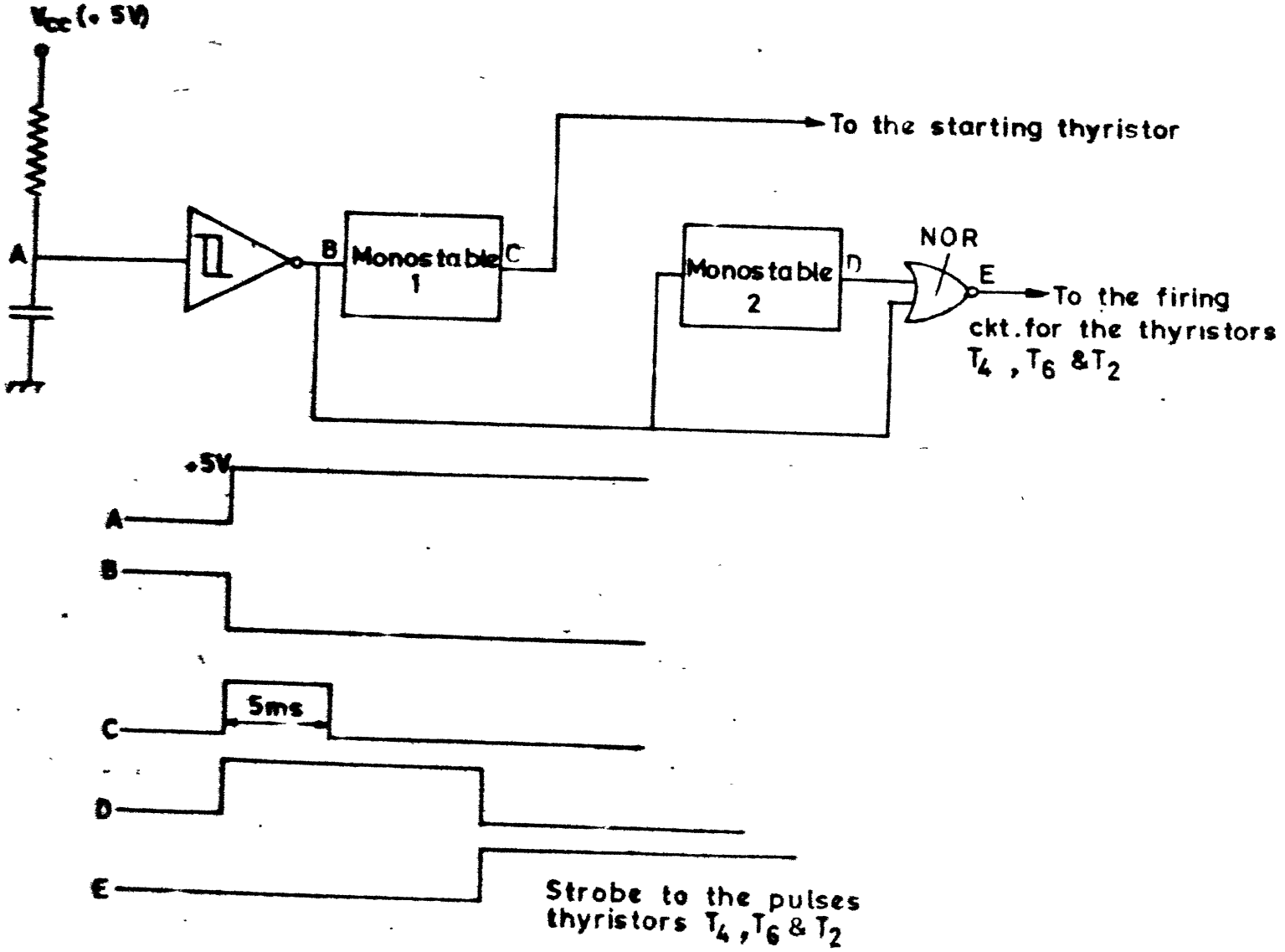

2.9 Control circuit for the starting thyristor and its pulse layout

at B and D are given to a NOR gate, the output of which will act as a strobe for the pulses of the thyristors T_2,T_4 and T_6. This circuit ensures that the starting thyristor is triggered during the initial period of starting. After the inverter is turned on, this circuit becomes inactive. No trigger pulses appear between gate-cathode terminals of the starting thyristor.

2.4.2 CONTROL CIRCUIT FOR THYRISTORS T_1,T_3 AND T_5

In this firing scheme, the number of firing pulses for T_1,T_3 and T_5 are chosen as four/phase/half cycle. The main reason is that in the inverter phase current, the lowest order harmonic present is 7th and all the other predominant harmonics are eliminated. This is theoretically determined and explained in chapter 3. The waveforms at different points of Fig.2.10 are illustrated in Fig.2.11. A synchronising signal A obtained from phase a is transformed into a square-wave B by a zero crossing detector (ZCD). This 50Hz. signal is used as a reference for the phase locked loop(PLL). The PLL output is fed to a divide by 12 counter which is reset at both the positive and negative edges of the ZCD, B by a monostable. This synchronises the signal output of the counter to the line frequency. The output of the PLL is passed through a negative zero crossing detector to obtain a $\pm$ 10V swing, C which is integrated and level shifted to obtain a triangular wave D. The triangular wave is compared with a dc signal X_C.

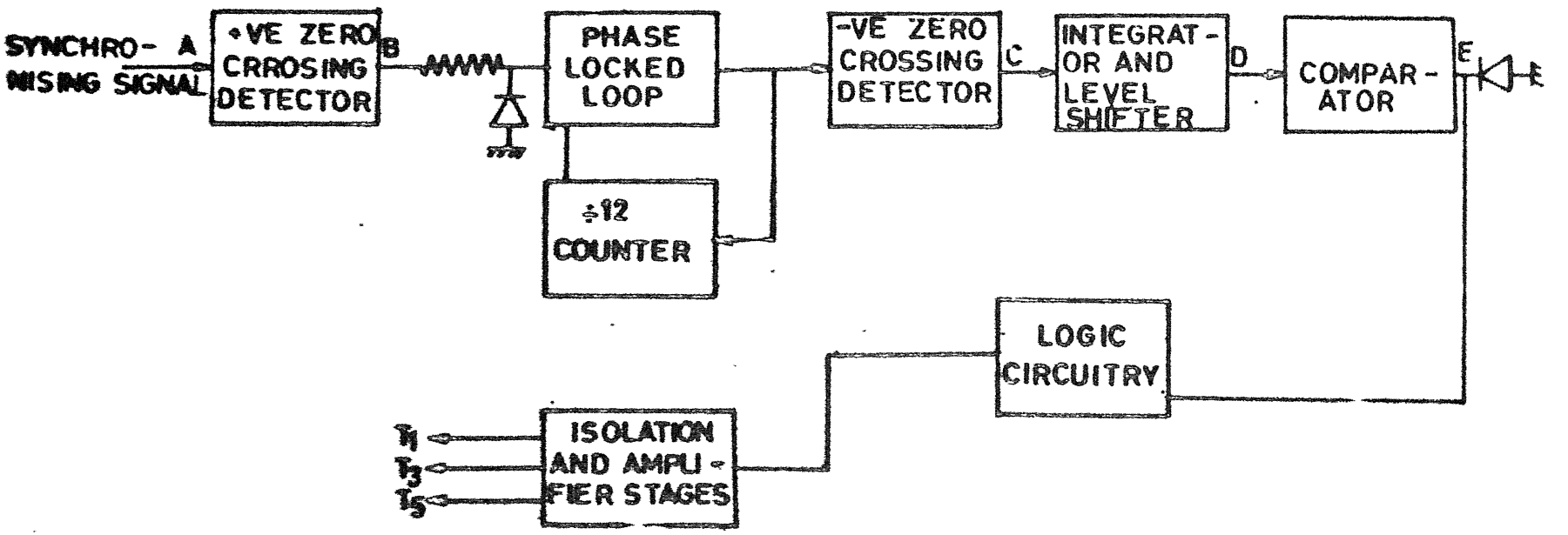

2.10 General block diagram of the control circuit for the thyristors T_1, T_3 and T_5

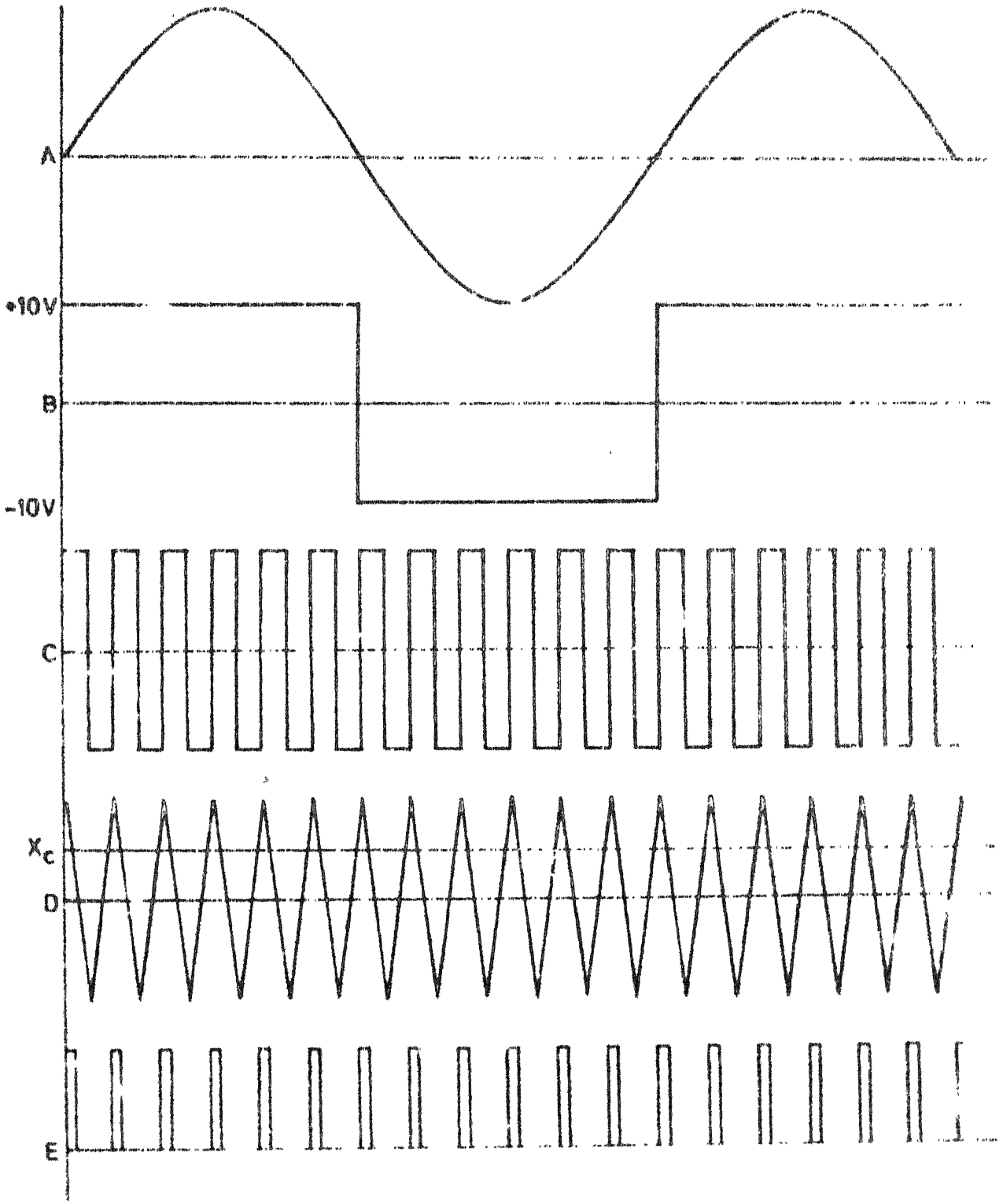

2.11 Wave forms at different stages for the firing CKT in Fig.2.9

The output of the comparator, E is a train of pulses which are to be distributed among T_1,T_3 and T_5 through the logic circuitry. Finally the pulses are passed through isolation and amplifier stages before they are applied to the gates of thyristors, T_1,T_3 and T_5.

2.4.3 CONTROL CIRCUIT FOR THYRISTORS T_4,T_6 AND T_2

The thyristors T_4,T_6 and T_2 are triggered by long pulses of 120° width. The general block diagram of the control circuit and the corresponding waveforms are shown in Figs. 2.12 and 2.13 respectively. The synchronising signal for the comparator stage is taken from the phase a. It is compared with a variable control voltage V_c. A monostable is triggered at the negative edge of the comparator output,C.A JK flip-flop used in the toggle mode divides the line frequency of the comparator output by two giving the waveform, D. The output of the JK flip-flop is given as one of the inputs to the phase comparators of the PLL. The PLL together with a divide by 12 counter achieves frequency multiplication. The VCO output of the PLL, E is 6 times the supply frequency. A pulse identified as the first pulse out of the six pulses has its positive edge coincident with the monostable output. Hence if the monostable output is given as the serial input to a 8 bit shift register and the VCO output of the PLL as its clock pulse, the first output of the shift register, F will shift with the variation of the control voltage. In this way,

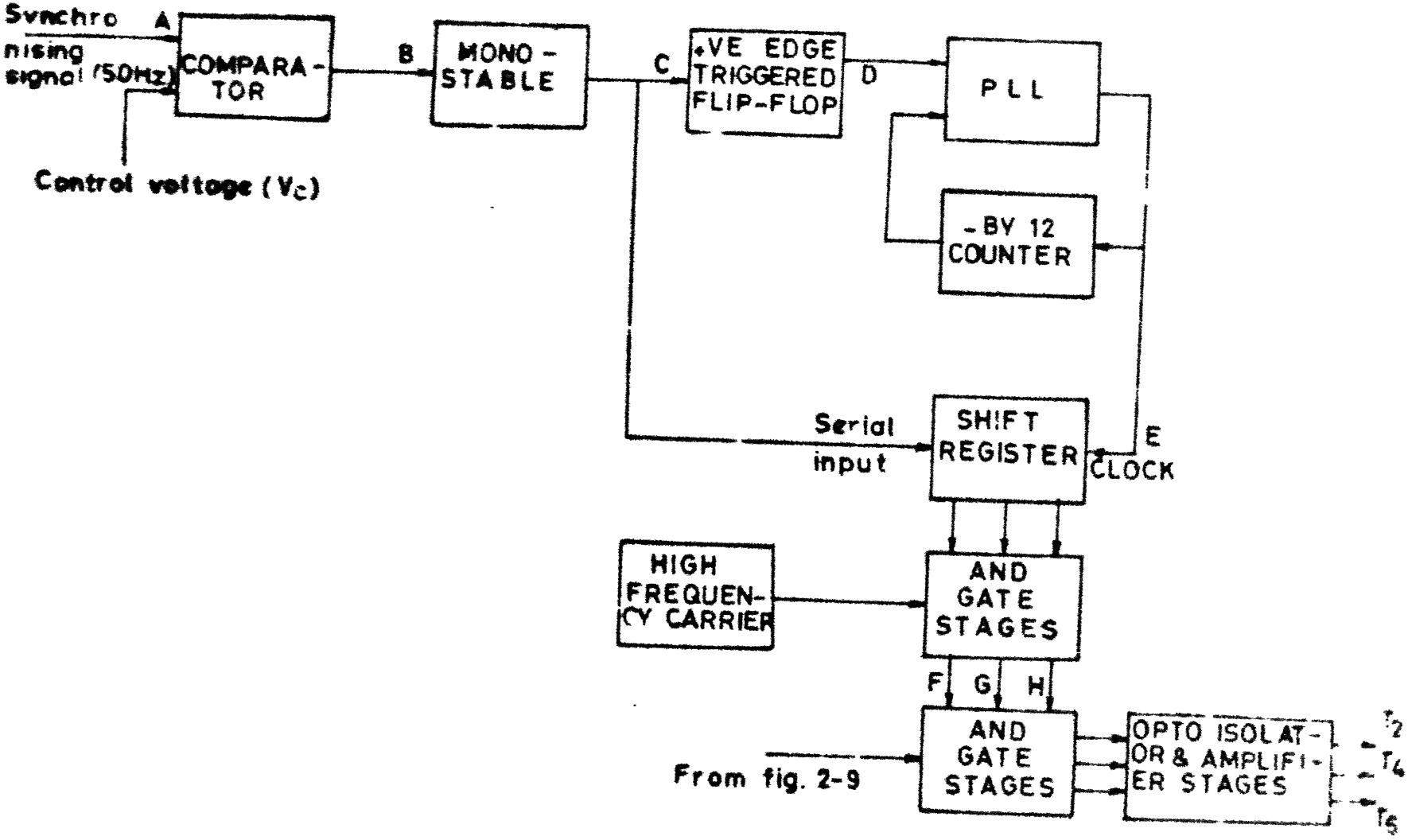

2.12 General block diagram of the control circuit for the thyristors T_2, T_4 and T_6

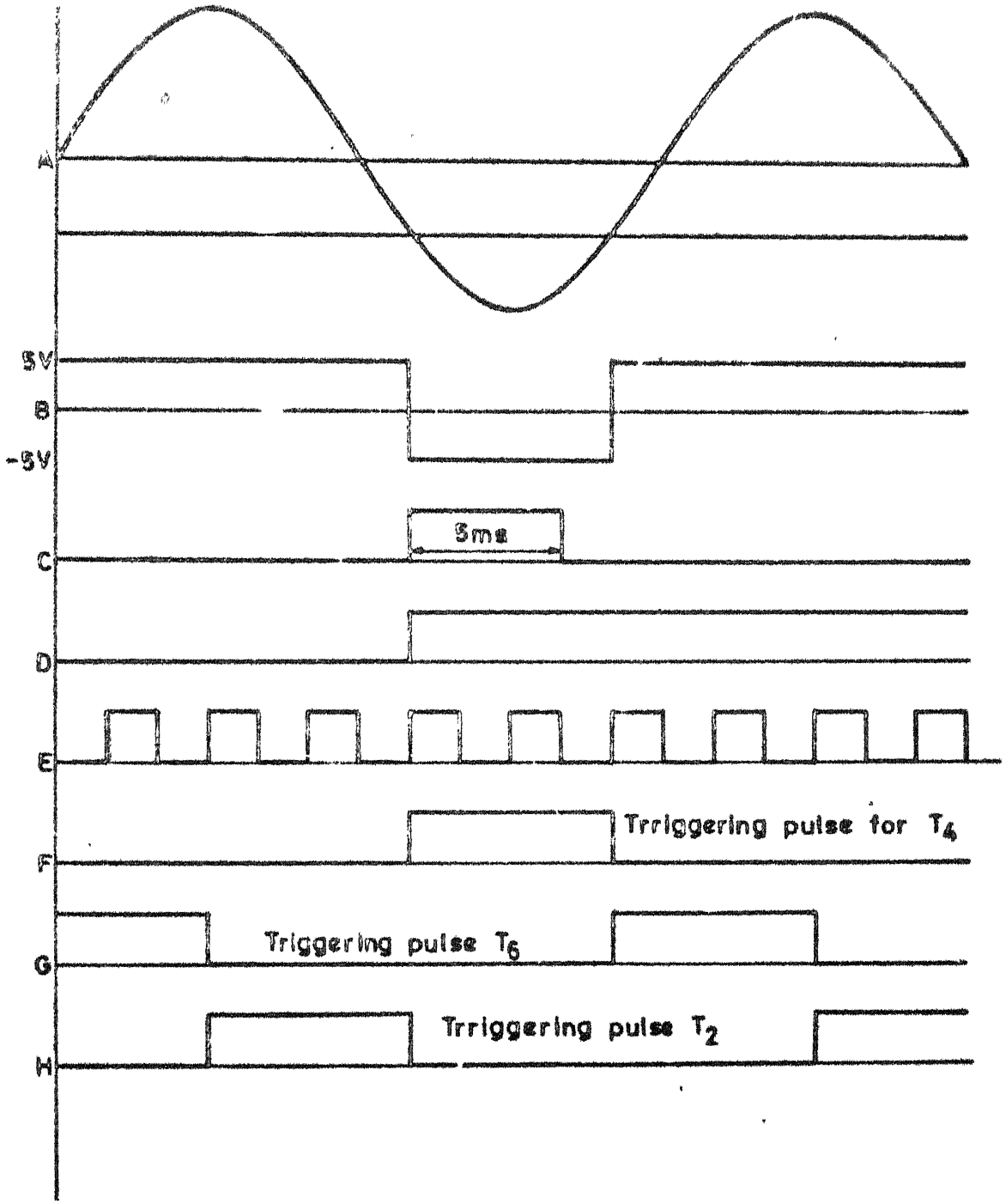

2.13 Wave forms at different stages for the firing circuit in Fig.2.12

the power factor of the inverter is controlled. Since phases b and c are shifted by 120° with respect to the phase a, so the third, g and fifth, H output of the shift register is taken as the triggering pulses for the thyristors in phases b and c respectively. They will also shift with the variation of the control voltage as in the case of first output of the shift register. The width of each pulse is 120° and this is achieved by making the width of the monostable output, C wider than one clock period. The outputs of the shift registers are ANDed with high frequency carrier and it is also ANDed with the strobe which is coming from the output stage of the control circuit for the starting thyristor, to ensure that the motor does not start through the inverter. The pulses are placed through isolation and amplifier stages and then applied to the gates of thyristors T_4, T_6 and T_2.

CHAPTER 3

STEADY STATE PERFORMANCE CHARACTERISTICS OF SLIP POWER RECOVERY SCHEME EMPLOYING PWM CONVERTER IN THE ROTOR CIRCUIT

3.1 INTRODUCTION

For slip ring induction motor with slip power recovery method of speed control, exact analysis is tedious, involving phasor calculations for motor fundamental and harmonic quantities and step by step analysis of the rectifier and inverter circuits.

The main problem in modelling and analysis of the drive system is that the phase of the voltage at the rotor terminals or the input to the diode bridge rectifier is not known. This problem is avoided by transferring the ac portion of the system to the dc side and accordingly dc equivalent circuit [7] can be developed. Using this model, we can study the torque-speed characteristics. In order to study the performance characteristics in the ac side, an ac equivalent circuit would be useful. In this method, the effect of the inverter is to generate a counter EMF opposing the rectified rotor EMF specially in the subsynchronous speed range. In fact, Lavi and Polge [4] have modelled and analysed the slip power recovery scheme using this concept. The same approach is followed for determining the supply performance.

3.2 DC EQUIVALENT CIRCUIT

Representing the induction motor by its approximate equivalent circuit and assuming that the no load current of the induction motor to be small in comparison with the primary current, the system can be represented by Fig.3.1(a) and is reduced to Fig.3.1(b) by transferring the stator impedance to the rotor side.

To transfer all the parameters to the dc side, the ac side resistance can be transferred to the dc side by power balancing. Assuming dc link current to be perfectly constant, the rotor current consists of alternate square pulses of $2\pi/3$ radians duration as shown in Fig.3.2(a). Fourier analysis of the rotor current gives,

$$I_2 = \sqrt{\frac{2}{3}}\, I_D \qquad \ldots\ (3.1)$$

$$I_{21} = \frac{3}{\pi}\, I_2 \qquad \ldots\ (3.2)$$

Hence, $3\, I_2^2\, R_{ac} = I_D^2 \cdot R_{dc}$, where R_{ac} is the total resistance referred to the rotor and R_{dc} is the ac side resistance when reflected to the dc side.

Due to the presence of the leakage reactances sX_1' and sX_2, the commutation of current between the diodes in the rectifier bridge is not instantaneous. There is an overlap period during which two phases conduct simultaneously. This causes a reduction in the output voltage by an amount given by $3s\,(X_1' + X_2)\cdot I_D/\pi$ [13] and the average output voltage of the diode bridge can be easily shown to be, $V_D = \frac{3\sqrt{6}}{\pi}\, sV/a$.

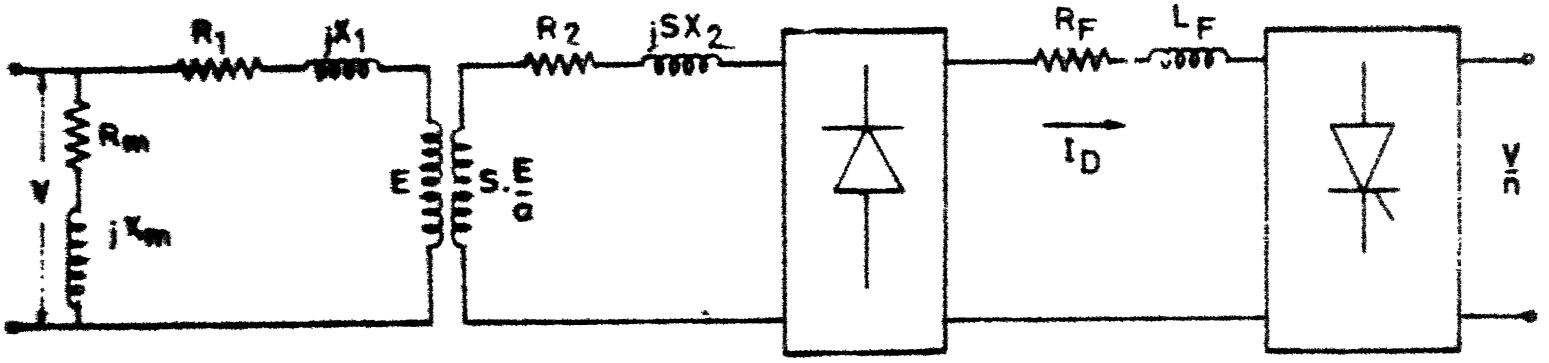

3.1(a) Representation of the drive system

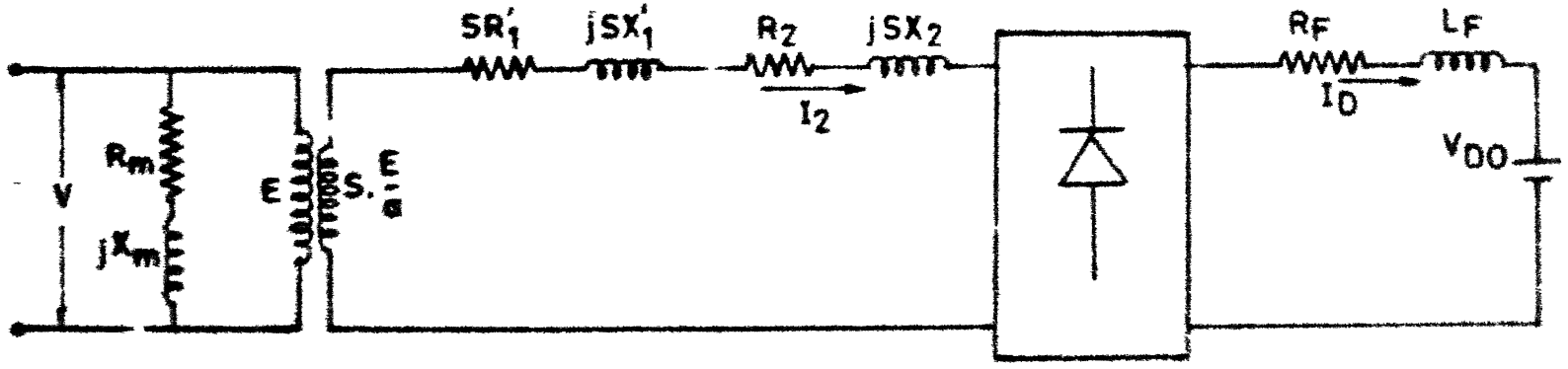

3.1(b) Representation of drive system by transferring the stator impedances to the rotor side

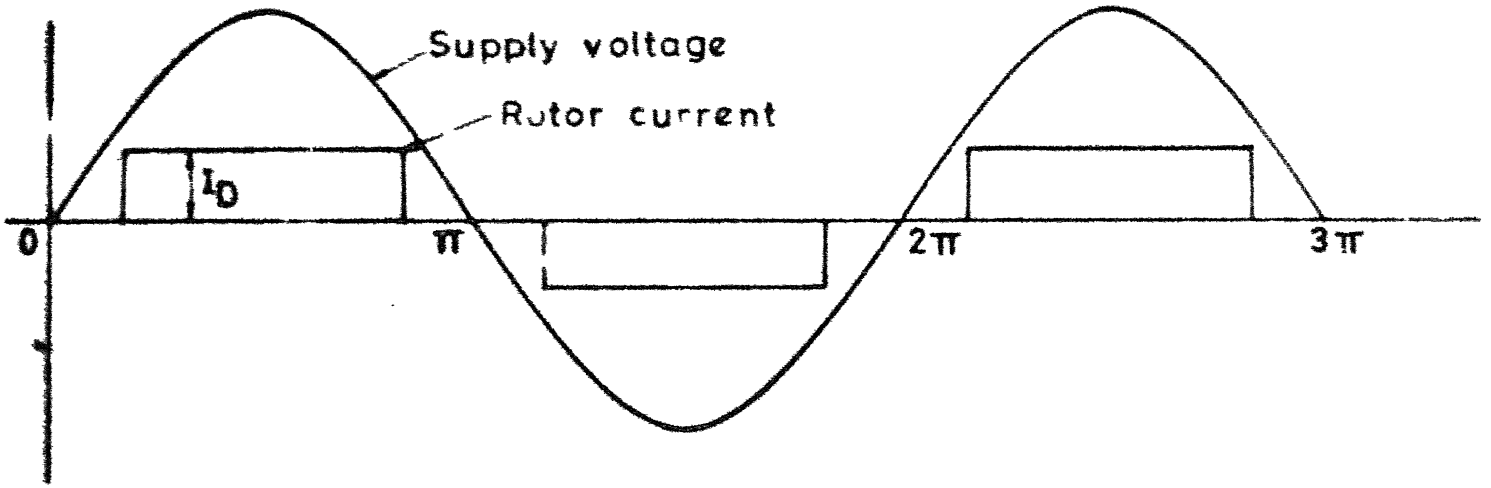

3.2(a) Rotor voltage and current

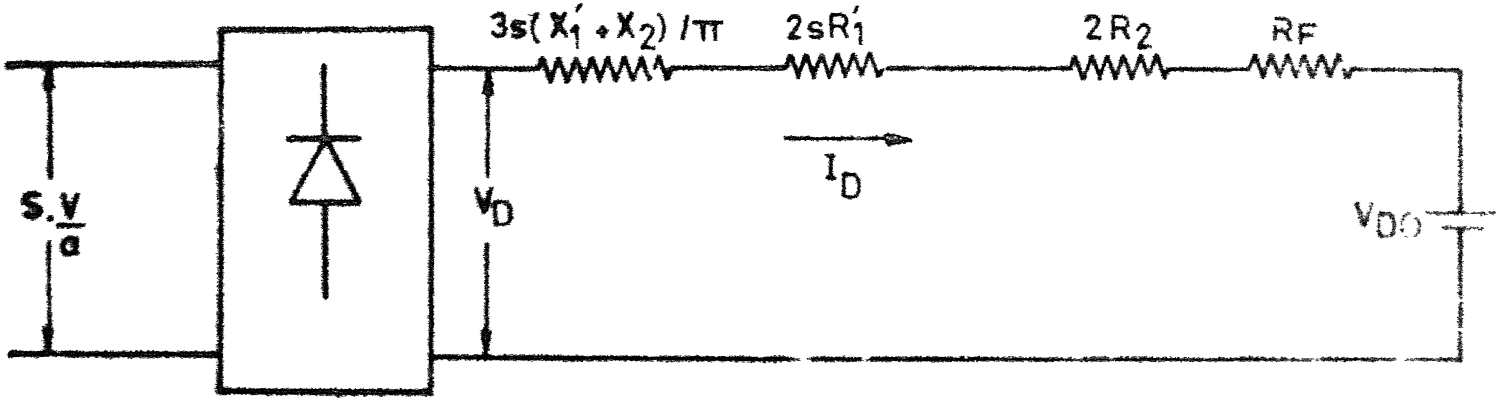

3.2(b) Derivation of DC equivalent circuit

If the magnetising current is neglected, the system can be represented by the dc equivalent circuit as shown in Fig. 3.2(b). Filter inductance L_F is not included because I_D is assumed to be perfectly constant and the circuit is considered to be in steady state only.

The output voltage of the inverter depends upon the pulse layout to the gate of thyristors T_1 to T_6. For a given modulation index, the output voltage waveform mainly depends upon the phase shift provided to the bottom group thyristors, T_4,T_6 and T_2. It was explained in Sec. 2.2.2 that the trigger pulses to thyristors T_4,T_6 and T_2 are controlled from 180° to 270° of the respective phase voltages. An examination of the output voltage waveform indicates that there are three distinct ranges as the phase shift is varied from 0° to 90°. These are : 0° to 30°, 30° to 60° and 60° to 90°. Typical waveforms of the output voltage of the inverter for a particular modulation index and a particular phase shift in each range are illustrated in Fig. 3.3 to 3.5. Since the waveforms repeat after every 360°, a full cycle must be taken into account while determing the average output voltage. The expressions for the output voltage in the three ranges are given in Appendix A. Equations (A.1), (A.2) and (A.3) are used to calculate the output voltage of the inverter. The variation of the average output voltage vs. speed for different values of the modulation index is shown in Fig.3.6.

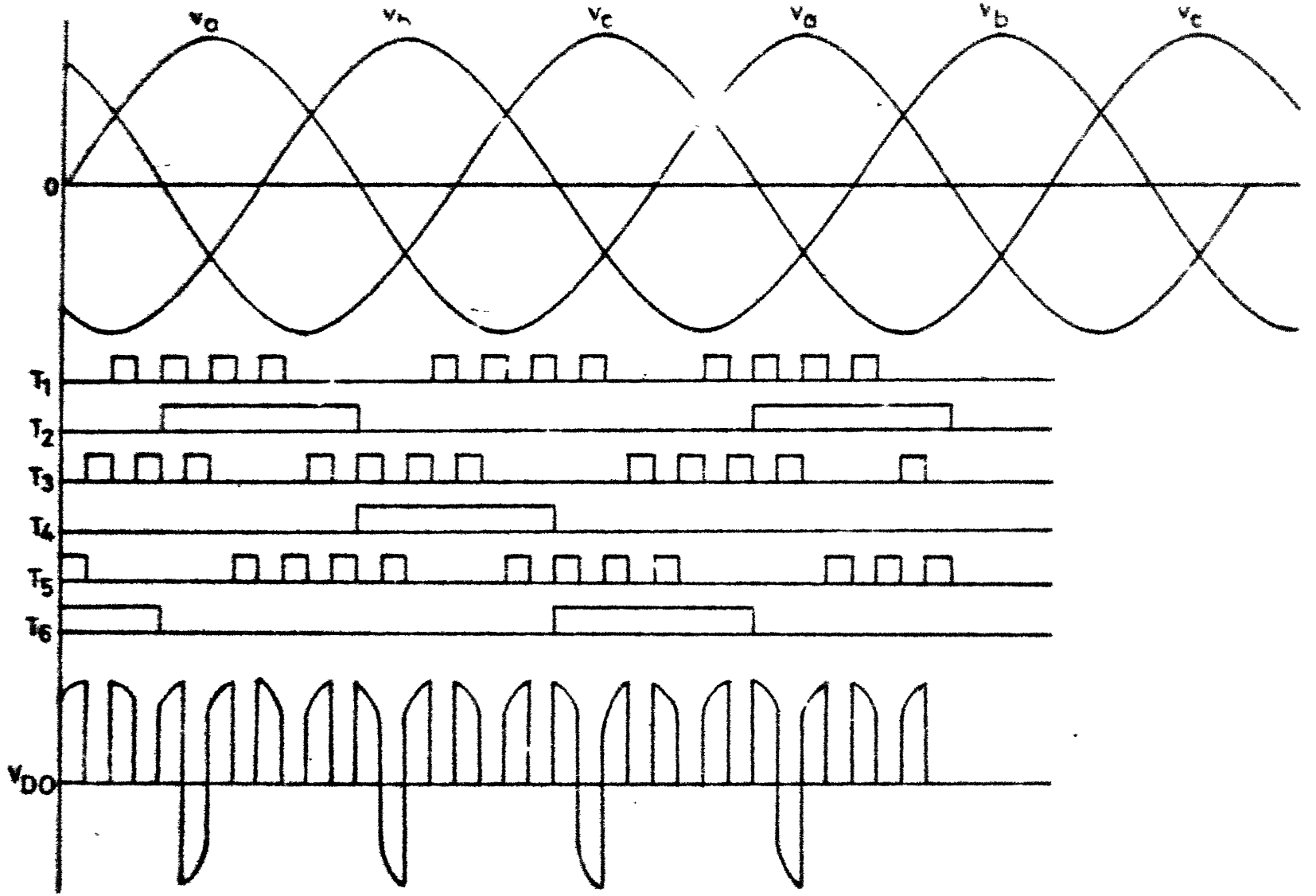

3.3 Pulse layout and the inverter counter EMF for the phase shift angle 0-30 degrees

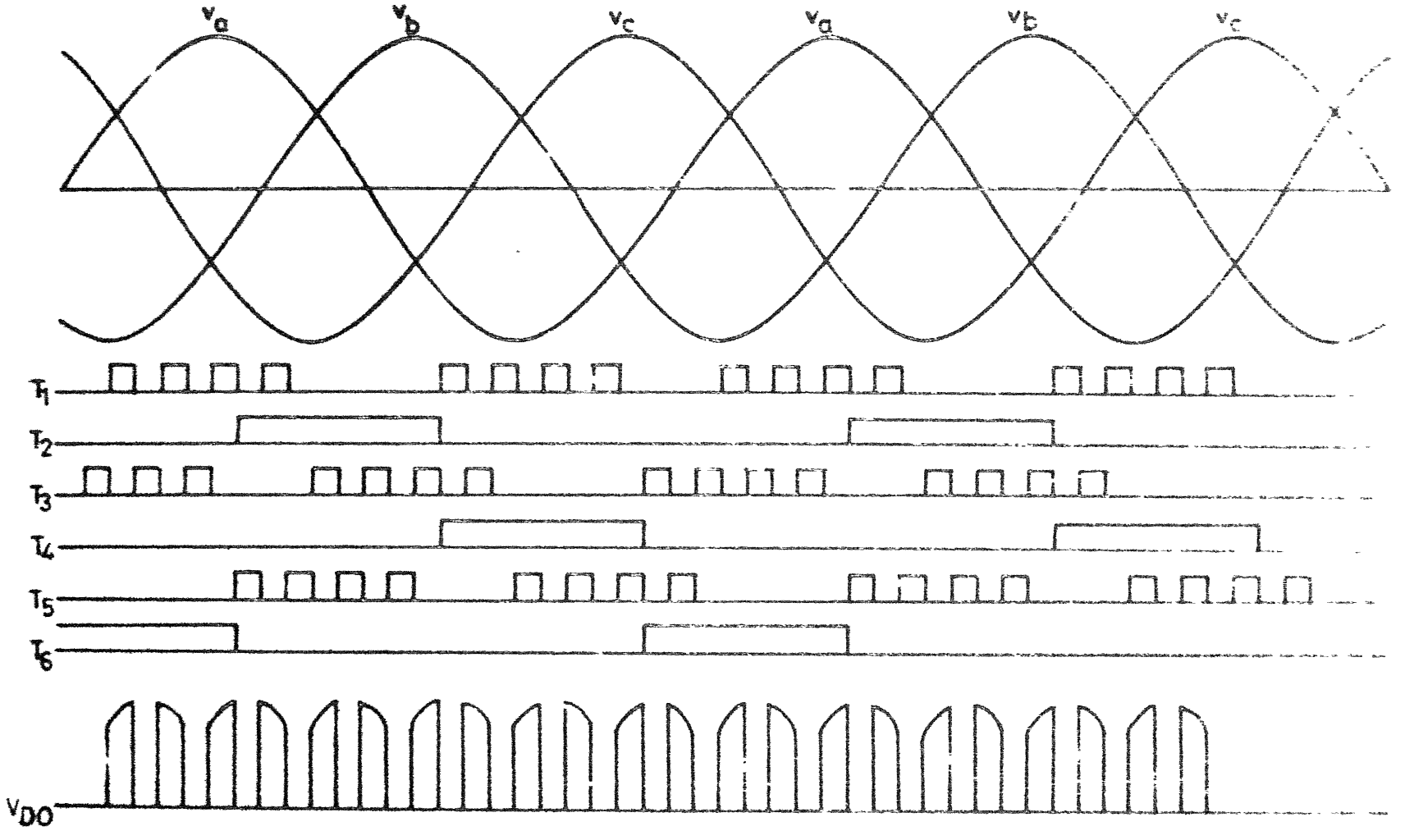

3.4 Pulse layout and the inverter counter EMF for the phase angle 30-60 degrees

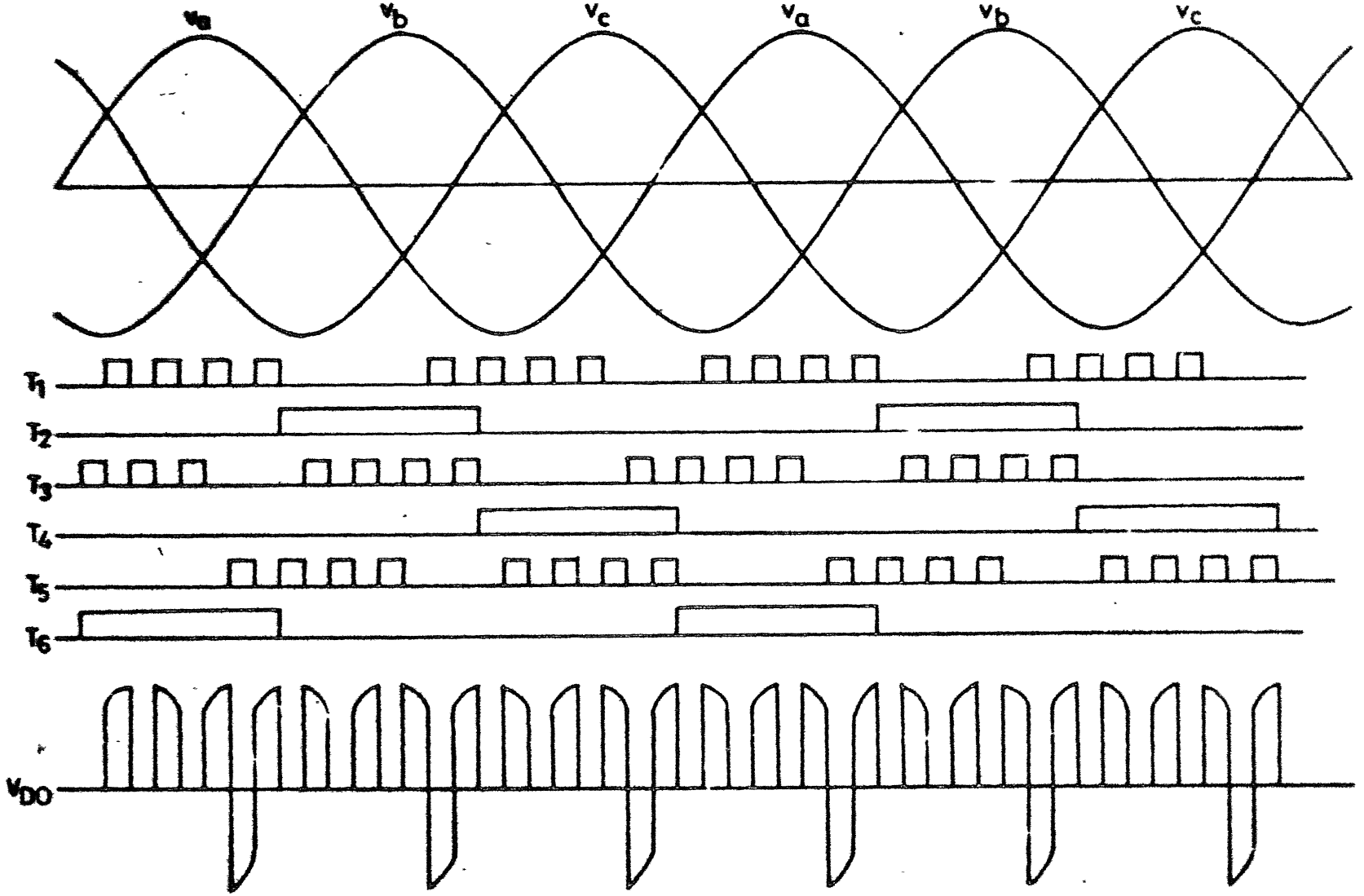

3.5 Pulse layout and the inverter counter EMF for the phase angles of 60-90 degrees

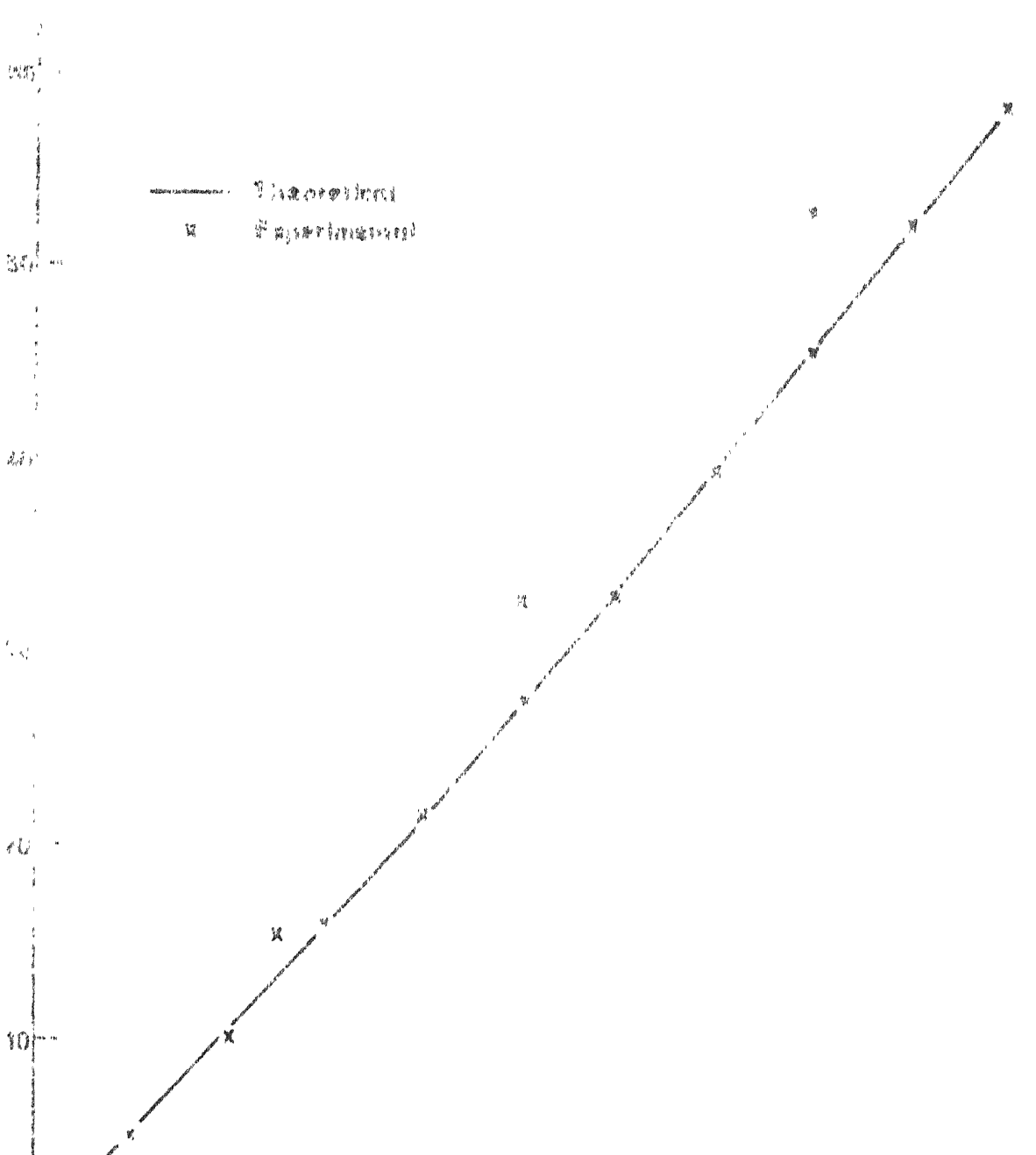

3.6 Inverter counter EMF vs. modulation index for a transformer turns ratio of 10:1

Thus from the dc equivalent circuit of Fig. 3.2(b), we get

$$V_D - \frac{3}{\pi} s\,(X_1' + X_2).\, I_D - I_D\,(2sR_1' + 2R_2 + R_F) - V_{DO} = 0$$

$$\text{or } I_D = \frac{V_D - V_{DO}}{\frac{3}{\pi}s\,(X_1' + X_2) + (2sR_1' + 2R_2 + R_F)} \qquad \ldots\ (3.3)$$

Let $\frac{3}{\pi}s\,(X_1' + X_2) = X_C$

$$\text{Therefore, } I_D = \frac{V_D - V_{DO}}{X_C + 2sR_1' + 2R_2 + R_F} \qquad \ldots\ (3.4)$$

The variation of the link current with speed is shown in Fig.3.7 using equation 3.4. The experimental values are also indicated in the same figure.

To derive the torque-speed characteristics, it is assumed that the torque produced by the harmonics is negligibly small. Lavi and Polge [4] has confirmed the validity of this assumption experimentally and theoretically.

From Fig. 3.2(b), rotor power $= [V_D - \frac{3}{\pi}s(X_1'+X_2).I_D - 2sR_1'.I_D]I_D$

$$\text{Therefore, Torque } T = \frac{[V_D - \frac{3}{\pi}s\,(X_1'+X_2).I_D - 2sR_1'.I_D].I_D}{s.w_s} \qquad \ldots\ (3.5)$$

Thus for a given slip and the modulation index of the inverter, I_D and T can be calculated by using equations 3.4 and 3.5, from which the speed-torque characteristics for different values of the modulation index can be determined. These are shown in Fig.3.8. The experimental values are also marked on the theoretically computed curves. There is a good agreement between theoretical and experimental results.

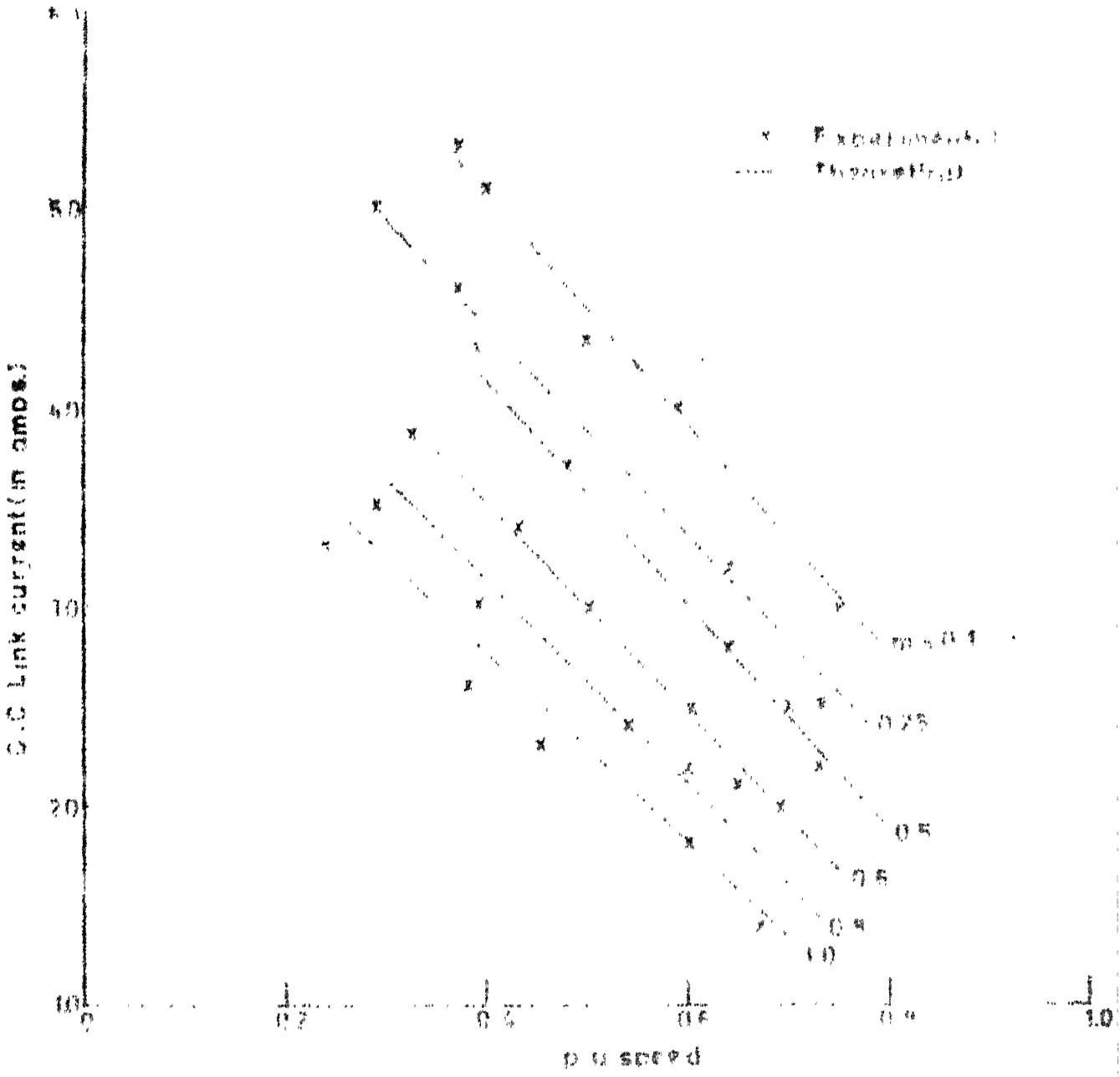

3.7 DC link current vs. speed for different values of modulation index

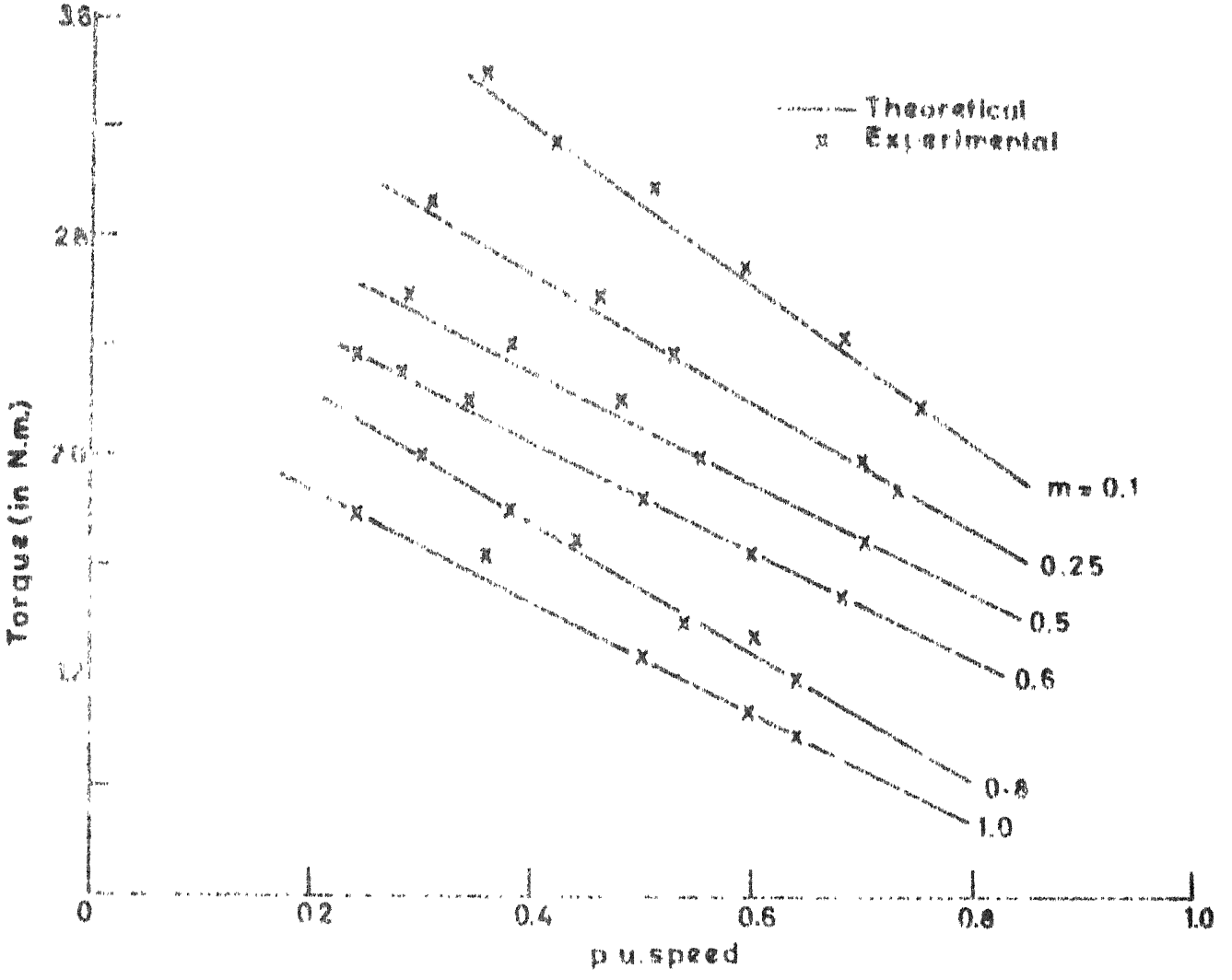

3.8 Torque vs. speed characteristics for different values of modulation index

3.3 AC EQUIVALENT CIRCUIT

The concept of the ac equivalent circuit is described in [4,14]. Writing the power balance equations for the rotor circuit, an ac equivalent circuit can be developed for the prediction of the steady state performance. The power loss in the dc side of the rectifier bridge, when reflected to the ac side and considered for each phase, is $\frac{I_D^2 \cdot R_F}{3}$. The expression relating power balance in each phase is,

$$E_2 I_{21} \cos\theta_{21} = \frac{R_F \cdot I_D^2}{3} + I_2^2 \cdot R_2 + P_{mech} + \frac{V_{DO} \cdot I_D}{3} \quad \ldots\ldots \quad (3.6)$$

Substituting $I_D = \sqrt{\frac{3}{2}}\, I_2$ in equation 3.6, we get

$$E_2 I_{21} \cos\theta_{21} = I_2^2 \left(R_2 + \frac{R_F}{2}\right) + P_{mech} + \frac{V_{DO} \cdot I_D}{3} \quad \ldots\ldots \quad (3.7)$$

Assuming that the mechanical torque developed by the fundamental component of the rotor current, P_{mech} is given by,

$$P_{mech} = \left[I_{21}^2 \left(R_2 + \frac{R_F}{2}\right) + \frac{V_{DO} \cdot I_D}{3} \right] \left(\frac{1}{s} - 1\right) \quad \ldots\ldots \quad (3.8)$$

Substituting the value of P_{mech} from equation 3.8 into equation 3.6 and using the relation $I_{21} = \frac{3}{\pi} I_2$, we get

$$E_2 I_{21} \cos\theta_{21} = \left(\frac{R_F}{2} + R_2\right) \cdot I_{21}^2 \cdot \left(\frac{\pi^2}{9} - 1\right) + \left(\frac{R_F}{2} + R_2\right) \cdot \frac{I_{21}^2}{s} + \frac{3\sqrt{6}}{\pi} \cdot \frac{V_{DO}}{s} \cdot I_{21} \quad \ldots\ldots \quad (3.9)$$

$$= R_X \cdot I_{21}^2 + \frac{R_y \cdot I_{21}^2}{s} + \frac{\pi}{3\sqrt{6}} \cdot \frac{V_{DO}}{s} \cdot I_{21} \quad \ldots\ldots \quad (3.10)$$

where $R_X = \left(R_2 + \frac{R_F}{2}\right) \left(\frac{\pi^2}{9} - 1\right)$ and $R_y = R_2 + R_F/2$

Considering the L.H.S. of equation 3.10, the first term represents the loss due to harmonics in the process of rectification, the second term gives the copper loss in the rotor and filter resistances and the third term accounts for the power returned to the ac supply source.

Equation 3.10 can be translated into an equivalent circuit as shown in Fig.3.9 referring all the quantities to the stator side. The phasor diagram for the corresponding circuit is shown in Fig.3.10. Both active and reactive powers corresponding to the fundamental component of the inverter current are returned to the supply source through the PWM inverter. In the ac equivalent circuit of Fig.3.9, the rotor fundamental current flowing through the inverter counter emf accounts for the active power being returned to the source, while the block connected to the supply terminals draws the reactive component of the inverter current. Since this component leads the supply voltage by 90^{o}, the net effect is to return the reactive power to the supply. This scheme of speed control in comparison with the reported schemes [4,5,6,9,10], provides significant improvement in the overall power factor. This is also confirmed experimentally as explained in section 3.3.2.

3.3.1 CALCULATION OF THE FUNDAMENTAL COMPONENT OF THE INVERTER CURRENT

The supply voltages to the inverter and the current in phase a are shown in Fig.3.11. The current on the dc side of the inverter is assumed to be constant.

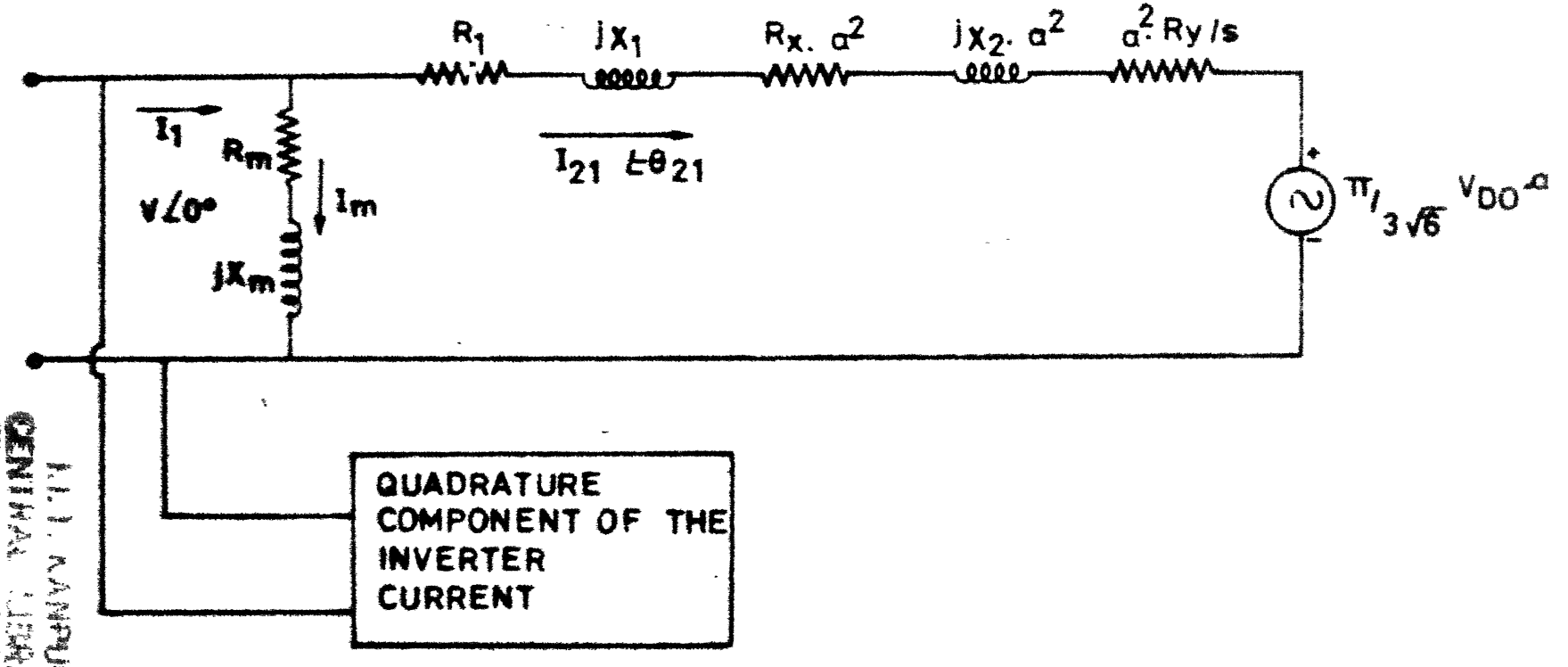

3.9 AC equivalent circuit referred to the stator

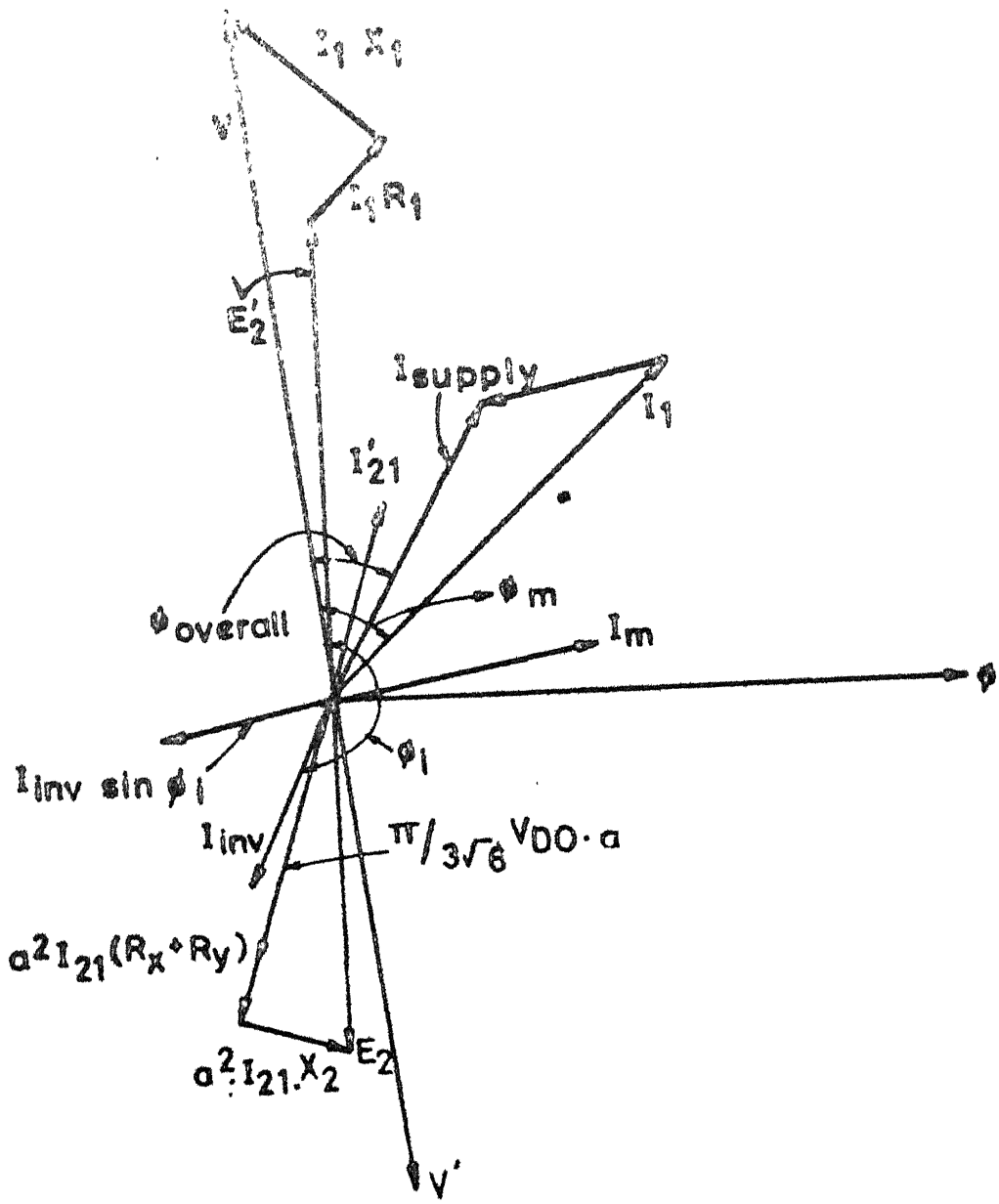

3.10 Phasor diagram of the AC equivalent circuit

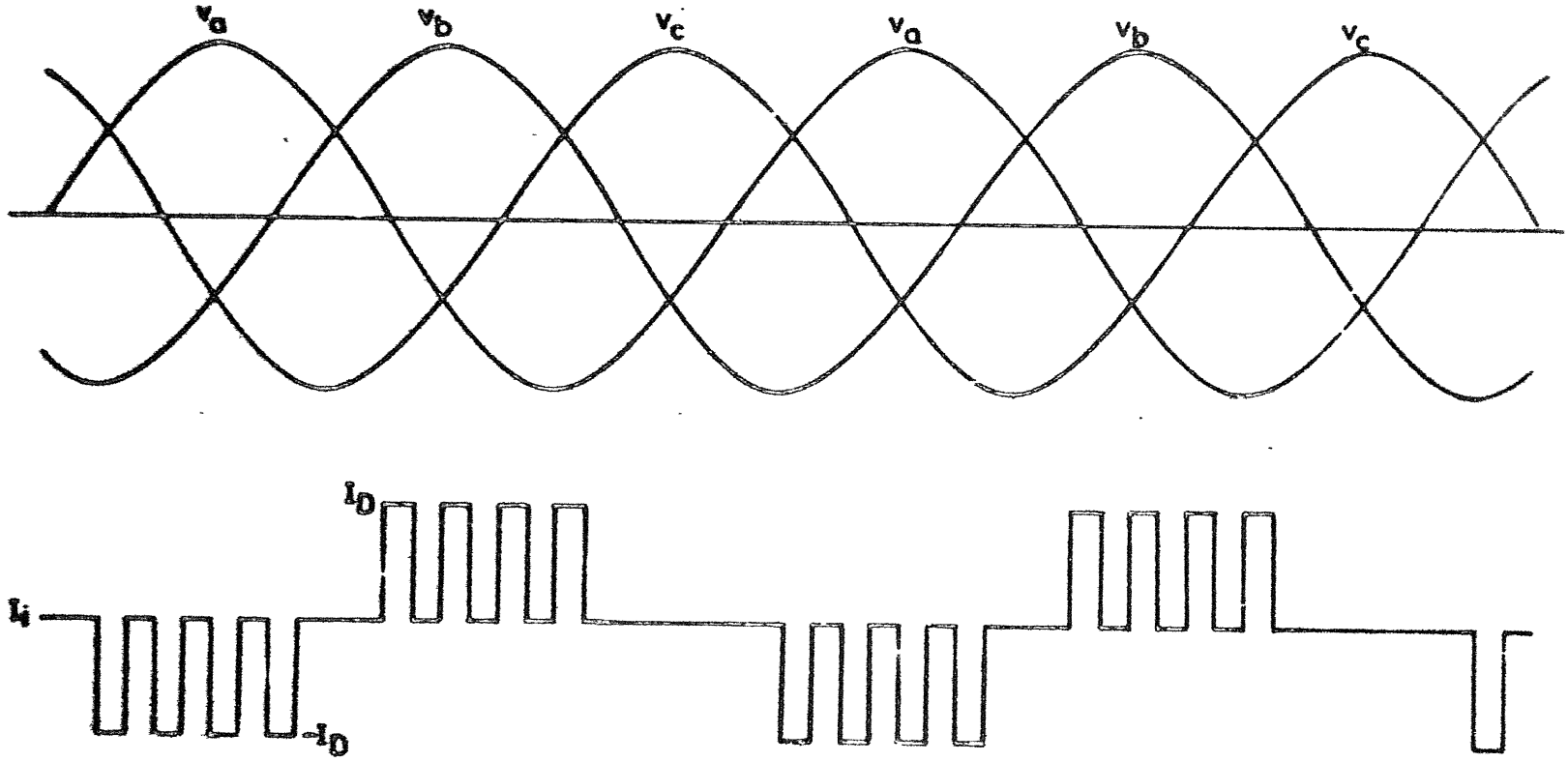

3.11 Phase to neutral voltages and inverter phase a current

This assumption is justified if there is a large inductior in the dc link. The ripple in the dc current can be neglected. The magnitude of the current in the link can be calculated using the equation 3.4, derived in section 3.2. Because of pulse width modulation, the output current in a given phase consists of a series of pulses. The phase current can be $+I_D$,0 or $-I_D$ as illustrated for phase a in Fig.3.11 for a particular modulation index and phase shift. Even harmonics are absent since the phase current possesses half-wave symmetry. The Fourier analysis of the current waveform along with the Fourier coefficients are given in Appendix B. The relative magnitude of the harmonics, taking the fundamental as 1 pu are plotted in Fig.3.12 as a function of the modulation index. The triplen harmonics are absent since the phases are displaced 120^o apart.

3.3.2 DETERMINATION OF THE OVERALL POWER FACTOR OF THE DRIVE

The supply current to the stator is assumed to be sinusoidal. The experimental observations also reveal that currents are almost sinusoidal. If ϕ_m is the phase difference between stator current and corresponding stator phase voltage, the active and reactive power supplied to the motor are $3V_aI_s\cos\phi_m$ and $3V_aI_s\sin\phi_m$ respectively. Let ϕ_i be the phase difference between the phase to neutral voltage and the fundamental component of the inverter phase current I_{if}. Then the total active and reactive powers returned by the inverter to the supply terminals are given by $3V_a.I_{if}.\cos\phi_i$ and $3V_a.I_{if}.\sin\phi_i$ respectively.

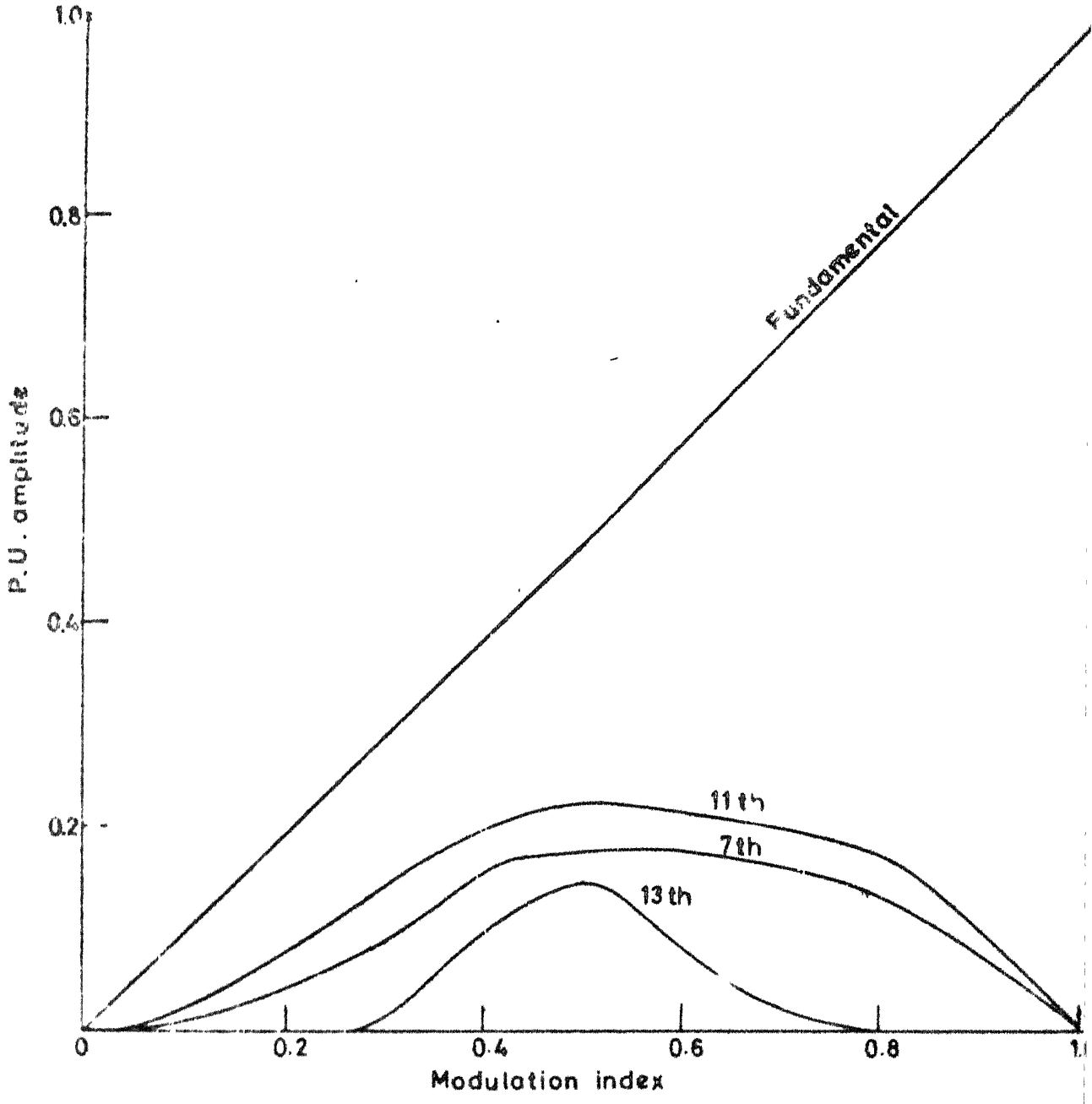

3.12 Inverter current harmonic spectrum

The net active power drawn from the source is

$$P = 3V_a I_s \cos\phi_m - 3V_a \cdot I_{if} \cdot \cos\phi_i \quad \ldots\ (3.11)$$

Similarly the net reactive power supplied from the source is

$$Q = 3V_a I_s \sin\phi_n - 3V_a \cdot I_{if} \cdot \sin\phi_i \quad \ldots\ (3.12)$$

The harmonic reactive power must be supplied by the source. The expression for the harmonics reactive power is

$$H = 3V_a \cdot \sum_{n=7,11,13,\ldots}^{\alpha} I_n^2 \quad \ldots\ (3.13)$$

The apparent power is given by, $VA = \sqrt{P^2+Q^2+H^2}$ ... (3.14)

Therefore the overall power factor of the drive at the source given by $PF = \frac{\text{Real power}}{\text{apparent power}} = \frac{P}{VA}$ .... (3.15)

The variation of the PF with speed for different values of the modulation index is given in Fig.3.13. The significant improvement in overall power factor can be clearly seen from Fig. 3.13. It increases slightly with an increase in speed for a particular modulation index. For a given speed, the power factor increases with an increase in the modulation index. The power factor is reasonably high at low speeds and low values of the modulation index. The new control strategy reported here has made it possible to achieve significant improvement in power factor. The slip power recovery schemes [4,5,6,9,10] reported so far have not achieved such an improvement in power factor.

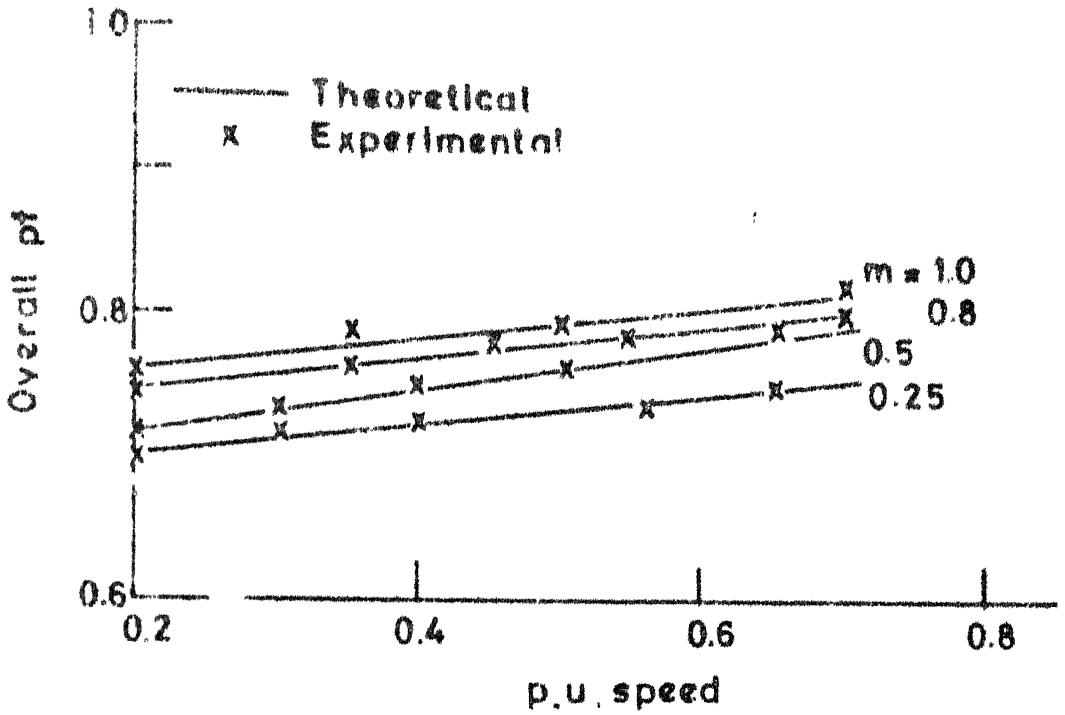

3.13 Power factor vs. speed for different values of modulation index

CHAPTER 4

CLOSED LOOP CONTROL OF THE NEW SLIP POWER RECOVERY SCHEME

4.1 OVERALL DESCRIPTION OF THE CLOSED LOOP SCHEME

In many industrial applications, very accurate speed control of the induction motor is required which is not possible in open loop conditions. For this, closed loop speed control must be incorporated. In the new slip power recovery scheme as described in Chapter 2, closed loop speed control scheme is incorporated with three loops as shown in Fig.4.1. It consists of an outer speed control loop with an inner current control loop incorporated to limit the value of the maximum current during change in speed. The third loop is for correction of power factor while change in speed occurs. The outer speed loop consists of a proportional plus integral controller, a speed limiter and a speed feedback filter. The proportional plus integral controller is used in the speed loop so that the steady state speed error becomes zero. The speed limiter restricts the value of the reference signal for the inner current control loop as a result of which current in d.c. link is controlled to remain within safe limits. The speed feedback is obtained from a DC tachogenerator and to reduce the ripple content in the output of the tachogenerator, the speed feedback filter is used.

The inner current control loop consists of a proportionate current controller and a bidirectional current limiter is incorporated. The current limiter is incorporated after the current controller to limit the input to the firing circuit which in turn will limit the modulation index. Since the modulation index should be varied from zero to one, so the limiter is designed as **bidirectional. i.e.** the output will vary between ± 10V. An opto-isolator based current sensing technique is employed to sense the d.c. current in the link for the information about the actual current. The details about the power factor loop is given in Sec.4.8.

4.2 ANALYTICAL MODEL FOR THE CLOSED LOOP

The exact model of the 3-phase induction motor is very complicated [20,21]. Miljanic [7] obtained a model involving average quantities by writing the voltage balance equations in the rotor circuit and using the well known result that the torque in an induction motor is equal to the electrical power input to the rotor divided by the slip. Applying Kirchoff's law to the DC equivalent circuit, given in Chapter-3.

$$\Delta V - \frac{3}{\pi} s\,(X_1' + X_2)\cdot I_D - (2R_1 s + 2R_2 + R_s + R_F)\cdot I_D - L_F \cdot \frac{dI_D}{dt} -$$

$$\Delta V - \Delta V' - V_{DO} = 0 \qquad \ldots\ldots \quad (4.1)$$

Substituting the value of equation (4.12) in (4.11), we get

$$T_{max} = \frac{1}{w_s} \cdot \frac{E^2}{4qR_1^f} \qquad \ldots\ldots (4.13)$$

Now from equation (4.10), we get,

$$i + T_e \cdot \frac{di}{dt} = s - sqi - s_o \qquad \ldots\ldots (4.14)$$

Now normalizing it, we get

$$\frac{i}{i_{max}} + T_e \cdot \frac{d}{dt}\left(i/i_{max}\right) = s - sq\,(i/i_{max}) - \frac{V_{DO}+\Delta V+\Delta V'}{E} \qquad \ldots\ldots (4.15)$$

and similarly we get

$$\frac{T}{T_{max}} = 4q \cdot \frac{i}{i_{max}}\left(1 - qi/i_{max}\right) \qquad \ldots\ldots (4.16)$$

Now to derive a simple mathemetical model, the following assumptions are made,

$$\left.\begin{array}{ll} \text{i)} & \Delta V,\ \Delta V' \ll E \\ \text{ii)} & q(i/i_{max}) \ll 1 \end{array}\right\} \qquad \ldots\ldots (4.17)$$

so, we get

$$\frac{i}{i_{max}} + T_e \frac{d}{dt}\left(i/i_{max}\right) = s + \frac{V_{DO}}{E} \qquad \ldots\ldots (4.18)$$

and $$\frac{T}{T_{max}} = 4q \cdot \frac{i}{i_{max}} \qquad \ldots\ldots (4.19)$$

The torque equation is given by $T = T_m \frac{dw}{dt} + Bw$ .....(4.20)

Therefore, $T = \frac{1}{sw_s} [s_o.E.I_D + L_F.I_D. \frac{dI_D}{dt} + R_1'. I_D^2]$ ..... (4.8)

Let $i = \frac{I_D}{E/R_1'}$ Therefore, $I_D = i. \frac{E}{R_1'}$

Therefore, $T = \frac{1}{sw_s} [s_o.E.I_D + L_F.I_D. \frac{E}{R_1'} . \frac{di}{dt} + \frac{i.E}{I_D} . I_D^2]$

$= \frac{1}{sw_s} [s_o.E.I_D + L_F. \frac{I_D.E}{R_1'} . \frac{di}{dt} + i.E.I_D]$

Let $T_e = L_F/R$ Therefore, $T = \frac{E.I_D}{s.w_s} [s_o + T_e. \frac{di}{dt} + i]$ ..... (4.9)

Let $q = \frac{\frac{3}{\pi}s(X_1+X_2) + 2R_1}{2R_2 + R_s + R_F} = \frac{R_1}{R_1'}$

From equation (4.5), we get

$sE - R_1. sI_D - R_1'.I_D - (V_{DO}+\Delta V +\Delta V') - L_F. \frac{dI_D}{dt} = 0$

or $s - sqi - i - s_o - T_e. \frac{di}{dt} = 0$ ..... (4.10)

From equations (4.9) and (4.10), we get

Torque $T = \frac{1}{w_s} . \frac{E^2}{R_1'} i [1 - qi]$ ..... (4.11)

Now from the expression of torque in (4.11), in order to find the maximum value of i, i.e. i_{max}, then differentiating T w.r.t. i, we get $\frac{dT}{di} = \frac{1}{w_s} . \frac{E^2}{R_1'} [1 - 2qi] = 0$

Therefore, $i_{max} = \frac{1}{2q}$ ..... (4.12)

where T_m = The mechanical time constant of the machine

B = Load constant.

Equations (4.18) to (4.20) give an approximate mathemetical model of the system. Though the parameters are variable, they can be assumed to be constant around an operating point. If the load is assumed to be a pure inertial one, then B can be neglected. The block diagram of the plant can be drawn as shown in Fig. 4.2.

4.3 TRANSDUCERS

4.3.1 SPEED-TRANSDUCER

A permanent magnet DC tachogenerator is coupled to the induction motor - DC generator set. Its constant is 100V/1000 rpm and is used as the speed transducer. By using a potential divider, the voltage is scaled down to 10V at 1440 rpm. To reduce the ripple content in the output of the tachogenerator, a filter is used.

4.3.2 CURRENT TRANSDUCER

A simple opto-isolator based current sensing technique is used to sense the current in the link which can give truly isolated current signal from the power circuit. The circuit diagram of this technique is given in Fig.4.3. Current is sensed with a small resistor (R_s) in the link circuit. This current is filtered using a low pass RC network. The filter time constant can be adjusted by the variable resistor R. The filtered signal is fed to an opto-isolator stage as shown in

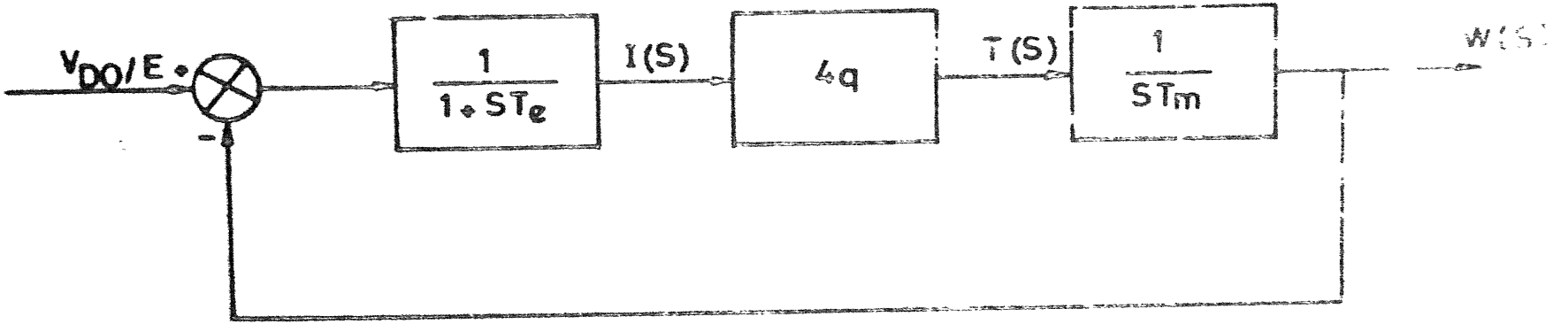

4.2 Simplified block diagram of the plant

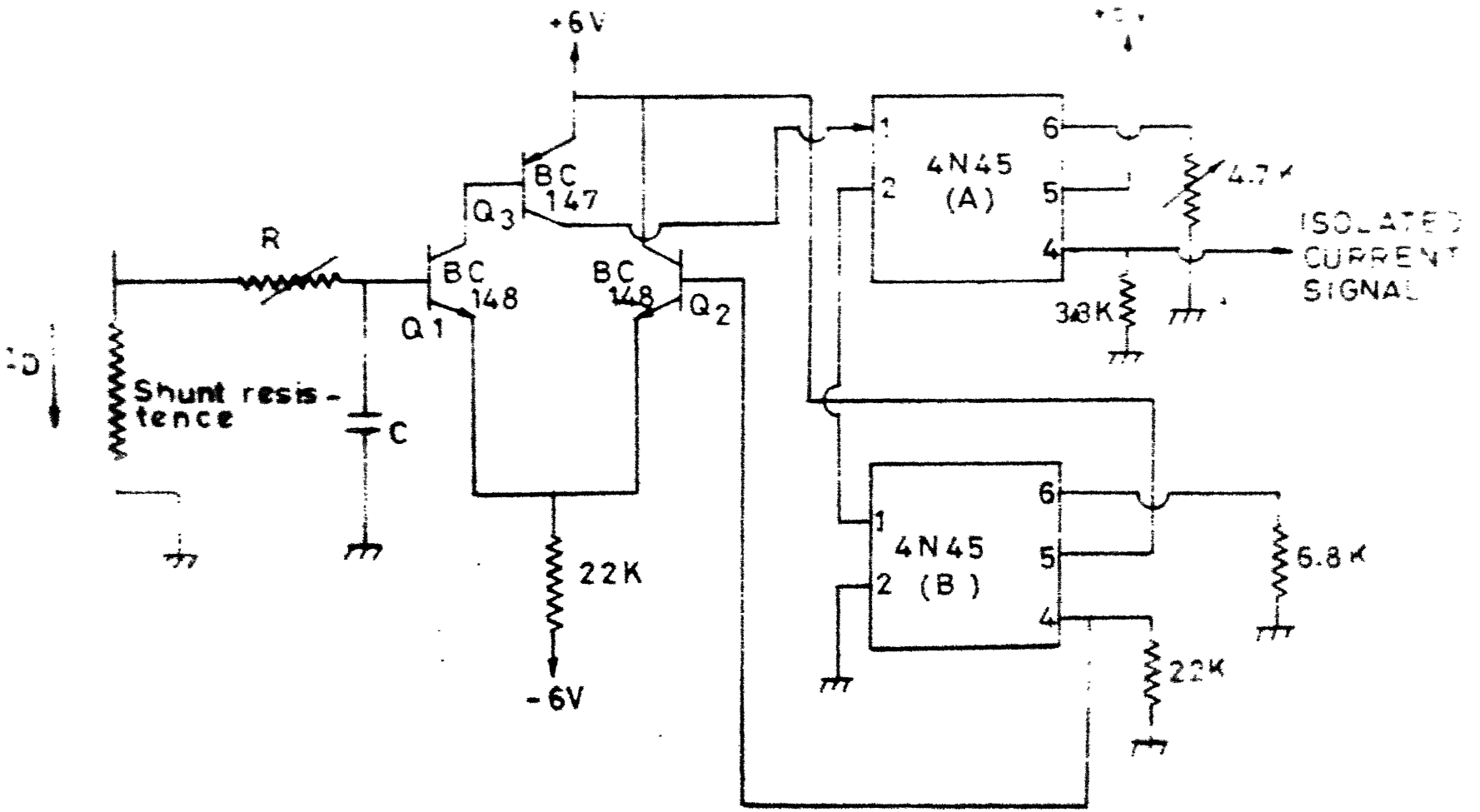

4.3 Sensing of link current using opto-isolator

Fig.4.3. The opto-isolator stages comprises of a differential amplifier stage and two opto-isolators (4N45). The current signal drives the base of the transistor Q_1 in the differential amplifier set up. The collector current of Q_3 which is proportional to the input voltage (at the base of Q_1) is passed through the inputs of the two opto-isolators A and B. The output of the opto-isolator B is fed back to the base of Q_2. Due to the high gain of the differential amplifier set up, the voltage at the base of Q_2 always tracks the input voltage at the base of Q_1.

Assuming A and B to be identical, the output of A is directly proportional to the output of B which in turn is proportional to the input current signal. A floating power supply, which is isolated from the power supply to A, is used for the differential amplifier and opto-isolator B. Hence, a current signal which is completely isolated from the power circuit is obtained.

4.4 FILTERS

4.4.1 SPEED FEEDBACK FILTERS

To reduce the ripple content in the tachogenerator output voltage, a first order filter is introduced in the speed feedback path with cut off frequency of 16Hz. i.e. with a time constant equal to 62ms. The steady state speed feedback factor H_v is chosen to be unity such that at 1440 rpm, the

speed feedback signal is of 10V.

Thus, $H_W = \frac{H_w}{1+sT_w} = \frac{1}{1+sx62x10^{-3}}$, where H_W is the transfer function of the speed feedback loop.

4.5 DERIVATION OF THE TRANSFER FUNCTIONS OF VARIOUS ELEMENTS

4.5.1 PWM INVERTER

The modulation index of the PWM inverter can be varied between 0 and 1. The working ac voltage of the inverter is kept at 40V and a modulation index of 0.5 is chosen as the operating point with the phase shift angle kept at 0^o. For this operating point, the pulse width for the negative voltage to commutate the starting thyristor is 15^o or 0.833ms.The inverter output voltage V_{DO} at this operating point is given by equation (A.1) of Appendix A. Substituting the values in equation (A.1), we get the value of V_{DO} as 43.34V.

Differentiating the expression of V_{DO} as in equation (A.1) w.r.t. the pulsewidth i.e. (2d), we get $\frac{\Delta V_{DO}}{\Delta(2d)} = 172.89$ after substituting all the values.

So, on normalization, it gives

$$\frac{\Delta V_{DO}/E}{\Delta(2d)/\pi/6} = \frac{\Delta V_{DO}/E}{6x\Delta(2d)/\pi} = \frac{\Delta V_{DO}}{E} \times \frac{\pi}{6x\Delta(2d)} = \frac{172.89 \times \pi}{83.33x2.34x6} = 0.46$$

Here, $2\pi/3$ is taken as the pulse width for the unity modulation index.

The firing units are designed such that the modulation index varies linearly from 0 to 1 for a variation of the control voltage from -10V to + 10V (which are the two extreme controllable voltages).

Thus, $\frac{\Delta(2d)/2\pi/3}{\Delta V_C/V_{Cmax}} = \frac{1}{2}$

There is a normal delay in the thyristor response. It can vary between 0 and 1.66ms. Taking the average, the time constant of the inverter is 0.83ms.

Therefore, the inverter transfer function is given by ,

$$\frac{V_{DO}(S)}{V_C(S)} = \frac{A}{1+sT_A} = \frac{0.46}{1+S\times0.83\times10^{-3}}$$

where A = The normalised gain of the thyristor inverter

T_A = The equivalent time constant of the inverter which includes the delays due to thyristors and diodes.

4.5.2 CURRENT CONTROLLER

A proportional controller has been chosen as the current controller whose transfer function is K_1, a pure gain.

4.5.3 SPEED CONTROLLER

A PI controller has been chosen as the speed controller and its transfer function is of the form $\frac{K_2(1+ST_2)}{ST_2}$.

4.6 LIMITERS

The value of the modulation index is to be varied between 0 and 1. The transfer function of the control circuit is given by $m = \frac{V_C}{V_{Cmax} - V_{Cmin}}$. Here $V_{Cmax} = 10V$, $V_{Cmin} = -10V$ and the value of V_C is to be calculated from the -10V level.

So, we can vary the V_C within the range of $\pm 10V$. The limiter which is incorporated after the speed PI controller limits the output voltage between -10V and +10V linearly. The limiter after the current controller is designed such that the output voltage level varies between -10V to +10V, linearly with the input voltage between 0 and +10V. The limiter circuits were designed with adjustable saturation levels.

4.7 DESIGN OF CONTROLLERS

4.7.1 CURRENT CONTROLLER

If the system mechanical time constant is very large compared to the response time of the current control loop, the effect of the speed variable on the transient respone of the current control loop can be neglected i.e. the speed feedback shown in Fig.4.2 can be omitted. The approximate block diagram of the current control loop is shown in Fig.4.4. The filter time constant in the opto-isolator based current sensing is 100ms. The steady state current feedback factor H_i, is adjusted

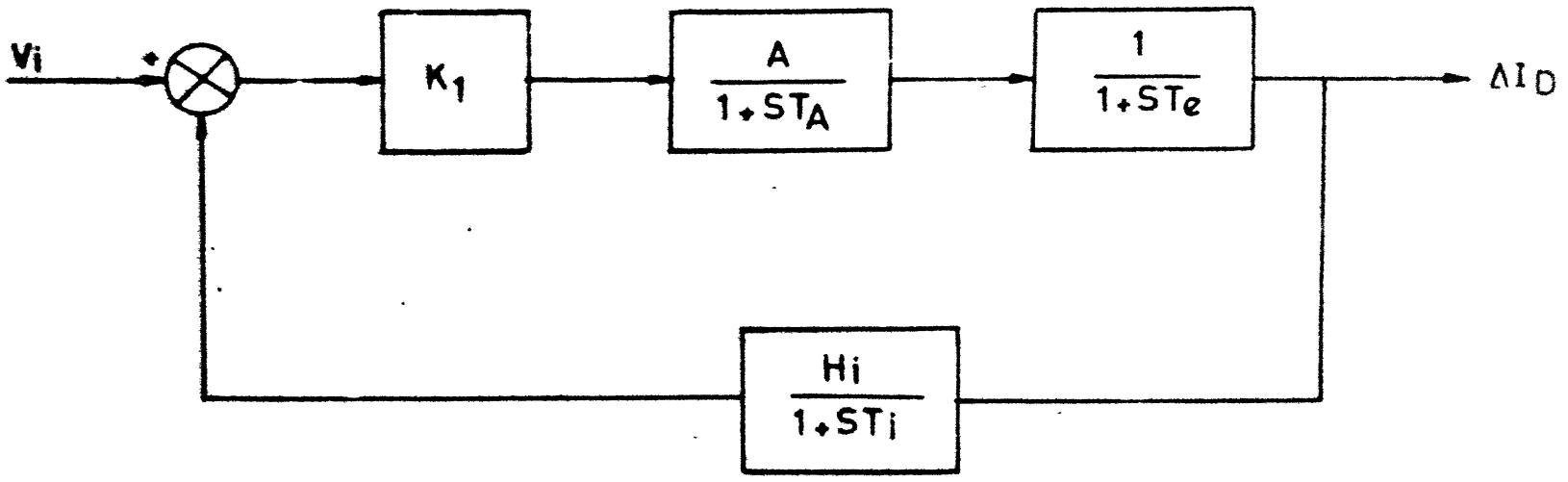

4.4 Block diagram of current control loop

in such a way that the feedback signal level is comparable to that of the reference signal for the current loop. As the maximum value of the output voltage of the speed loop limiter is 10V, then H_i is adjusted such that when the rated current of 12.24A is flowing in the rotor circuit, the feedback signal level is also 10V. The filter time constant is choosen quite high in order to reduce the level of ripple.

Thus, $\frac{V_i}{I_D} = \frac{10}{12.24} = 0.816$

Now $H_i = \frac{V_i/V_{Cmax}}{I_D/I_{Dmax}}$ and $I_{Dmax} = \frac{E}{2R_2+Rs+R_F}$

Therefore, neglecting R_F, we get $I_{Dmax} = 28.93A$

Therefore, $H_i = \frac{V_i}{I_D} \times \frac{I_{Dmax}}{V_{Cmax}} = 0.816 \times 28.93/10 = 2.4$

So the transfer function for the current filter is given by

$$H_I = \frac{H_i}{1+ST_i} = \frac{2.4}{1+Sx100x10^{-3}}$$

The current loop gain $GH_I(S)$ is given by

$$GH_I(S) = \frac{K_1.A.H_i}{(1+ST_A)(1+ST_e)(1+ST_i)} \quad \ldots\ldots \quad (4.21)$$

For all practical purposes, we can neglect the filter time constant T_i. So the block diagram for the current control loop can be modified using a unity feedback gain. The new block diagram is shown in Fig.4.5.

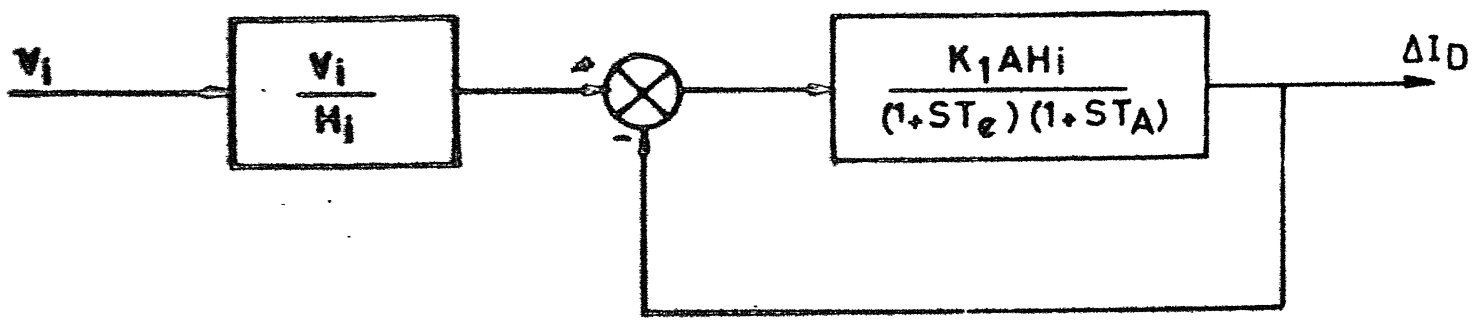
Vi
Vi / Hi
+
-
K1AHi / (1+STe)(1+STA)
ΔID

The loop gain of the modified current control loop is given by

$$GH_I(S) = \frac{K_1 AH_i}{(1+ST_c)(1+ST_A)} \qquad \ldots\ldots \quad (4.22)$$

The closed loop transfer function is given by $\frac{GH_I(S)}{1+GH_I(S)} =$

$$\frac{\frac{K_1 AH_i}{(1+ST_A)(1+ST_e)}}{1+\frac{K_1 AH_i}{(1+ST_A)(1+ST_e)}} = \frac{K_1 AH_i}{(1+ST_A)(1+ST_e)+K_1 AH_i} =$$

$$\frac{K_1 AH_i}{1+S(T_A+T_e)+S^2 T_A T_e+K_1 AH_i}$$

Now in the above expression, T_e is much larger than T_A. Hence $\frac{1}{T_e}$ can be neglected compared to $\frac{1}{T_A}$. Similarly $K_1 AH_i$ is also larger than 1.

Therefore, $\frac{GH_I(S)}{1+GH_I(S)} = \frac{K_1 AH_i}{S(T_A+T_e)+S^2 T_A T_e+K_1 AH_i} =$

$$\frac{K_1 AH_i/T_A T_e}{S^2+S(\frac{1}{T_A}+\frac{1}{T_e})+\frac{K_I AH_i}{T_A T_e}} = \frac{H_i \; K_I AH_i/T_A T_e}{S^2+S.\frac{1}{T_A}+\frac{K_1 AH_i}{T_A T_e}} \qquad \ldots\ldots \quad (4.23)$$

Comparing the denominator of equation (4.23) with a standard 2nd order equation, we get,

$$w_n^2 = K_1 AH_i / T_A T_e$$

$$2\xi w_n = 1/T_A$$

$$\xi^2 = \frac{1}{4T_A^2} \cdot \frac{T_A T_e}{4K_1 AH_i} = \frac{T_e}{4K_1 AH_i \cdot T_A} \qquad \ldots\ldots (4.24)$$

Let the current controller gain be designed for 10/ overshoot, then the value of the current controller will be given by

$$K_1 = \frac{T_e}{4\xi^2 AH_i T_A} = \frac{0.718\ T_e}{AH_i\ T_A} \qquad \ldots\ldots (4.25)$$

4.7.2 REALISATION OF THE CURRE T CONTROLLER

The realisation of the current controller is done by using a simple operational amplifier with a gain K_1 and is shown in Fig.4.6. The R_1,R_2 and R_3 values are choosen according to the value of K_1 and the steady state feedback factor of the current feedback filter i.e. H_i. The gain of the current controller is given by $K_1 = \frac{R_s}{R_1}$ ..... (4.26)

As the H_i factor is chosen such that with the rated current in the rotor circuit, the magnitude of the feedback signal V_{fi} is equal to the current controller reference signal V_{Ri}, the values of R_1 and R_2 should be equal.

4.7.3 SPEED CO TROLLER

While designing the speed controller, the current loop has been approximated by a first order system of an equivalent gain [17,18] of $K' = \frac{1}{H_i} = 0.417$ and an equivalent time

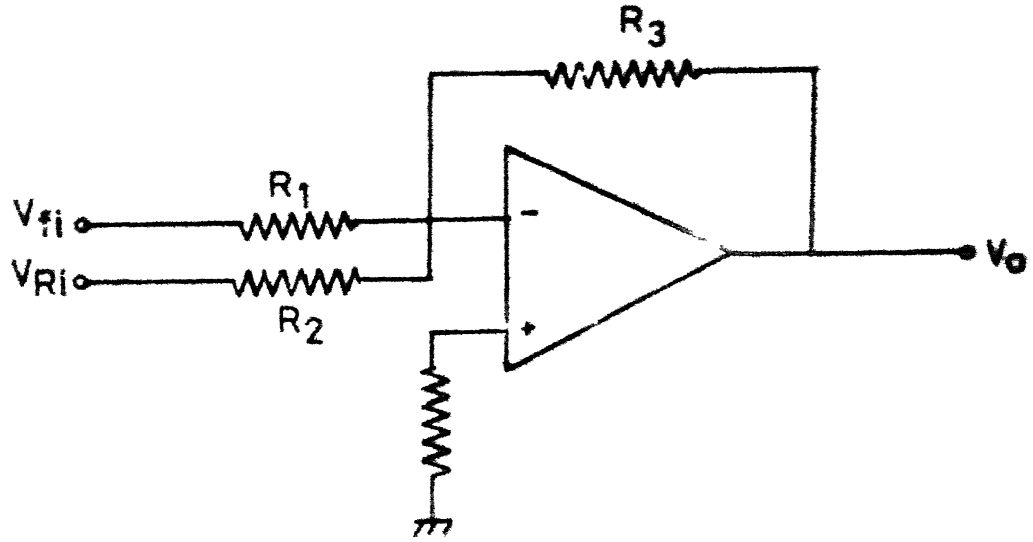

4.6 Circuit diagram of the current controller

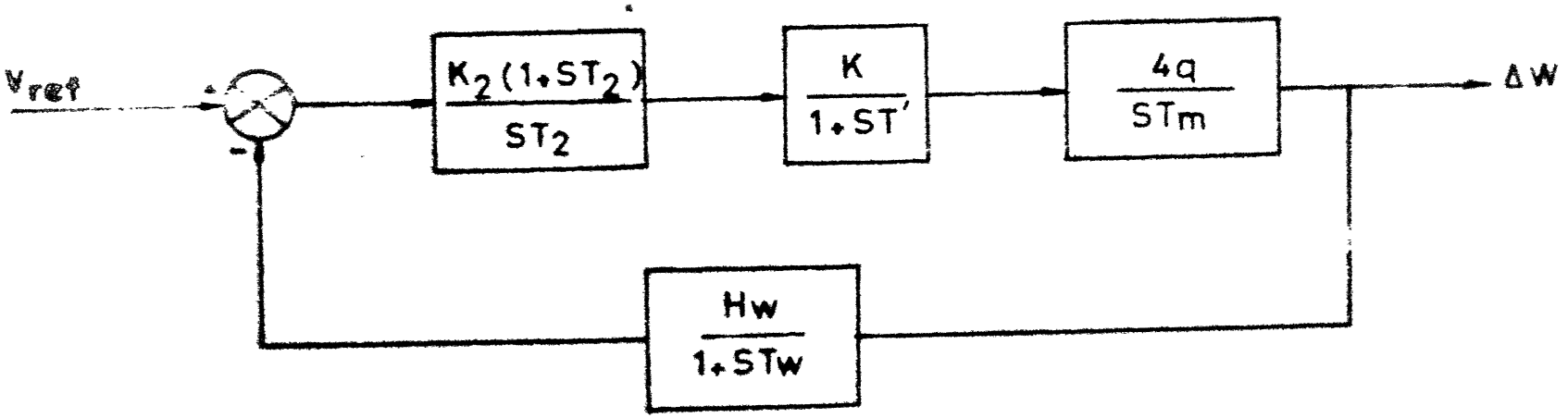

4.7 Block diagram of speed controller loop

$$\text{or} \quad \frac{T_2(1+w^2T_w^2) - T_w(1+w^2T_2^2)}{(1+w^2T_2^2)(1+w^2T_w^2)} = 0$$

$$\text{or} \quad T_2(1+w^2T_w^2) - T_w(1+w^2T_2^2) = 0$$

$$\text{or} \quad T_2+w^2T_w^2T_2 - T_w - w^2T_2^2T_w = 0$$

$$\text{or} \quad w^2T_wT_2\,(T_w - T_2) = T_w - T_2 \quad \text{or} \quad w^2 = \frac{1}{T_wT_2}$$

Therefore $w = \sqrt{\frac{1}{T_wT_2}}$ ..... (4.30)

i.e. $w_c/_{\text{minimum phase lag}} = \sqrt{\frac{1}{T_wT_2}}$

Let $T_2 = x^2T_w, \quad x > 1$

Therefore, $w_c/_{\text{minimum phase lag}} = \frac{1}{\sqrt{T_w \cdot x^2T_w}} = \frac{1}{xT_w} =$

$$\frac{x^2}{x.T_2} = \frac{x}{T_2} \qquad \ldots\ldots \quad (4.31)$$

Therefore, the magnitude of $GH_w(S)$ at this frequency is

$$/GH_w(w_c)/ = \frac{K_2K'4qH_w(1+w_c^2\,T_2^2)^{1/2}}{w_c^2\,T_2T_m(1+w_c^2\,T_w^2)^{1/2}} = 1 \qquad \ldots\ldots \quad (4.32)$$

$$\text{or} \quad \frac{K_2K'4qH_w(1+x^2)^{1/2}}{\frac{x^2}{T_2} \cdot T_m\,(1+\frac{1}{x^2})^{1/2}} = 1$$

$$\text{or} \quad \frac{K_2K'4qH_w.T_2}{x\,T_m} = 1$$

Therefore, $K_2 = \frac{xT_m}{K'4qH_w.T_2}$ ..... (4.33)

Now from equations (4.28) and (4.33), we get $GH_w(S) = \frac{(1+ST_2).x}{S^2.T_2^2(1+ST_w)}$

$$= \frac{(1+Sx^2T_w).x}{S^2x^4T_w^2(1+ST_w)} = \frac{(1+Sx^2T_w)}{x^3T_w^2S^2(1+ST_w)} \quad \ldots\ldots \quad (4.34)$$

Now the characteristic equation of the transfer function of the speed loop is given by

$$1+GH_w(S) = 1 + \frac{(1+Sx^2T_w)}{x^3T_w^2S^2(1+ST_w)} = 0 \text{ or } x^3T_w^2S^2(1+ST_w) + 1 + Sx^2T_w = 0$$

$$\text{or } x^3T_w^2S^2 + x^3T_w^3S^3 + Sx^2T_w + 1 + x^2T_w^2S^2 - x^2T_w^2S^2 + xT_wS - xT_wS = 0$$

$$\text{or } (1+xT_wS)\,[1+x^2T_w^2S^2 + x(x-1)\,T_wS] = 0 \quad \ldots\ldots \quad (4.35)$$

The value of 'x' is to be chosen from the consideration of the damping ratio of the system. Comparing the second order equation in (4.35) with a standard second order equation and choosing the damping ratio of 0.707 for the speed loop, we get

$$S^2 + \frac{(x-1)}{xT_w} \cdot S + \frac{1}{x^2T_w^2} = 0 \quad \text{Therefore, } w_n^2 = \frac{1}{x^2T_w^2},$$

$$2\xi w_n = \frac{x-1}{xT_w} \quad \text{Therefore, } \xi^2 = \frac{(x-1)^2}{4} = 0.5$$

Therefore $x = 1+\sqrt{2}$ $\ldots\ldots$ (4.36)

Therefore, $T_2 = x^2T_w = (1+\sqrt{2})^2 . T_w$ $\ldots\ldots$ (4.37)

$$K_2 = \frac{xT_m}{K'4qH_wT_2} = \frac{xT_m}{K'4qH_wx^2T_w} = \frac{T_m}{(1+\sqrt{2})4qK'H_wT_w} \quad \ldots\ldots (4.38)$$

Substituting the values, we get q = 0.62

Therefore, $K_2 = \frac{0.4375}{(1+\sqrt{2}) \times 4 \times 0.62 \times 0.417 \times 62 \times 10^{-3}} = 2.82$

$T_2 = (1+\sqrt{2})^2 \times T_w = (1+\sqrt{2})^2 \times 62 = 361.4ms.$

4.7.4 REALISATION OF SPEED CONTROLLER

The realisation of the speed controller is as shown in Fig. 4.8. The values are given $T_2 = R_3C$, $K_2 = R_3/R_1$

4.8 POWER FACTOR CORRECTION LOOP

The schematic diagram of the power factor correction loop is shown in Fig.4.9. The zero crossing of both phase to neutral voltage V_a and the stator current I_s in sensed. The zero crossing of the phase to neutral voltage is sensed with the help of a monostable. The ZCD of the phase to neutral voltage (V_a) which is the input to the monostable is taken from Fig.2.10 in Chapter 2. Similarly the stator current signal I_s taken across a 0.5 shunt is given to a ZCD for squaring. The ZCD is then passed through an opto-isolator stage to provide isolation for the power factor correction loop from the power stage. The inverted ZCD from the opto-isolator stage is then provided to a monostable to sense its falling edge which will be the positive

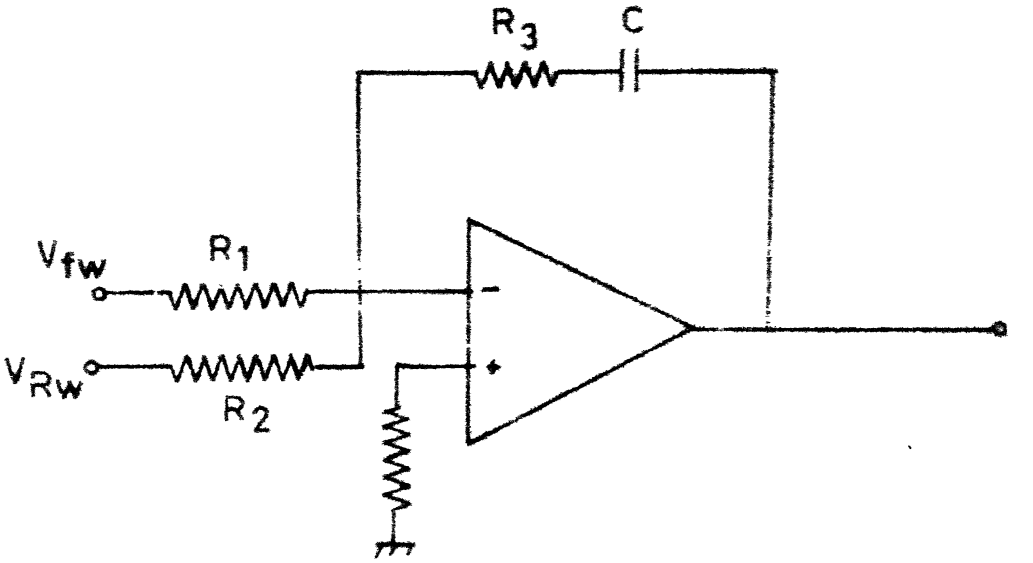

4.8 Realization of the speed-controller

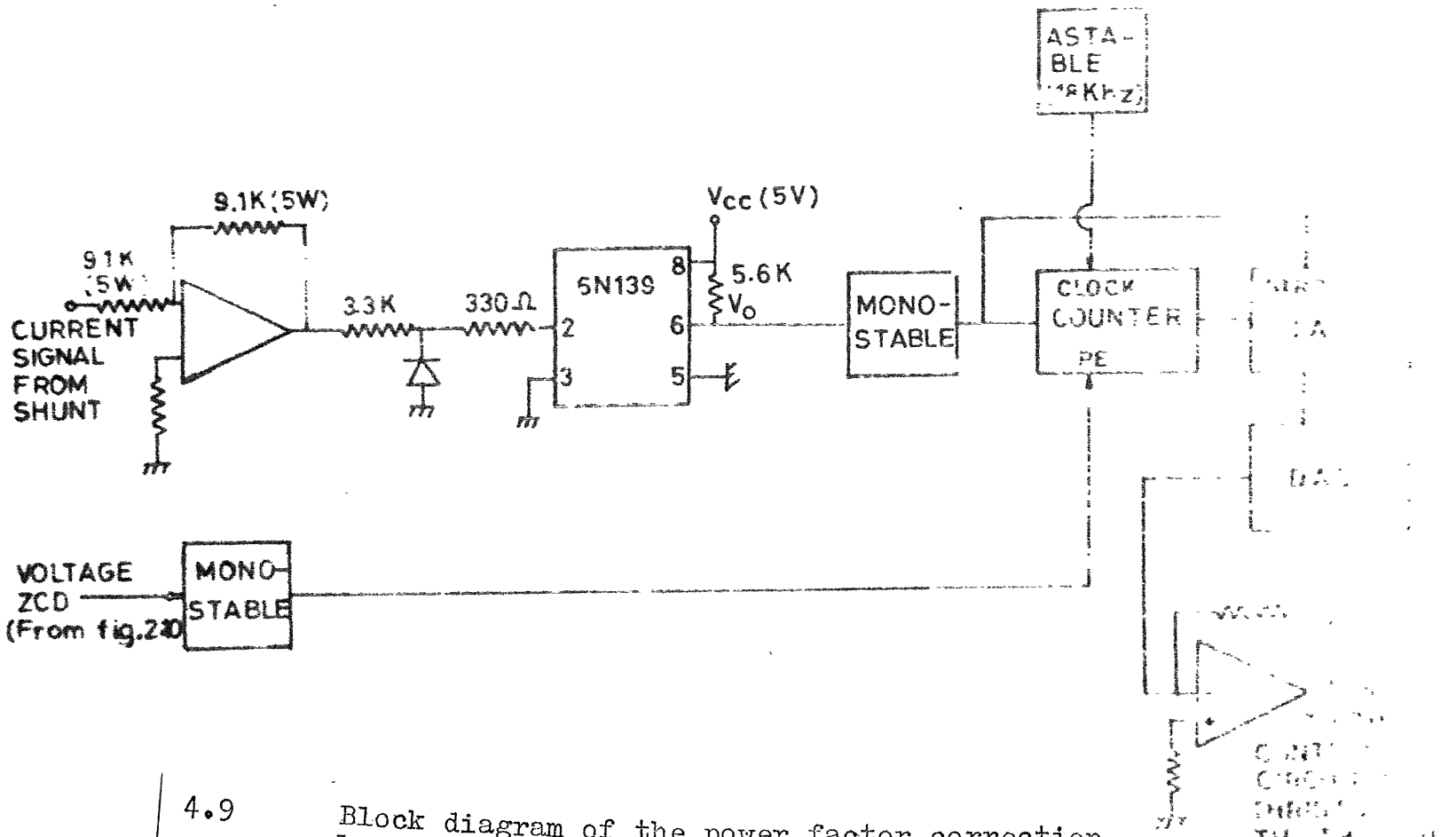

4.9 Block diagram of the power factor correction loop

zero-crossing edge of the current signal. Two 4 bit counter stages are cascaded to form a counter which will start counting at the zero crossing edge of the phase to neutral voltage (V_a). Since we have to count from zero to ninety in the time duration of the quarter of a cycle, so the clock frequency of the counter, which is supplied from a astable,has a frequency of 90 x 4 x 50 = 18 KHz. The output of the counter is given to a 8282 latch. The $\overline{OE}$ output of the latch is kept permanently grounded. The output of the monostable which is used to sense the positive zero crossing of the stator current signal is used as a strobe signal for the latch. This is done in order to make the latches transparent at the positive zero crossing edge of the stator current signal so that the count registered in the counter, which is directly proportional to the phase difference between V_a and I_s, goes at the output of the latch. At the high to low transition of the strobe signal, the data from the counter gets latched. The output of the latch is given to a DAC to give the analog value of the corresponding count registered in the counter. The reference voltage of the DAC is kept at +5V. The output of the DAC will give the value of output between 0 and 5V. Since the DAC is a constant current source, hence a current to voltage converter is necessary at the output of the DAC. The output of the current to voltage converter will var y between zero to -5V which is used as a control signal X_c for the firing circuit shown in Fig. 2.12 of Chapter 2.

The system block diagram is shown in Fig.4.10. The values of all the parameters are given in Appendix D.

Using the control system described in the above sections, the speed-torque characteristics were obtained. Fig. 4.11 shows the speed-torque characteristics with all the control loops on, at various initial speeds.

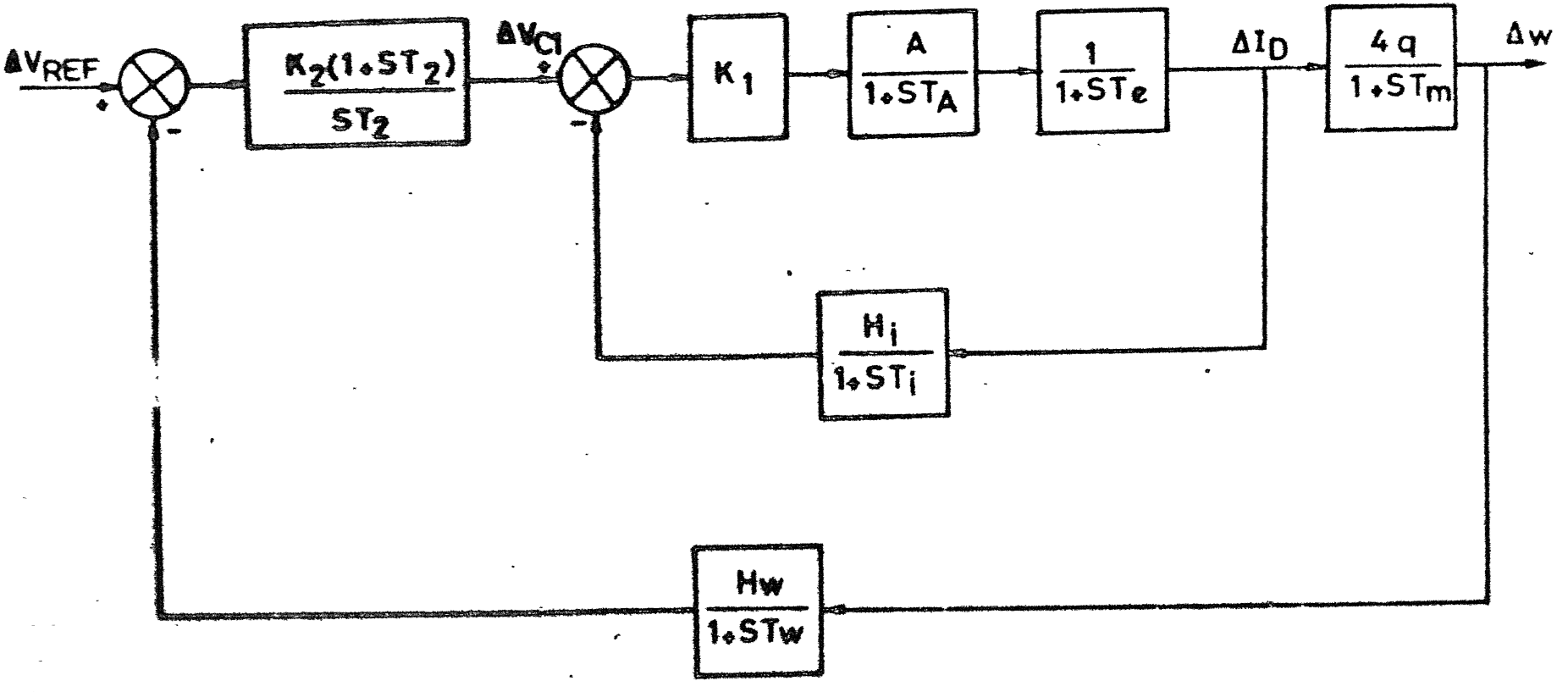

4.10 System block diagram

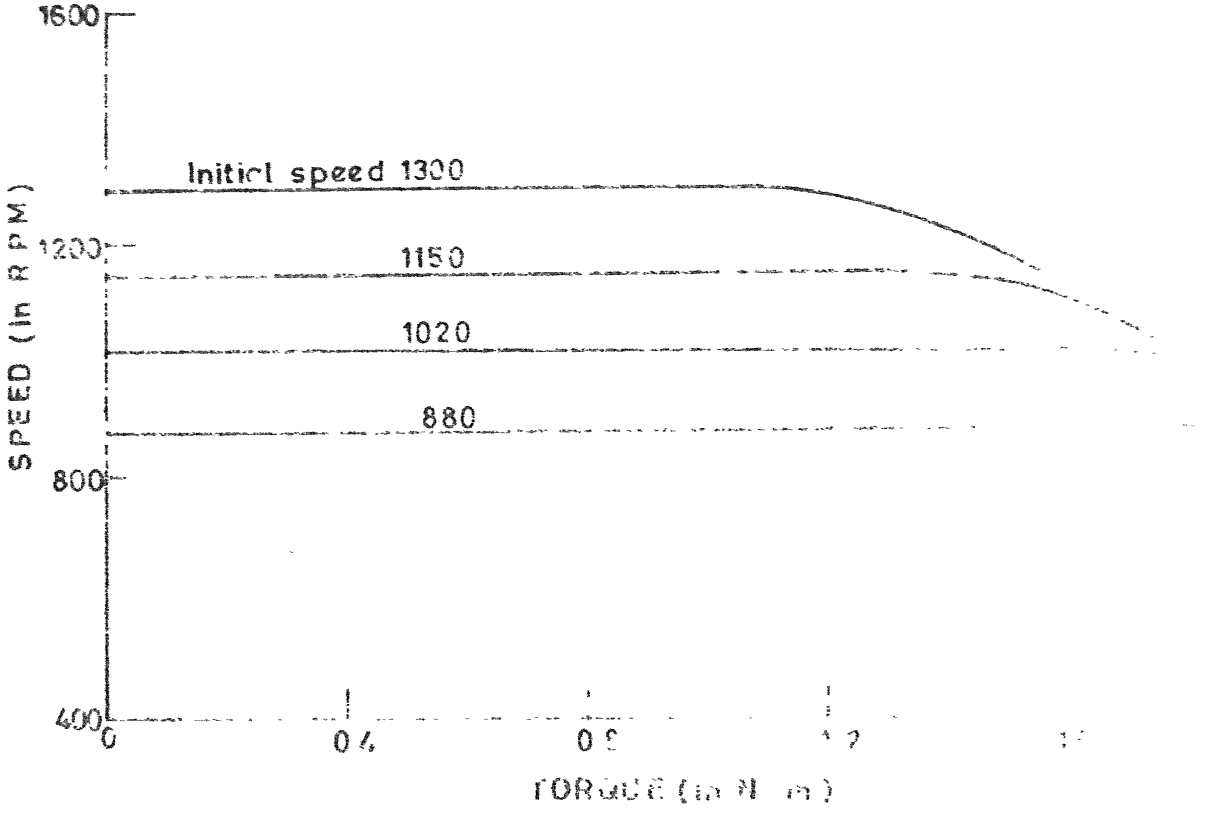

4.11 Closed loop speed-torque characteristics

CHAPTER 5

CONCLUSIONS

The slip power recovery scheme with a new control strategy has improved the supply power factor of the drive to a great extent. Such an improvement is definitely not possible with the schemes reported so far [1 - 8]. Because of multipulse width modulation, the ripple in the direct current is considerably reduced and the inverter harmonic current spectrum has shifted from lower order to higher order. A novel method of starting the drive is explained. The starting thyristor is automatically turned off by the gating pulses of the inverter. No forced commutation circuitry is needed to turn off the starting thyristor. The steady state performance characteristics have been determined by simple DC and AC equivalent circuits which have provided results to a satisfactory accuracy as revealed by the experimental verification. This new slip power recovery scheme in comparison with the earlier reported schemes is somewhat complex since it employs forced commutation. However, the significant improvement in performance makes it highly desirable for industrial applications where induction motor drives are preferred. The study has also revealed versatile speed-torque characteristics similar to those of a separately excited dc motor.

A new method for controlling the supply power factor of the drive under closed-loop operation is suggested. The transfer function of various blocks in the closed-loop operation are derived. A simple procedure for predicting the closed-loop performance is delineated.

APPENDIX A

In this appendix, the expression for average counter emf is determined as a function of the pulse width. In equal pulse width modulation, since the modulating signal is a dc level, hence the change of pulse widths with a change in modulation index is linear. For unity modulation index, the width of each pulse is 1.66m sec. In determining the expression for the average counter emf, the modulation index is varied from unity to zero in steps of 0.1 i.e. with a change in pulse width of 0.0166m sec. Hence the average counter emf will be a function of the pulse width which is also a function of the modulation index.

Let $V_{ab} = \sqrt{6}\ V \sin(wt + 30^{o})$, $V_{bc} = \sqrt{6}\ V \sin(wt - 90^{o})$, $V_{ca} = \sqrt{6}\ V \sin(wt - 210^{o})$, where V is the rms phase voltage. Let 2d be the width of each pulse and m be the number of pulses/phase/half-cycle. The expression for the average counter emf V_{DO} for the phase shift range of 0^{o} to 30^{o} is :

$$V_{DO} = \frac{V}{\pi}\left[\int_{0}^{2d} -\sqrt{6}\sin(wt-\pi/2)d(wt) + \int_{2\pi/3m}^{2\pi/3m+2d} \sqrt{6}\sin(wt+\pi/6)d(wt) - \right.$$

$$\int_{4\pi/3m}^{4\pi/3m+2d} \sqrt{6}\sin(wt-7\pi/6)\,d(wt) - \int_{2\pi/m-2d}^{2\pi/m} \sqrt{6}\sin(wt-\pi/2)\,d(wt) -$$

$$\int_{2\pi/m}^{2\pi/m+2d} \sqrt{6}\sin(wt-7\pi/6)d(wt) - \int_{8\pi/3m}^{8\pi/3m+2d} \sqrt{6}\sin(wt-7\pi/6)d(wt) + \int_{10\pi/3m}^{10\pi/3m+2d} \sqrt{6}\sin(wt-\pi/2)d($$

$$-\int_{\pi}^{\pi+2d} \sqrt{6}\sin(wt+\pi/6)d(wt) - \int_{\pi+2\pi/3m-2d}^{\pi+2\pi/3m} \sqrt{6}\sin(wt-7\pi/6)d(wt) -$$

$$\int_{\pi+2\pi/3m}^{\pi+2\pi/3m+2d} \sqrt{6}\sin(wt+\pi/6)d(wt) - \int_{\pi+4\pi/3m}^{\pi+4\pi/3m+2d} \sqrt{6}\sin(wt+\pi/6)d(wt) + \int_{\pi+2\pi/m}^{\pi+2\pi/m+2d} \sqrt{6}\sin(wt-7\pi/6)d(wt)$$

$$\int_{\pi+8\pi/3m}^{\pi+8\pi/3m+2d} \sqrt{6}\sin(wt-\pi/2)d(wt) - \int_{\pi+10\pi/3m-2d}^{\pi+10\pi/3m} \sqrt{6}\sin(wt+\pi/6)d(wt) - \int_{\pi+10\pi/3m}^{\pi+10\pi/3m+2d} \sqrt{6}\sin(wt-\pi/2)d(wt)]$$

$$= \frac{\sqrt{6}V}{\pi}\Big[\,[\cos(wt-\pi/2)]_0^{2d} - [\cos(wt+\pi/6)]_{2\pi/3m}^{2\pi/3m+2d} +$$

$$[\cos(wt-7\pi/6)]_{4\pi/3m}^{4\pi/3m+2d} + [\cos(wt-\pi/2)]_{2\pi/m-2d}^{2\pi/m} + [\cos(wt-7\pi/6)]_{2\pi/m}^{2\pi/m+2}$$

$$+ [\cos(wt-7\pi/6)]_{8\pi/3m}^{8\pi/3m+2d} - [\cos(wt-\pi/2)]_{10\pi/3m}^{10\pi/3m+2d} +$$

$$[\cos(wt+\pi/6)]_{\pi}^{\pi+2d} + [\cos(wt-7\pi/6)]_{\pi+2\pi/3m-2d}^{\pi+2\pi/3m} +$$

$$[\cos(wt+\pi/6)]_{\pi+2\pi/3m}^{\pi+2\pi/3m+2d} + [\cos(wt+\pi/6)]_{\pi+4\pi/3m}^{\pi+4\pi/3m+2d} -$$

$$[\cos(wt-7\pi/6)]_{\pi+2\pi/m}^{\pi+2\pi/m+2d} + [\cos(wt-\pi/2)]_{\pi+8\pi/3m}^{\pi+8\pi/3m+2d} +$$

$$[\cos(wt+\pi/6)]_{\pi+10\pi/3m-2d}^{\pi+10\pi/3m} + [\cos(wt-\pi/2)]_{\pi+10\pi/3m}^{\pi+10\pi/3m+2d}\,]$$

$$= \frac{2\sqrt{6}V}{\pi}\Big[\frac{\cos(2d-\pi/2)}{2} + \sin d\,[2\sin(2\pi/3m+\pi/6+d) - \sin(4\pi/3m+d-7\pi/6)$$

$$- \sin(2\pi/m-\pi/2-d) - 2\sin(2\pi/m+d-7\pi/6) - \sin(8\pi/3m-7\pi/6+d) +$$

$$\sin(2\pi/3m-7\pi/6-d) + \sin(4\pi/3m+d+\pi/6) + \sin(8\pi/3m+d-\pi/2) +$$

$$\sin(10\pi/3m-d+\pi/6)] - \frac{\cos(2d+\pi/6)}{2} + 0.433] \qquad \ldots\ (A.1)$$

Similarly the expression for the average counter emf in the range of phase shift angles between 30^{o} and 60^{o} is given by :

$$V_{DO}= \frac{V}{\pi}\left[\int_{0}^{2d} - \sqrt{6}\sin(wt-\pi/2)d(wt) + \int_{2\pi/3m}^{2\pi/3m+2d} \sqrt{6}\sin(wt+\pi/6)d(wt) + \right.$$

$$\int_{4\pi/3m}^{4\pi/3m+2d} \sqrt{6}\sin(wt+\pi/6)d(wt) + \int_{2\pi/m}^{2\pi/m+2d} \sqrt{6}\sin(wt+\pi/6)d(wt) - \int_{8\pi/3m}^{8\pi/3m+2d} \sqrt{6}\sin(wt-7\pi/6)d(wt)$$

$$+ \int_{10\pi/3m}^{10\pi/3m+2d} \sqrt{6}\sin(wt-\pi/2)d(wt) + \int_{\pi}^{\pi+2d} \sqrt{6}\sin(wt-\pi/2)d(wt) +$$

$$\int_{\pi+2\pi/3m}^{\pi+2\pi/3m+2d} \sqrt{6}\sin(wt-\pi/2)d(wt) - \int_{\pi+4\pi/3m}^{\pi+4\pi/3m+2d} \sqrt{6}\sin(wt+\pi/6)d(wt) + \int_{\pi+2\pi/m}^{\pi+2\pi/m+2d} \sqrt{6}\sin(wt-7\pi/6)d(wt)$$

$$+ \int_{\pi+8\pi/3m}^{\pi+8\pi/3m+2d} \sqrt{6}\sin(wt-7\pi/6)d(wt) + \left.\int_{\pi+10\pi/3m}^{\pi+10\pi/3m+2d} \sqrt{6}\sin(wt-7\pi/6)d(wt)\right]$$

$$\text{or } V_{DO} = \frac{V\sqrt{6}}{\pi}\left[[\cos(wt-\pi/2)]_{0}^{2d} - [\cos(wt+\pi/6)]_{2\pi/3m}^{2\pi/3m+2d} - \right.$$

$$[\cos(wt+\pi/6)]_{4\pi/3m}^{4\pi/3m+2d} - [\cos(wt+\pi/6)]_{2\pi/m}^{2\pi/m+2d} + [\cos(wt-7\pi/6)]_{8\pi/3m}^{8\pi/3m+2d}$$

$$- [\cos(wt-\pi/2)]_{10\pi/3m}^{10\pi/3m+2d} - [\cos(wt-\pi/2)]_{\pi}^{\pi+2d} - [\cos(wt-\pi/2)]_{\pi+2\pi/3m}^{\pi+2\pi/3m+2d}$$

$$+ [\cos(wt+\pi/6)]_{\pi+4\pi/3m}^{\pi+4\pi/3m+2d} - [\cos(wt-7\pi/6)]_{\pi+2\pi/m}^{\pi+2\pi/m+2d} -$$

$$\left.[\cos(wt-7\pi/6)]_{\pi+8\pi/3m}^{\pi+8\pi/3m+2d} - [\cos(wt-7\pi/6)]_{\pi+10\pi/3m}^{\pi+10\pi/3m+2d}\right]$$

$$\text{or} \quad V_{DO} = \frac{2\sqrt{6}V}{\pi} [\sin(2d)+\sin d[\sin(2\pi/3m+\pi/6+d)+2\sin(4\pi/3m+\pi/6+d)$$

$$+ \sin(2\pi/m+\pi/6+d)- 2\sin(8\pi/3m-7\pi/6+d)+ \sin(10\pi/3m-\pi/2+d) -$$

$$\sin(2\pi/3m-\pi/2+d) + \sin(2\pi/m-7\pi/6+d) - \sin(10\pi/3m+d-7\pi/6)]] \quad \ldots\ (A.2)$$

Similarly the expression for the average counter EMF in the range of phase shift angles between 60° and 90° is given by :

$$V_{DO} = \frac{\sqrt{6}V}{\pi} [\int_{0}^{2d} \sin(wt-7\pi/6)d(wt)+\int_{2\pi/3m}^{2\pi/3m+2d} \sin(wt+\pi/6)d(wt) +$$

$$\int_{4\pi/3m}^{4\pi/3m+2d} \sin(wt+\pi/6)d(wt) + \int_{2\pi/m}^{2\pi/m+2d} \sin(wt+\pi/6)d(wt) + \int_{8\pi/3m-2d}^{8\pi/3m} \sin(wt-\pi/2)d(wt) +$$

$$\int_{8\pi/3m}^{8\pi/3m+2d} \sin(wt+\pi/6)d(wt) + \int_{10\pi/3m}^{10\pi/3m+2d} \sin(wt-\pi/2)d(wt) + \int_{\pi}^{\pi+2d} \sin(wt-\pi/2)d(wt) +$$

$$\int_{\pi+2\pi/3m}^{\pi+2\pi/3m+2d} \sin(wt-\pi/2)d(wt) + \int_{\pi+4\pi/3m-2d}^{\pi+4\pi/3m} \sin(wt-7\pi/6)d(wt) + \int_{\pi+4\pi/3m}^{\pi+4\pi/3m+2d} \sin(wt-\pi/2)d(wt) +$$

$$\int_{\pi+2\pi/m}^{\pi+2\pi/m+2d} \sin(wt-7\pi/6)d(wt) + \int_{\pi+8\pi/3m}^{\pi+8\pi/3m+2d} \sin(wt-7\pi/6)d(wt) + \int_{\pi+10\pi/3m}^{\pi+10\pi/3m+2d} \sin(wt-7\pi/6)d(wt) +$$

$$\int_{2\pi-2d}^{2\pi} \sin(wt+\pi/6)d(wt)]$$

$$\text{or } V_{DO} = \frac{\sqrt{6}V}{\pi} \left[- [\cos(wt-7\pi/6)]_{0}^{2d} - [\cos(wt+\pi/6)]_{2\pi/3m}^{2\pi/3m+2d} \right.$$

$$- [\cos(wt+\pi/6)]_{4\pi/3m}^{4\pi/3m+2d} - [\cos(wt+\pi/6)]_{2\pi/m}^{2\pi/m+2d} - [\cos(wt-\pi/2)]_{8\pi/3m-2d}^{8\pi/3m}$$

$$- [\cos(wt+\pi/6)]_{8\pi/3m}^{8\pi/3m+2d} - [\cos(wt-\pi/2)]_{10\pi/3m}^{10\pi/3m+2d} - [\cos(wt-\pi/2)]_{\pi}^{\pi+2d}$$

$$- [\cos(wt-\pi/2)]_{\pi+2\pi/3m}^{\pi+2\pi/3m+2d} - [\cos(wt-7\pi/6)]_{\pi+4\pi/3m-2d}^{\pi+4\pi/3m} -$$

$$[\cos(wt-\pi/2)]_{\pi+4\pi/3m}^{\pi+4\pi/3m+2d} - [\cos(wt - 7\pi/6)]_{\pi+2\pi/m}^{\pi+2\pi/m+2d} -$$

$$[\cos(wt-7\pi/6)]_{\pi+8\pi/3m}^{\pi+8\pi/3m+2d} - [\cos(wt-7\pi/6)]_{\pi+10\pi/3m}^{\pi+10\pi/3m+2d} -$$

$$\left. [\cos(wt+\pi/6)]_{2\pi-2d}^{2\pi} \right]$$

$$\text{or } V_{DO} = \frac{2\sqrt{6}V}{\pi} \left[\frac{\cos(2d-\pi/2)}{2} + \cos(\pi/6-2d) - 0.866 + \right.$$

$$\sin d[\sin(2\pi/3m+\pi/6+d) + \sin(4\pi/3m+d+\pi/6) + \sin(2\pi/m+d+\pi/6) +$$

$$\sin(8\pi/3m-d-\pi/2) + \sin(8\pi/3m+\pi/6+d) + \sin(10\pi/3m+d-\pi/2) -$$

$$\sin(2\pi/3m+d-\pi/2) - \sin(4\pi/3m-d-7\pi/6) - \sin(4\pi/3m+d-\pi/2) -$$

$$\left. \sin(2\pi/m+d-7\pi/6) - \sin(8\pi/3m+d-7\pi/6) - \sin(10\pi/3m+d-7\pi/6)] \right.$$

APPENDIX B

From Fig.3.11, the fundamental component of the inverter current is determined as,

$$a_1 = \frac{2}{\pi}\left[\int_{2\pi/3m}^{2\pi/3m+2d} -I_D\cos wt\, d(wt) + \int_{4\pi/3m}^{4\pi/3m+2d} -I_D\cos wt\, d(wt) + \int_{2\pi/m}^{2\pi/m+2d} -I_D\cos wt\, d(wt) + \int_{8\pi/3m}^{8\pi/3m+2d} -I_D\cos wt\, d(wt)\right]$$

$$= -\frac{2I_D}{\pi}\left[\left[\sin wt\right]_{2\pi/3m}^{2\pi/3m+2d} + \left[\sin wt\right]_{4\pi/3m}^{4\pi/3m+2d} + \left[\sin wt\right]_{2\pi/m}^{2\pi/m+2d} + \left[\sin wt\right]_{8\pi/3m}^{8\pi/3m+2d}\right]$$

$$= -\frac{2I_D}{\pi}[\sin(2\pi/3m+2d) - \sin(2\pi/3m) + \sin(\tfrac{4\pi}{3m} + 2d) - \sin(4\pi/3m) + \sin(2\pi/m+2d) - \sin(2\pi/m) + \sin(8\pi/3m+2d) - \sin(8\pi/3m)]$$

$$= -\frac{4I_D}{\pi}[\cos(2\pi/3m+d).\sin d + \cos(4\pi/3m+d).\sin d + \cos(2\pi/m+d).\sin d + \cos(8\pi/3m+d).\sin d]$$

$$= -\frac{4I_D}{\pi}[\sin d[\cos(2\pi/3m+d) + \cos(4\pi/3m+d) + \cos(2\pi/m+d) + \cos(8\pi/3m+d)]] \quad \ldots\ (B.1)$$

$$b_1 = \frac{2}{\pi}\left[\int_{2\pi/3m}^{2\pi/3m+2d} -I_D \sin wt\, d(wt) + \int_{4\pi/3m}^{4\pi/3m+2d} -I_D \sin wt\, d(wt) + \right.$$

$$\left. \int_{2\pi/m}^{2\pi/m+2d} -I_D \sin wt\, d(wt) + \int_{8\pi/3m}^{8\pi/3m+2d} -I_D \sin wt\, d(wt)\right]$$

$$= \frac{2I_D}{\pi}\left[[\cos wt]_{2\pi/3m}^{2\pi/3m+2d} + [\cos wt]_{4\pi/3m}^{4\pi/3m+2d} + [\cos wt]_{2\pi/m}^{2\pi/m+2d} + \right.$$

$$\left. [\cos wt]_{8\pi/3m}^{8\pi/3m+2d}\right]$$

$$= \frac{2I_D}{\pi}[\cos(2\pi/3m+2d) - \cos(2\pi/3m) + \cos(4\pi/3m+2d) - \cos(4\pi/3m)$$

$$+ \cos(2\pi/m+2d) - \cos(2\pi/m) + \cos(8\pi/3m+2d) - \cos(8\pi/3m)\,]$$

$$= -\frac{4I_D}{\pi}[\sin d[\sin(2\pi/3m + d) + \sin(4\pi/3m + d) + \sin(2\pi/m + d)$$

$$+ \sin(8\pi/3m + d)\,] \qquad \ldots\ (B.2)$$

Therefore, fundamental component of inverter current

$$I_{if} = \sqrt{a_1^2 + b_1^2} \qquad \ldots\ (B.3)$$

$$\text{RMS value of the } I_{if} = \frac{\sqrt{a_1^2+b_1^2}}{\sqrt{2}} \qquad \ldots\ (B.4)$$

In general, the Fourier coefficients are given by,

$$a_n = \frac{2}{\pi}\left[\int_{2\pi/3m}^{2\pi/3m+2d} -I_D \cos nwt\, d(wt) + \int_{4\pi/3m}^{4\pi/3m+2d} -I_D \cos nwt\, d(wt) + \right.$$

$$\left. \int_{2\pi/m}^{2\pi/m+2d} -I_D \cos nwt\, d(wt) + \int_{8\pi/3m}^{8\pi/3m+2d} -I_D \cos nwt\, d(wt)\right]$$

$$= -\frac{2I_D}{n\pi}\left[\left[\sin nwt\right]_{2\pi/3m}^{2\pi/3m+2d} + \left[\sin nwt\right]_{4\pi/3m}^{4\pi/3m+2d} + \left[\sin nwt\right]_{2\pi/m}^{2\pi/m+2d} + \left[\sin nwt\right]_{8\pi/3m}^{8\pi/3m+2d}\right]$$

$$= -\frac{2I_D}{n\pi}\left[\sin n(2\pi/3m+2d) - \sin 2n\pi/3m + \sin n(4\pi/3m+2d) - \sin 4n\pi/3m + \sin n(2\pi/m+2d) - \sin 2n\pi/m + \sin n(8\pi/3m+2d) - \sin 8n\pi/3m\right]$$

$$= -\frac{4I_D}{n\pi}\left[\cos n(2\pi/3m+d).\ \sin nd + \cos n(4\pi/3m+d).\ \sin nd + \cos n(2\pi/m+d).\ \sin nd + \cos n(8\pi/3m+d).\ \sin nd\right]$$

$$= -\frac{4I_D}{n\pi}\left[\sin nd\left[\cos n(2\pi/3m+d) + \cos n(4\pi/3m+d) + \cos n(2\pi/m+d) + \cos n(8\pi/3m+d)\right]\right] \quad \ldots\ (B.5)$$

Similarly,

$$b_n = \frac{2}{\pi}\left[\int_{2\pi/3m}^{2\pi/3m+2d} -I_D \sin nwt\ d(wt) + \int_{4\pi/3m}^{4\pi/3m+2d} -I_D \sin nwt\ d(wt) + \int_{2\pi/m}^{2\pi/m+2d} -I_D \sin nwt\ d(wt) + \int_{8\pi/3m}^{8\pi/3m+2d} -I_D \sin nwt\ d(wt)\right]$$

$$= \frac{2I_D}{n\pi} \left[\left[\cos nwt\right]_{2\pi/3m}^{2\pi/3m+2d} + \left[\cos nwt\right]_{4\pi/3m}^{4\pi/3m+2d} + \left[\cos nwt\right]_{2\pi/m}^{2\pi/m+2d} \right.$$

$$\left. + \left[\cos nwt\right]_{8\pi/3m}^{8\pi/3m+2d} \right]$$

$$= -\frac{4I_D}{n\pi} \left[\sin nd \left[\sin n(2\pi/3m+d) + \sin n(4\pi/3m+d) + \sin n(2\pi/m+d) \right.\right.$$

$$\left.\left. + \sin n(8\pi/3m+d) \right] \right. \quad \ldots\ldots \quad (B.6)$$

Therefore, Fourier components are given by

$$I_n = \sqrt{a_n^2+b_n^2} \quad \ldots\ldots \quad (B.7)$$

RMS values is given by $\frac{\sqrt{a_n^2 + b_n^2}}{\sqrt{2}}$

APPENDIX C

DETAILS OF THREE PHASE SLIP-RING INDUCTION MOTOR, LOADING GENERATOR AND TACHOGENERATOR

1. Three phase slip-ring induction motor

   3HP, 1440rpm, 400V, 50Hz.

   Rated Stator Current : 5.0A

   Rated Rotor Current : 10.0A

   Rated Rotor Voltage : 145.0V

   Stator/Rotor Turns Ratio : 2.76

   The per phase equivalent circuit parameters, referred to stator, are given below :

   R_1 = 1.6 Ω

   X_1 = 2.9 Ω

   R_m = 40.8 Ω

   X_m = 79.2 Ω

   X_2 = 2.9 Ω

   R_2 = 3.37 Ω

2. DC Loading Generator (Seperately Excited)

   5HP, 240V, 19.7A

   Speed : 1150/2800rpm

   Field Current : 1.06/0.34A

   Field Resistance : 174 Ω

APPENDIX D

K_2 = 2.82

T_2 = 361.4 msec.

K_1 = 17.23

A = 0.46

T_A = 83 msec.

T_e = 22 msec.

q = 0.62

T_m = 437.5 [22]msec.

H_i = 2.4

T_i = 100 msec.

H_w = 1

T_w = 62 msec.

REFERENCES

[1]. Fitzerald, Kinsley and Kusko, 'Electric Machinery', Maegraw - Hill.

[2]. J.M.D. Murphy, 'Thyristor control of AC Motors', Pergamon press, Oxford, 1973.

[3]. M.S. Erlicki, 'Inverter Rotor Drive of an Induction motor', IEEE Trans. on Power Apparatus and Systems, Vol. PAS - 84, No. 11, pp. 1011 - 1016, November 1965.

[4]. A. Lavi and R.J. Polge, 'Induction motor speed control with static inverter in the rotor', IEEE Trans., Vol. PAS - 85, No. 1, pp. 76 - 84, January 1966.

[5]. W. Shepherd and J. Stanway, 'Slip Energy recovery in an Induction motor by the use of a thyristor inverter', IEEE Trans., Vol. IGA - 5, No. 1, pp. 74 - 82, January/February 1969.

[6]. W. Shepherd and A.Q. Khalil, 'Capacitive compensation of thyristor controlled slip energy recovery system', IEE proc., Vol. - 117, No. 5, pp. 948 - 956, May 1970.

[7]. P.N. Miljanic, 'The through pass inverter and its application to the speed control of wound rotor induction machine', IEEE Trans., Vol. PAS - 87, No. 1, pp. 234 - 239, January 1968.

[8]. W. Drury, B.L. Jones and J.E. Brown, 'Applications of controlled flywheeling to the recovery bridge of a Static Kramer Drive', IEEE proc., Vol. 130, pt. B, No. 3, pp. 73 - 85, March 1983.

[9]. N.N. Rao, G.K. Dubey and S.S. Prabhu, 'Slip power recovery scheme employing a fully controlled converter with half controlled characteristics, IEE proc., Vol. 130, pt. B, No. 1, pp. 33 - 38, January 1983.

[10]. Guy Oliver and Victor Stefanovic, 'Evaluation of phase commutated converters for slip power control in Induction drives', IEEE Trans., Vol. 19, No. 1, pp. 105 - 112, January/February 1983.

[11]. G.A. Smith, 'A current - source inverter in the secondary circuit of a wound rotor induction motor provides sub and suber synchronous operation', IEEE Trans., Vol. IA - 17, No. 4, pp. 399 - 406, July/August 1981.

[12]. G.N. Revankar, S.K. Pillai, M.C. Srisailam and Y.R. Shah, 'Reduction of commutation period in current source Inverters', Journal of the Institution of Engineers (Electrical Engg. Division), Vol. 62, Part El 4, February 1982.

[13]. Moltgen Gottfried, 'Line commutated thyristor converters', Pitman Publishing, 1972.

[14]. P.C. Sen and K.H.J.Ma, 'Rotor Chopper Control for induction motor drive : TRC strategy', IEEE Trans., Vol. IA-11 No. 1, pp. 43 - 49, January/February 1975.

[15]. B. Ray, 'Modelling of Static Kramer Drive', IIT, Kanpur thesis, July 1983.

[16]. B.K. Bose, 'A review of AC drives technology', Report No. 81CRD127, General Electric, June 1981.

[17]. T. Krishnan and B. Ramaswami, 'A fast-response DC motor control system', IEEE Trans., Vol. IA - 10, No. 5, September/October 1974, pp. 643 - 651.

[18]. B. Adkins, 'The Generalised Theory and Electrical Machines', New York, Willey, 1957.

[19]. T. Krishnan and B. Ramaswami, 'Slip-ring induction motor speed-control using a thyristor inverter', Automatica, Vol. 11, 1975, p.419.

[20]. C. Concordia, 'Synchronizing Machines', New York, Willey, 1951.

[21]. J.D. Azzo and C. Houpis, 'Control system analysis and synthesis', New York, Mcgraw Hill, 2nd Edition, 1951.

[22]. N.S. Wani, 'Thyristor controllers for slip ring induction motor', Ph.D. Thesis, IIT, Kanpur, India, 1978.